A Mechanistic Study of Sulphur, Nitrogen and Oxygen Donor Bidentate Ligand Interactions on the Rhenium (I) Tricarbonyl Core

by

PHEELLO ISAAC NKOE

A dissertation submitted to meet the requirements for the degree of

MAGISTER SCIENTIAE

In the

DEPARTMENT OF CHEMISTRY
FACULTY OF NATURAL AND AGRICULTURAL SCIENCES

At the

UNIVERSITY OF THE FREE STATE

SUPERVISOR: DR. MARIETJIE SCHUTTE-SMITH
CO-SUPERVISOR: DR. ALICE BRINK

December 2015

ACKNOWLEDGEMENTS

First and foremost, I would like to thank God for giving me the strength and courage to complete this work. I am very blessed!

Prof André Roodt, it is a great honour to be known as one of your students. Thank you for giving me the opportunity and also the inspiration through your passion for chemistry. I am proud of myself because of you.

I would like to express my gratitude to Dr Chantel Swart-Pistor and Miss SE Saaiman at the Department of Microbial, Biochemical and Food Biotechnology at the UFS for her inputs, effort and time spent on the testing of the compounds.

A big thank you to the crystallographers Renier Koen, Dumisane Kama (Tom), Thabo Marake and Carla Pretorius for their time and help with the crystallographic part of this work. Prof Deon Visser, thank you for all your assistance, time and effort with the interpretations and understanding of the work. I appreciate your help a lot!

Dr Marietjie Schutte-Smith the best supervisor, I don't know how to thank you. You were always next to me during times that I did not have hope, ever since 2013. I would like to gratefully thank you for your patience, understanding and your guidance. You are the best supervisor I could ask for. Dr Alice Brink, to be honest with you, you are a great co-supervisor. Your wisdom, knowledge and commitment inspires me. Thanks a lot for your encouragement and your support through tough times. Drs Schutte-Smith and Brink, my eyes are open and my mind is open because of you. BIG THANKS TO YOU!!

I would like to thank my second family, the Inorganic Chemistry group at the University of the Free State for being there for me when I needed you. Your assistance with the happy faces that expressed 'It's a pleasure, PLEASE come again, we will help you!' I would like to specifically mention Pule Molokoane, Nina Marogoa, Mampotso Tsosane, Lebohang Mphure, Teboho Alexander (Orbett), Penny Mokolokolo and Sibongile Mamusa. With your jokes, all the funny moments, talks, encouragement, going out for drinks and not giving up on me, you guys made this work much simpler for me.

I would like to thank Hlengiwe Mnculwane, Lumanyano Ntoi, Qinisile Vilakazi, Gontse Malefo for the lunches, fun and crazy moments we shared during this time. You guys are the best. Special thanks to my Brandwag neighbours Neo Qhala (Tuna), Tshepo

Matebesi and Neo Segalo. Thanks guys for being such good friends to me; without all the fun we had on Saturdays, this work would have been much less exciting.

To my family, I really don't know how to thank you. The word 'thanks' is not enough. My late Mother, Nobelongu Maria Nkoe, you did more than your part for our family. I am what I am because of you. You taught me to close my mouth and open my ears. You sacrificed a lot in order for us to have a good education. My father, Tshotleho Andres Nkoe, you are the best father in the world. Thanks for the support you gave me, the encouragement you offered and sacrifices you made for me during my studies. My brothers Tatolo, Khotso and Lehlohonolo Nkoe - I would like to thank you for being there for me when I need you, for putting your faith in me and allowing me to be as ambitious as I want. Very special thanks to this beautiful lady, Rose Palesa Khumalo for your support, patience and encouragement through this tough time from 2013. You never gave up on me, THANKS!!

TABLE OF CONTENTS

ABBREVIATIONS

º	Degrees
Å	Angstrom
α	Alpha
β^-	Beta
γ	Gamma
β^+	Positron
v_{CO}	C=O stretching frequency
2,3-diMeANAOXH	5-(2,3-diMephenyl)azo-8-hydroxyquinoline
2,5-PicoH_2	2,5-Pyridinedicarboxylic acid
2,6-diMeANAOXH	5-(2,6-diMephenyl)azo-8-hydroxyquinoline
3,4-diMeANAOXH	5-(3,4-diMephenyl)azo-8-hydroxyquinoline
3-ClPy	3-Chloropyridine
4-Pic	4-Picoline
ANAOX	5-Phenylazo-8-hydroxyquinoline
BSBr	5-Bromo-2,2`-bithiophene
BSC	2,2′-Bithiophene-5-carboxylic acid
BSOC	Methyl benzo[b]thiophene-2-carboxylate
BSOH	Benzothiophene-2-methanol
BSOPhH_2	2-Mercaptophenol
BSOPhCH	2-Methoxythiophenol
BSPhH_2	Benzene-1,2-dithiol
CH_3CN	Acetonitrile
Conc	Concentration
DMAP	4-Dimethylaminopyridine

Abbreviations

DMS	Dimethylsulfide
fac	facial
HEDP	Hydroxyethylidene diphosphonate
HNO_3	Nitric acid
IR	Infrared Spectroscopy
Isa	Isatin
k_1	First-order rate constant for forward reaction
k_{-1}	Rate constant for reverse reaction
K_1	equilibrium constant
L,L'-Bid	Bidentate ligand with L,L' donor atoms
L,L',L"-Tri	Tridentate ligand with L,L',L'' donor atoms
MIBI	2-Methoxy-2-methylpropylisocyanide
m-TolANAOXH	5-(m-Tol)azo-8-hydroxyquinoline
m-TolBSPhH	Toluene-3,4-dithiol
$[NEt_4]^+$	Tetraethylammonium cation
NMR	Nuclear Magnetic Resonance Spectroscopy
PPh_3	Triphenylphosphine
Py	Pyridine
Pyz	Pyrazine
ReAA	*fac*-$[NEt_4]_2[Re(CO)_3(Br)_3]$
$t_{1/2}$	Half-life
THT	Tetrahydrothiophene
Trop	Tropolone
TS	2,2`-Thiodiethanethiol
TU	Thiourea
UV/Vis	Ultraviolet/Visible Spectroscopy

Abbreviations

XRD	X-ray Diffraction

ABSTRACT

The nuclear properties of rhenium ($^{186/188}$Re) and technetium (^{99m}Tc) are used for their application as diagnostic and therapeutic radiopharmaceuticals. Researchers have shown a significant interest in rhenium and technetium tricarbonyl complexes of the form *fac*-$[M(CO)_3X(L,L'\text{-Bid})]^n$ where M = Tc(I) or Re(I), X = entering monodentate ligand and L-L'-Bid = different donor atom bidentate ligands, as potential diagnostic and therapeutic radiopharmaceuticals. These *fac*-$[M(CO)_3X(L,L'\text{-Bid})]^n$ type complexes are prepared from the starting synthons *fac*-$[M(CO)_3(Br_3)]^{2-}$ and *fac*-$[M(CO)_3(H_2O)_3]^+$ that was initially prepared by Alberto *et al.* in 1999. This starting synthon is a favourite all around for the synthesis of potential radiopharmaceuticals due to the easy preparation and the stability of *fac*-$[M(CO)_3(H_2O)_3]^+$ in aqueous solution in the pH range of 2 - 12 for several hours. The carbonyl ligands are tightly coordinated to the metal and form the stable *fac*-$[M(CO)_3]^+$ core. The three bromido or water ligands can be easily substituted by different functional groups such as thioethers, thiols, phosphines and amines.

The aim of this study was to investigate the ability of the chosen donor atom N,O; S,S'; S,O bidentate and S,S'S" tridentate ligands to coordinate to the *fac*-$[Re(CO)_3]^+$ core. The results were compared to previous studies reported on N,O and O,O' bidentate ligand systems to observe the variation in coordination behaviours. The chosen ligands include: 5-phenylazo-8-hydroxyquinoline, 5-(m-Tol)azo-8-hydroxyquinoline, 5-(2,3-diMephenyl)azo-8-hydroxyquinoline, 5-(2,6-diMe phenyl)azo-8-hydroxyquinoline, 5-(3,4-diMe phenyl)azo-8-hydroxyquinoline, methyl benzo[b]thiophene-2-carboxylate, benzothiophene-2-methanol, 2-mercaptophenol, 2-methoxythiophenol, 5-bromo-2,2`-bithiophene, 2,2′-bithiophene-5-carboxylic acid, benzene-1,2-dithiol, toluene-3,4-dithiol, and 2,2`-thiodiethanethiol.

The synthesis of the complexes are described in Chapter 4 and characterized by IR, UV/Vis, NMR (^{1}H and ^{13}C) and elemental analysis. The following crystal structures were obtained *fac*-$[Re_2(CO)_6(TS)(Py)]$ (**1**), *fac*-$[Re_2(CO)_6PPh_3(BSOPhC)_2(Py)]$ (**2**), *fac*-$[NEt_4][Re_2(CO)_6(BSOPhC)_3]$ (**3**) and *fac*-$[Re_2(CO)_6(m\text{-TolBSPh})_2]$ (**4**). All four of the structures has four molecules per unit cell (Z = 4). (**1**) and (**4**) crystallized in the $P\bar{1}$ space group while (**2**) and (**3**) crystallized in a monoclinic space group. In all four these structures the ligands form sulphur bridges between two rhenium (I) centres. The Re-

CO bond distances of all the crystal structures range from 1.88(3) Å to 1.95(10) Å and the Re-S bond distances vary from 2.44(2) Å to 2.56(7) Å. (**2**) has a Re-P bond distance of 2.51(12) Å and a Re-N bond distance of 2.24(4) Å. The S-Re-S bond angles range from 76.26(3) ° to 94.99(8) ° and the Re-S-Re bond angles from 87.28(9) ° to 100.60(4) ° with the non-bonding rhenium to rhenium distances of 3.796(8) Å for (**1**), 3.845(10) Å for (**2**), 3.488(10) Å for (**3**) and 3.654(16) Å for (**4**). The non-bonding Re…Re distances are directly proportional to the Re-S-Re angles and follow the following trend: (**3**) < (**4**) < (**1**) < (**2**).

A fairly good comparison could be made between previously reported structures with S,S'; S,O; N,O and O,O'-bidentate ligands coordinated to the *fac*-$[Re(CO)_3]^+$ core. The structure of (**4**) has been reported before and a very good correlation is found between this structure and the reported structure.

After an in depth study it was confirmed that the structures of all the compounds with S,O; S,S' and S,S',S'' ligands have to be analysed by single crystal XRD or at least a quantitative NMR study. For one ligand system (BSOPhC), two different structures were obtained with only a slight change in the synthetic procedure. It is not that easy to determine and speculate the bonding modes of these type of ligands. Therefore a complete crystallographic study will form part of the future work for this project.

Excellent results were obtained for anti-mitochondrial activity screening for five compounds. The next step will be to improve the solubility of these complexes, especially in water as solvent; this illustrates the possible use of these compounds as potential radiopharmaceuticals.

OPSOMMING

Die kern eienskappe van renium ($^{186/188}$Re) en tegnesium (^{99m}Tc) word gebruik vir hulle toepassing in diagnostiese en terapeutiese radiofarmasie. Navorsers het reeds beduidende belangstelling getoon in renium en tegnesium trikarboniel komplekse van die vorm *fas*-[M(CO)$_3$X(L,L'-Bid)]^n, waar M = Tc(I) of Re(I), X = inkomende monodentate ligand en L-L'-Bid = verskillende skenkeratoom bidentate ligande, vir toepassing as potensiële diagnostiese en terapeutiese radiofarmaseutiese middels. Hierdie *fas*-[M(CO)$_3$X(L,L'-Bid)]^n tipe komplekse is voorberei vanaf *fas*-[M(CO)$_3$(Br$_3$)]$^{2-}$ en *fas*-[M(CO)$_3$(H$_2$O)$_3$]$^+$ wat aanvanklik deur Alberto *et al.* in 1999 berei is. Hierdie begin sinton is 'n algemene gunsteling vir die sintese van potensiële radiofarmaseutiese middels danksy die maklike bereiding en stabiliteit van *fas*-[M(CO)$_3$(H$_2$O)$_3$]$^+$ in wateroplossing in 'n pH reeks van 2 tot 12 vir verskeie ure. Die karboniel ligande is stewig aan die metaal gekoördineer en vorm die stabiele *fas*-[M(CO)$_3$]$^+$ kern. Die drie bromido of water ligande kan maklik deur verskillende funksionele groepe soos tioësters, tiole, fosfiene en amiene gesubstitueer word.

Die doel van hierdie studie was om die vermoë van die gekose skenkeratoom N,O; S,S'; S,O bidentate en S,S'S" tridentate ligande aan die *fas*-[Re(CO)$_3$]$^+$ kern te koördineer te ondersoek. Die resultate is met vorige studies rakende N,O en O,O' bidentate ligandstelsels vergelyk ten einde die variasie in koördinasiegedrag waar te neem. Die gekose ligande sluit in: 5-fenielaso-8-hidroksiekinolien, 5-(m-Tol)aso-8-hidroksiekinolien, 5-(2,3-diMe-feniel)aso-8-hidroksiekinolien, 5-(2,6-diMe-feniel)aso-8-hidroksiekinolien, 5-(3,4-diMe-feniel)aso-8-hidroksiekinolien, metiel benso[b]tiofeen-2-karboksilaat, bensotiofeen-2-metanol, 2-merkaptofenol, 2-metoksietiofenol (BSOFCH), 5-bromo-2,2`-bitiofeen, 2,2′-bitiofeen-5-karboksielsuur, benseen-1,2-ditiol, tolueen-3,4-ditiol (m-TolBSFH$_2$) en 2,2`-tiodietaantiol (TSH$_2$).

Die sintese van die komplekse word in Hoofstuk 4 beskryf en is gekarakteriseer deur IR, UV/Vis, KMR (^{1}H en ^{13}C) en elementanalise. Die volgende kristalstrukture is verkry: *fas*-[Re$_2$(CO)$_6$(TS)(Py)] (**1**), *fas*-[Re$_2$(CO)$_6$PF$_3$(BSOFC)$_2$(Py)] (**2**), *fas*-[NEt$_4$][Re$_2$(CO)$_6$(BSOFC)$_3$] (**3**) en *fas*-[Re$_2$(CO)$_6$(m-TolBSF)$_2$] (**4**). Al vier van die strukture het vier molekule per eenheidsel (Z = 4). (**1**) en (**4**) kristalliseer in die $P\bar{1}$ ruimtegroep terwyl (**2**) en (**3**) in 'n monokliniese kristalstelsel kristalliseer. In al vier van hierdie strukture vorm die ligande swael brûe tussen twee renium (I) kerne. Die Re-CO

bindingsafstande van al die kristalstrukture wissel van 1.88(3) Å tot 1.95(10) Å en die Re-S bindingsafstande wissel van 2.44(2) Å tot 2.56(7) Å. (**2**) het ŉ Re-P bindingsafstand van 2.51(12) Å en ŉ Re-N bindingsafstand van 2.24(4) Å. Die S-Re-S bindingshoeke wissel vanaf 76.26(3) ° na 94.99(8) ° en die Re-S-Re bindingshoeke tussen 87.28(9) ° en 100.60(4) ° met die ongebonde renium na renium afstande van 3.796(8) Å vir (**1**), 3.845(10) Å vir (**2**), 3.488(10) Å vir (**3**) en 3.654(16) Å vir (**4**). Die ongebonde Re…Re afstande is direk eweredig aan die Re-S-Re hoeke en volg die volgende tendens: (**3**) < (**4**) < (**1**) < (**2**).

ŉ Betreklik goeie vergelyking kon getref word tussen voorheen gemelde strukture met S,S'; S,O; N,O en O,O' bidentate ligande wat aan die *fas*-$[Re(CO)_3]^+$ kern gekoördineer is. Die struktuur van (**4**) is voorheen gerapporteer en ŉ baie goeie ooreenkoms tussen hierdie struktuur en die gerapporteerde struktuur is gevind.

Na ŉ deeglike studie is dit bevestig dat die strukture van alle verbindings met S,O; S,S' en S,S',S'' ligande deur middel van enkelkristal X-straal diffraksie of ten minste ŉ kwantitatiewe KMR studie geanaliseer moet word. Vir een ligandstelsel (BSOFC) is twee verskillende strukture verkry met slegs ŉ geringe verandering in die sintetiese prosedure. Dit is nie maklik om die bindingsmodusse van hierdie tipe ligande vas te stel en daaroor te spekuleer nie, daarom vorm ŉ volledige kristallografiese studie deel van die toekomstige doelwitte vir hierdie projek.

Uitstekende resultate is vir die anti-mitokondriese aktiwiteitsifting vir vyf verbindings verkry. Die volgende stap is die verbetering van die oplosbaarheid van hierdie komplekse, veral in water as oplosmiddel; dit illustreer die moontlike gebruik van hierdie verbindings as radiofarmaseutiese middels.

1 INTRODUCTION AND AIM

1.1 Nuclear medicine

In November 1895, Wilhelm Conrad Roentgen was the first person to discover X-rays; after that other researchers began to investigate the possibility that X-rays may kill germs.[1] Antoine Henri Becquerel discovered radioactivity from a sample of uranium[1] after Roentgen's findings, and a few years later Marie and Pierre Curie isolated radium and polonium. Radium was used to cure many diseases in the 1900's.[2] In 1935, Irene Curie and Frederic Joliot managed to successfully produce artificial radionuclides, which led to the development of radiotracers studied by Georg de Hevesy who received the Nobel Prize in chemistry in 1943.[2]

According to the theory behind nuclear medicine, and with the help of Georg de Hevesy, nuclear medicine was established following the application of the 'radiotracer theory'. This led us to the point where nuclear medicine was defined as a speciality in medicine which deals with the use of radiopharmaceuticals or radiotracers.

1.2 Radiopharmaceuticals

Metal coordination compounds are widely used in the medical field. In the case of radiopharmaceuticals, the drugs are used for different applications e.g. cisplatin and carboplatin are used for the treatment of cancer, while gadolinium compounds are used as magnetic resonance imaging (MRI) agents.[3] Radiopharmaceuticals are defined as

[1] Treichel, P. M. *Kirk-Othmer Encyclopaedia of Chemical Technology (*3rd Ed). John Wiley and Sons. New York. 1982.
[2] Mathews, C. K. Van Holde, K. E*. Biochemistry*, Benjamin/Cummings Publishing Company, Inc., Redwood City. 1990**.**
[3] Perera, T. PhD thesis. University of Colombo. Sir Lanka. 2004.

drugs that are pharmaceutical formulations consisting of radioactive substances used in nuclear medicine for the diagnosis or therapy of diseases, such as radioisotopes or molecules labeled with radioisotopes. The radioactivity serves as a signal or tracking device in the former case or it can be used to kill diseased cells in the latter case of therapeutic applications. Radiopharmaceuticals can also be small inorganic or organic molecules or organometallic complexes that can contain a biologically active molecule or not. These biologically active molecules may be macromolecules, like monoclonal antibodies, antibody fragments, small peptides, inhibitors or substrates of enzymes among others.[4] Other radiopharmaceuticals may consist of a ligand and a metal nuclide. The radionuclides of interest for this particular study have focused on the organometallic complexes containing rhenium ($^{186/188}$Re) and technetium (^{99m}Tc).

1.3 Aim of the study

In this study, the main objective was to synthesize rhenium (I) tricarbonyl complexes and fully characterize it in order to fully understand the chemical complexity of the molecules. The results will be compared to previous studies where N,O and O,O' bidentate ligand systems were used to observe the change in coordination behaviour. The stepwise goals of this study are summarized below:

1. Syntheses of new rhenium (I) tricarbonyl complexes using a wide range of bidentate and tridentate ligand systems (N,O; S,O; S,S' and S,S',S''). The specific ligand systems which will be evaluated are listed below:
    - N,O bidentate ligands: 5-phenylazo-8-hydroxyquinoline (ANAOXH), 5-(m-tol)azo-8-hydroxyquinoline (m-TolANAOXH), 5-(2,3-dimephenyl)azo-8-hydroxyquinoline (2,3-diMeANAOXH), 5-(2,6-dimephenyl)azo-8-hydroxyquinoline (2,6-diMeANAOXH) and 5-(3,4-diMephenyl)azo-8-hydroxyquinoline (3,4-diMeANAOXH);

[4] Dilworth, J.R. Parrott, S.J. *Chem. Soc. Rev.* **27** (1998), 43-55.

- S,O bidentate ligands: methyl benzo[b]thiophene-2-carboxylate (BSOC), benzothiophene-2-methanol (BSOH), 2-mercaptophenol ($BSOPhH_2$) and 2-methoxythiophenol (BSOPhCH);
- S,S' bidentate ligands: 5-bromo-2,2`-bithiophene (BSBr), 2,2′-bithiophene-5-carboxylic acid (BSCH), benzene-1,2-dithiol ($BSPhH_2$) and toluene-3,4-dithiol (m-Tol$BSPhH_2$);
- S,S',S"-tridentate ligand: 2,2`-thiodiethanethiol (TSH_2).

2. Characterization of the complexes using various analytical techniques such as infrared spectroscopy, UV/Vis spectroscopy, nuclear magnetic resonance (i.e.^{1}H NMR and ^{13}C NMR), elemental analysis as well as single crystal X-ray diffraction.
3. The possible solid state and solution state differences of these complexes will be evaluated to further understand the formation of mononuclear vs. dinuclear complexes.
4. Some of the compounds and ligands will be tested for anti-mitochondrial (specifically anti-cancer) activity using the bio-assay coupled to Auger-architectonics.
5. Preliminary kinetic investigation of the rhenium (I) tricarbonyl complexes.

2 LITERATURE STUDY OF RHENIUM AS APPLIED IN NUCLEAR MEDICINE

2.1 Brief history of rhenium

Understanding the link between nuclear medicine and chemistry plays a fundamental role in the knowledge of rhenium, element number 75 especially for the development of new radiopharmaceuticals.

Rhenium (Re), that was named after the Rhine river (in *greek* “Rhenus”) was discovered by the German scientists Ida Tacke Noddack, Walter Noddack and Otto Berg in 1925.[1,2] Rhenium was the last natural occurring element discovered and as a mixture of two non-radioactive isotopes, ^{185}Re and ^{187}Re, with abundances of 37.4% and 62.6%, respectively. Rhenium was detected spectroscopically in Russian platinum ores and it is also found in trace amounts in minerals such as columbite, gadolinite and molybdenite.[3,4] In 1928, researchers managed to extract one gram of pure rhenium from 660 kilograms of molybdenite. Pure rhenium is platinum-like, hard and can only be shaped when heated. It melts at 3186 ˚C, has a boiling point ranging from 56300 to 59000 ˚C and has a density of 21.04 g/cm^3.[3,4]

[1] Megger, F.W. *J. Res. Natl. Bur. Stand*. **49** (1952) 87-216.
[2] Weeks, M.E. *J. Chem. Educ*. **10** (1933) 223-227.
[3] Dabek, J., Halas, S. *Geochronometria*. **27** (2007) 23-26.
[4] Dilworth, J.R., Parrott, S.J. *Chem. Soc. Rev*. **27** (1998) 43-55.

2.2 Rhenium metal in radiopharmaceuticals

The term 'radiopharmaceutical' refers to molecules containing a radioactive nuclide and a molecular entity which is used specifically for medical applications. The radionuclide is responsible for the radiation signal that is detectable outside the targeted organism and the molecular structure determines the course of the radiopharmaceutical within the organism.[5] Radiopharmaceuticals are used for two major purposes namely the diagnosis and/or therapeutic treatment of a human disease. Approximately 95 % of radiopharmaceuticals today are used for diagnostic purposes while the rest are used for therapy.[6,7]

Fundamental organometallic chemistry of technetium (diagnosis) and rhenium (therapy) are of considerable interest in radiopharmacy for nuclear medical purposes.[8,9] Novel complexes containing radioactive nuclides of rhenium are used for the therapeutic treatment of diseases due to its production method, properties and decay characteristics. Understanding the fundamental chemistry of rhenium will determine the success in designing future pharmaceuticals.

There are two radionuclides of rhenium which are important and have been studied for nuclear medicinal applications namely ^{186}Re and ^{188}Re.[10] Table 2.1 reports the characteristics of these two rhenium isotopes used in nuclear medicine.[11]

Table 2.1: Nuclear properties of Rhenium-186 and Rhenium-188. [12]

Radionuclide	^{186}Re	^{188}Re
Half-life ($t_{1/2}$)	90 hr	16.9 hr
Beta Particle, MeV (%)	1.069 (71%) 0.932 (21.54%) 0.581 (5.78%) 0.459(1.69%)	2.120 (71.1%) 1.965 (25.6%) 1.487 (1.65%)
Gamma Photon, KeV (%)	136 (9%)	155 (15%)
Tissue range (mm)	5	11
Direct Production Mode	^{185}Re(n,γ)^{186}Re	^{187}Re(n,γ)^{188}Re
Decay product	^{186}W (EC, 7,47%) ^{186}Os (β-, 92.43%)	^{186}Os (β-, 100%)

[5] Wadsak, W., Mitterhauser, M. *Eur. J. Radiol*. **73** (2010) 461-469.
[6] Malvi, R., Bajpai, R., Jain, S. *Int. J. Pharm. Biol. Sci. Arch*. **3** (2005) 487-492.
[7] Saha, G.B., *Fundamentals of Nuclear Pharmacy*, 5th Edition, Springer-Verlag, New York, 2003.
[8] Alberto, R., Schibli, R., Schubiger, P. A. *Polyhedron*. **15** (1996) 1079-1089.
[9] Braband, H., Abram, U. *J. Organomet. Chem*. **689** (2004) 2066-2072.
[10] Leddicotte, W. G. *The Radiochemistry of Rhenium*. National Research Council, Tennessee, 1961.
[11] Strominger, D., Hollander, J.M., Seaborg, G. T. *Rev. Mod. Phys*. **30** (1958) 585-904.
[12] Pillai, M.R.A., Dash, A., Knapp Jr, F.F. *Curr. Radiopharm*. **5** (2012) 228-243.

By looking at the radiation properties, both the rhenium isotopes can be used in therapy. From the tissue range it is clear that ^{186}Re is more suitable for small tumours and is attractive for clinical use whereas ^{188}Re is more suitable for large masses and is an excellent candidate for therapy.

2.2.1 Rhenium-186

Rhenium-186 (^{186}Re) was suggested for the treatment of osseous metastases from 1979 to 1986, when a therapeutically useful bone-seeking compound was generated. The original mixture reported by Mathieu[13] was purified by Deutsch and Maxon.[14] Rhenium-186-hydroxyethylidene diphosphonate (^{186}Re-HEDP) was first prepared at the University of Cincinnati.[13] HEDP was concentrated on the primary and metastatic bone lesions *in vivo*, however *in vitro* it is absorbed on hydroxyapatite.[14] The use of ^{186}Re-HEDP has been proved to be highly justified and efficient in bone pain palliation from multiple metastases. Advances in imaging enable us to measure the specific distribution of radioactivity in normal organs and tumours over time. In nuclear medicine, ^{186}Re-HEDP is used as a bone-seeking radiopharmaceutical in patients with bone metastases that originated from breast or prostate cancer with regard to pharmacokinetics, toxicity and bone marrow dosimetry. Therefore, bone-seeking radiopharmaceuticals are used to image tumours in bone depending on the energy of the radioactive label and carrier ligand.[15,16,17]

The most important advantage of using ^{186}Re is that it can be produced in many nuclear reactors around the world. It is produced by direct neutron activation of enriched ^{185}Re in low specific activity. A 90 hour half-life often permits distribution to sites distant from the production facility. ^{186}Re is also produced by proton bombardment of an enriched tungsten target, and a high specific activity is obtained for antibody and peptide radiolabeling. Preparation of phosphonates for bone pain palliation and use of intravascular radiotherapy for inhibition of coronary restenosis after angioplasty is possible with a lower specific activity. There are a large number of different opinions

[13] Mathieu, L., Chevalier, P., Galy, G., Berger, M. *Int. J. Appl. Radiat. Isot*. **30** (1979) 725-727.
[14] Deutsch, E., Libson, K., Vanderheyden, J.L., Ketring, A.R., Maxon, H.R. *Int. J. Rad. Appl. Instrum* B. **13** (1986) 465-477.
[15] De Klerk, J.M., Zonnenberg, B.A., Blijham G.H. *Anticancer Res.* **17** (1997) 1773-1777.
[16] Lyra, M., Limouris, G.S., Frantzis, A.P. *Eur J Nuc Med*. **26** (1999) 1191.
17 Lewington, V.J. *Eur. J. Nucl. Med*. **20** (1993) 66-74.

found in literature about the excitation function of the $^{186}W(p,n)/^{186}Re$ reaction.[18,19,20,21,22,23,24]

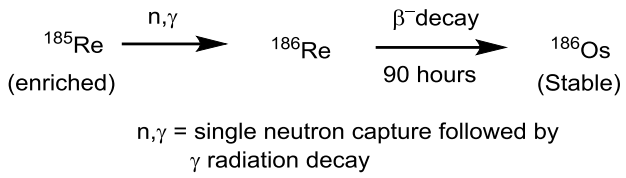

Scheme 2.1: Illustration of the reactor production of rhenium (^{186}Re).

In order to improve the quality of producing multi-mCi levels of ^{186}Re for therapeutic applications through the $^{186}W(p,n)/^{186}Re$ reaction, re-measurement of the excitation function were performed. The stacked foil techniques were used for the cross section of the production of ^{186}Re for proton energies up to 17.6MeV from natural tungsten.[25]

^{186}Re is the well-known beta-emitting radionuclide with a physical half-life of 89.3 hours (3.78 days) with maximum energies of $E_{max,1}$ = 1.069 MeV (71 %) and $E_{max,2}$ = 0.932 MeV (21.54 %) respectively. It has a gamma-emission with energy E_γ = 137 KeV (9 %) that enables molecular scintigraphic imaging during therapy and biodistribution assessment for patient-specific dosimetry calculations. According to research, ^{186}Re was found to be the best emerging candidate for radioimmunotherapy due to its ideal half-life of 3.72 days and decay properties. However, ^{186}Re is also a predicting candidate for tumour therapy from millimetre to centimetre range.[26,27,28]

2.2.2 Rhenium-188

According to the physical properties and production of Rhenium-188 (^{188}Re) *in situ* by an $^{188}W/^{188}Re$ generator, ^{188}Re is a most attractive radioisotope. ^{188}Re is the

[18] Zhang, X., Li, W., Fang, K. *Radiochim Acta* **86** (1999) 11-16.
[19] Shigeta, N., Matsuoka, H., Osa, A. *Radioanal Nucl Chem*. **205** (1996) 85-92.
[20] Kinuya, S., Yokoyama, K., Izumo, M. *Cancer Lett*. **219** (2005) 41-48.
[21] Kinuya, S., Yokoyama, K., Izumo M. *J Cancer Res Clin Oncol*. **129** (2003) 392-396.
[22] Van Gog, F.B., Visser, G. W. M., Klok, R. *J. Nucl. Med*. **37** (1996) 352-362.
[23] Marnix, G.E.H., Klerk, J.M.H., Rijk, P.P. *Eur J Nucl Med Mol Imaging*. **31** (2004) S162-S170.
[24] Quirijnen, J. M. S. P., Han, S. H., Zonnenberg, S. H. H. *J. Nucl. Med*. **37** (1996) 1511-1515.
[25] Moustapha, E.M., Ehrhardt, G.J., Smith, C.J., Szajek, L.P., Eckelman, W.C., Jurisson, S.S. *J Nucl Med Biol*. **33** (2006) 81-89.
[26] Eckerman, K.F., Bolch, W.E., Zankl, M., Petoussi-Henss, N. *Rad Prot Dos*.**127** (2007) 1-4.
[27] Jia, W., Ehrhardt, G.J. *Radiochim Acta.* **79** (1997) 131-136.
[28] Bolch, W.E., Shah, A.P., Watchman, C.J. *Rad Prot Dos.* **127** (2007) 169-173.

radionuclide of choice for therapy and there are several research groups[29,30,31,32,33] working on the development of therapeutic radiopharmaceuticals with ^{188}Re, eluted from an ^{188}W/^{188}Re generator. It is used in the treatment of liver tumours and non-Hodgkin`s lymphomas, experimentally for endovascular brachytherapy, breast tumours and treatment of ovarian cancer.[34]

^{188}Re is produced by two reactions in a nuclear reactor. The first reaction is: ^{187}Re→^{188}Re→^{188}Os (stable) where metallic rhenium is targeted. However, this reaction is not routinely used. ^{188}Re has an important advantage as it is produced by an ^{188}W/^{188}Re generator system. The double neutron capture form the parent radionuclide ^{188}W from ^{186}W and produces ^{188}Re *via* the decay of a beta-particle (2.120 MeV, 71.1 %) and a gamma-photon (155 KeV, 15 %).[35,36,37]

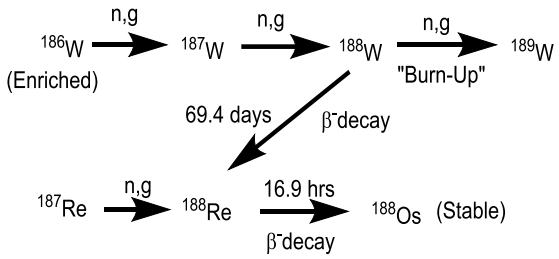

Scheme 2.2: Illustration of the reactor production of rhenium (^{188}Re).[34]

From Scheme 2.2 the production reaction is: ^{186}W → ^{187}W → ^{188}W (69.4 days, β$^-$-decay) → ^{188}Re (16.9 hours, β⁻decay) → ^{188}Os (stable). From an alumina generator containing ^{188}W as tungstic acid, ^{188}Re is eluted with saline. The ^{188}W/^{188}Re generator that has been studied extensively is similar in function to the ^{99}Mo/^{99m}Tc generator system. The production process of ^{188}W results in a carrier-added ^{188}W product unlike ^{99}Mo that is produced from the fission of ^{235}U. However, the adsorption column of the ^{99}Mo/^{99m}Tc generator is significantly smaller than that of the ^{188}W/^{188}Re generator at

[29] Pillai, M.R., Dash, A., Knapp., F. F. *Curr. Radiopharm*. **5** (2012) 228-243.
[30] Li, S., Liu, J., Zhang, H., Tian, M., Wang, J., Zheng, X. *Clin. Nucl. Med*. **26** (2001) 919-922.
[31] Knapp, F. F., Beets, A. L. Nuclear Medicine Group. Oak Ridge National Laboratory. Oak Ridge, Tennessee. United State of America.
[32] Pinkert, J., Krop,J. University Hospital Carl Gustav Carus. Technical University Dresden. Dresden. Germany.
[33] Konior, W., Iller, E. Mod. Chem. appl. **2** (2004) 1-2.
[34] Lyra, M. E., Andreou, M. Georgantzoglou, A., Kordolaimi, S., Lagopati, Ploussi, A., Salvara, A., Vamcaks, I.*Curr. Med. Imaging Rev*. **9** (2013) 51-75.
[35] Vučina, J., Lukić, D. *Phys, Chem. and Tech.* **2** (2002) 235-243.
[36] Hsieh, B., Lin, W., Luo, T., Chen, K. *J. Radianal. Nucl. Chem.* **274** (2007) 569-573.
[37] Jeong, J.M., Knapp, F. F. *Semin. Nucl. Med*. **38** (2008) S19-S29.

the same radioactivity. In order to elute ^{188}Re at a reasonable quantity, a large amount of elution is required. This problem is maintained by using concentration methods.[15,38]

2.3 Design of radiopharmaceuticals

2.3.1 General considerations

The radiopharmaceuticals are used on different nuclear medicine testing. The radiopharmaceuticals have specific requirements for intended tests.[39] Some agents satisfy the nuclear medicine community and no further investigation and development are necessary to replace them, like ^{99m}Tc-methylene diphosphonate (MDP) which is widely used for bone imaging. However, agents that supplies minimal diagnostic value during the testing process should be replaced. Researchers are investigating the improvement of these radiopharmaceuticals based on the following commonly used mechanisms of localization in a given organ.[39]

- Cell sequestration - sequestration of the heart-damaged ^{99m}Tc-labeled red blood cells by the spleen.
- Capillary blockage - ^{99m}Tc-macro-aggregated albumin (MAA) particles are trapped in the lung capillaries.
- Chemotaxis - ^{111}In-labeled leukocytes to localize infections.
- Passive diffusion - ^{111}In-DTPA in cisternography, ^{133}X and ^{99m}Tc-DTPA aerosol in the ventilation image and ^{99m}Tc-DTPA in brain imaging
- Receptor binding - ^{11}C-dopamine binding to the dopamine receptors in the brain.
- Active transport - ^{131}I uptake in the thyroid, ^{201}TI uptake in the myocardium.
- Compartmental localization - ^{99m}Tc-labeled red blood cells used in the gated blood pool study.
- Phagocytosis – removal of ^{99m}Tc-sulfur colloid particles by the reticuloendothelial cells in the liver, bone marrow and spleen.

[38] Knapp, F.F., Callahan, A.P., Beets, A.L. *Appl. Radiat. Isot*. **45 (**1994) 1123-1128.
[39] Saha, G.B. *Fundamentals of Nuclear Pharmacy*, 6th Edition, Springer-Verlag, New York, (2010).

- Antigen-antibody complex formation - ^{111}In-, ^{131}I- and ^{99m}Tc-labeled antibodies to localize tumors.
- Ion exchange - ^{99m}Tc-phosphonate complexes in bone.
- Metabolism - ^{18}F-FDG uptake in myocardial and brain tissues.

It is possible to design a radiopharmaceutical to assess the function and the structure of a specific organ from these mechanisms. It is crucial that the methods to develop radiopharmaceuticals are easy, simple and reproducible. However it should not alter the desired properties of the labelled compound.[39]

The pH, ionic strength, molar ratio and temperature should be maintained and established for maximum efficacy. After the radiopharmaceutical has been developed and successfully formulated, its clinical efficacy should be evaluated by testing it in animals and then subsequently in humans. In order to use the drug in humans a Notice of Claimed Investigational Exemption for a New Drug (IND) of the U.S should be available for the Food and Drug Administration (FDA) that regulate human trials of drugs. If the administration of a radiopharmaceutical cause any dangerous effect in humans, the radiopharmaceutical is discarded.[39]

2.3.2 Essential factors influencing the design of radiopharmaceuticals

There are certain factors or aspects that need to be kept in mind during the preparation of new radiopharmaceuticals. The following aspects are considered to be important in the design of radiopharmaceuticals.

- Compatibility - The chosen nuclide should have the ability to bind with the exploited ligand. This will only be successful if the chemical properties of both the nuclide and the ligand are known.[40,41,42]
- Stoichiometry - The nuclide quantity should be known in order to add the correct amount of reducing agent. It is also important that an adequate amount of chelating agent be added to get maximum labelling. Ideally, but not necessarily, these ratios should be 1:1.[39,40,41]

[40] Van Der Merwe, K. A. MSc dissertation. University of the Free State, Bloemfontein, South Africa, 2011.
[41] Engelbrecht, H. P. PhD thesis. University of the Free State. Bloemfontein, South Africa. 2001.
[42] Whitehead, T. D., Nemanich, S. T, Dence, C., Shongi, K. I. *J. Nucl. Med*. **54** (2013) 1812-1819.

- Charge of the molecule - This is crucial since it specifies the solubility of a chemical compound in various solvents as well as its site-specific biodistribution.[40,41]
- Size of the molecule - The absorption rate and excretion are influenced by the size of the molecule. Small molecules (M_r < 60 000) are filtered by the glomeruli of the kidneys and will therefore accumulate in the liver while too large molecules accumulate in the pulmonary tissue of the lungs.[40,41]
- Protein binding - The plasma proteins (albumin or globulin) bind to all drugs to some degree and this binding is regulated by pH, the coordination site available (i.e. O-, S-, N-donor atoms), charge of the molecule, nature of the protein and the anion concentration in the plasma. The abnormal tissue distribution or slow plasma clearance of the radiopharmaceutical cause the negative result in protein binding due to the poor uptake in the organs.[40,41]
- Solubility - Most neutral drugs are not soluble in saline and it needs to be protonated first. In order to introduce a radiopharmaceutical (drug) to a human body, the pH need to be similar to that of the blood, which is approximately 7.4.[39,40]
- Stability - The compound must be stable and should not change in structure whether it is *in vivo* or *in vitro* to avoid major problems.[39,40]
- Biodistribution - This is important when measuring the usefulness and efficiency of the radiopharmaceutical and involves tissue distribution, urinary/faecal excretion and plasma clearance.[40,41]

2.3.3 Choice of radionuclide for therapy

Successful radionuclide therapy rely on the collaboration among scientists that are specialized in different fields such as immunology, radiation physics (e.g. dosimetry), biochemistry, oncology, haematology, nuclear medicine, radiochemistry, pathology and biotechnology. The choice of radionuclide and labelling method are crucial like the choice of the targeting peptide or protein. Therefore the radiochemistry is very important, not only to choose the best method for stable attachment of a given nuclide to a given peptide or protein but also to consider the variety of biological and pharmacological factors. [39]

2.3.3.1 General considerations

The most important requirement for a therapeutic radiopharmaceutical is the delivery of a low radiation or no dose to the healthy tissue and a high local radiation dose to the tumour cells. The energy released during the decay of the nuclide should be deposited locally so that the whole body irradiation is low. The following are the general requirements of physical properties for a radionuclide to be used in therapy:[39]

1. Each radionuclide emits particular radiation i.e. (β) beta-, (α) alpha- particles and Auger or conversion electrons to maintain cytotoxic action.
2. A cost-effective way to develop the radionuclide.
3. According to *in vivo* pharmacokinetics of the targeting agent, the best physical half-life seems be 1 to 14 days.
4. High-energy gamma components is unsuitable at high abundance because it causes whole-body irradiation, therefore imaging such as dosimetry and therapy monitoring are in favour of low abundance photons (100 - 200 KeV).
5. Radiocatabolites must be removed from the body without too much accumulation in normal tissue or organs.
6. The radionuclide should be produced with a high amount of radioactivity and a desirable specific radioactivity.
7. High-yield labelling of proteins should be enabled by the chemical properties of the radionuclide.

2.3.3.2 Half-life of the radionuclide for therapy

The half-life is the rate of radioactive decay and it characterizes every radionuclide. It is unique for every radionuclide and is denoted by $t_{1/2}$. Half-life is defined as the time it takes for the radioactivity to decrease to one-half of its original value. For example, if there are 40 atoms of a radionuclide with a half-life of one minute, there will be one-half of that number, or 20 atoms, of the original radionuclide left after one minute. Two minutes later, there will be 10 atoms of the original radionuclide left.[43]

[43] Toutain, P.L., Bousoquet-Melou. A. *J. Vet. Parmacol. Therap*. **27** (2004) 427–439.

2.3.3.3 Biochemical properties

The biochemical properties of the radionuclide are important because of the redistribution of radioactivity after the metabolism of the carrier molecule. The residual molecules might have a different distribution pattern compared to the original agent and might lead to undesirable irradiation of non-target tissue.

2.3.3.4 Reliability

Radionuclides must be pure, of good quality and constricted within the range of reliability. Other trace amounts will result in wrong labelling. There are different sources of radiometals namely: cyclotrons, generators, accelerators and nuclear reactors. By considering the cost implication, generators are the economical choice in radiopharmaceuticals.[44] Solvent extraction or ion exchange chromatography is used to separate the long-lived parent isotopes and short-lived daughter radionuclides. Other sources of radiometals have the disadvantage of making one isotope at a time and are more expensive.

2.3.4 Method of radiolabelling

Radiolabelling is the chemical reaction whereby the desired molecule reacts with the radionuclide to give the radiotracer. The method of radiolabelling depends on the proposed studies.[45] Radiolabelling has grown substantially in different fields such as in biochemical, medical and other related fields. In the medical field, β- and γ - emitting radionuclides are used more often. β-emitting radionuclides curtailed to therapeutic treatment and *in vitro* experiments while γ- emitting radionuclides are restricted to *in vivo* imaging of various organs and has wide applications.[7] In the labelling process, there are two primary methods used for the preparation of receptor-specific targeting molecules namely the bifunctional approach and the intrinsic approach.

2.3.4.1 Bifunctional approach

The bifunctional approach agent (BFCA) is defined as a molecule containing a strong metal chelating unit and a reactive functional group. It consists of two parts, one part

[44] Velilkyan, I. *Molecules*. **20** (2015) 12913-12943.

[45] Vanessa, G. *PhD thesis*. Universitat Ramon Liull, Escola Tecnica Superior IQS, Barcelona. 2009.

is a ligand capable of coordinating to the chosen metal ion and the second part is a functional group that can react to and produce a stable covalent bond with the carrier.[46,47] The metal ion (the probe) is linked to the biomolecule (the carrier) *via* the BFCA. Several BFCAs has been reported in literature. Some of the BFCAs that have been reported are polyaminopolycarboxylic ligands that are the most efficient (Figure 2.1). The main advantage of these BFCAs are that they form highly stable complexes with different metal ions.[48] Selecting the right ligand is very important when designing the final conjugate. The BFCAs can also be divided into two parts. The first part is acyclic i.e. as those based on the EDTA (ethylenediaminetetraaceticacid) type ligands. These ligands do not need rough conditions but they are prone to release the metal ion *in vivo* due to the transmetallation by endogenous metal ion competition by the endogenous ligands.[49] The second part is macrocyclic i.e. those based on DOTA (1,4,7,10-tetraazacyclododecane-1,4,7,10-tetraacetic acid) type ligands. These ligands form very stable compounds that are thermodynamically stable, kinetically inert during the formation.

[46] De Leon-Rodriguez, L. M., Kovacs, Z. *Boiconjugate. Chem*. **19** (2008) 391-402.
[47] Fichna, J., Janecka, A. *Bioconjugate. Chem*. **14** (2003) 3-17.
[48] Anderegg, A., Amoud-Neu, F., Delgado, R., Felcman, J., Popov, K. *Pure Appl. Chem*. **77** (2005) 1445-1495.
[49] Morcos, S.K. *Eur. J. Radiol*. **66** (2008) 175-179.

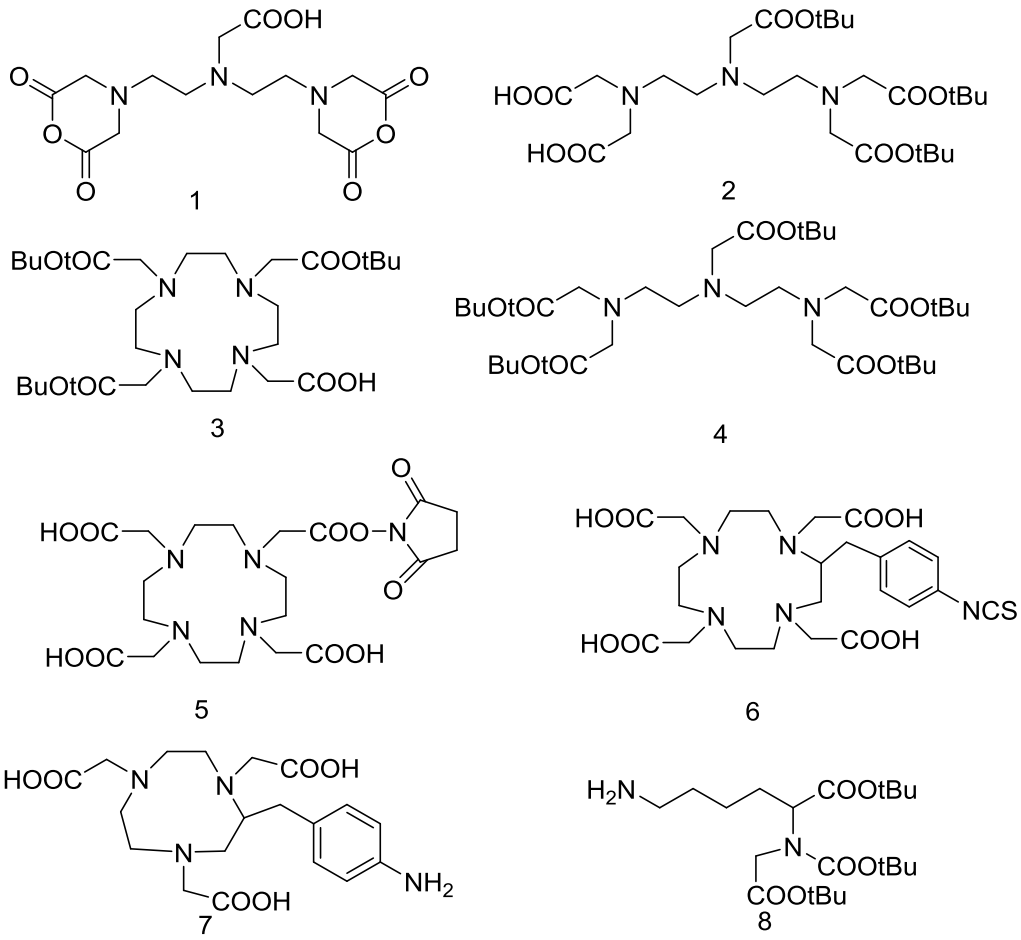

Figure 2.1: Examples of a few reported BFAC structures.[50]

2.3.4.2 Intrinsic approach

This approach helps to improve the stability of the radiopharmaceutical since the radionuclide-chelate replace the high affinity receptor ligand and is then integrated into the targeting moiety. This approach have a few disadvantages during the process, where there is a decrease in receptor binding and a more challenging target molecule needs to be synthesized. Synthesizing a metal compound that mimics a biomolecule binding site is a significant challenge in this intrinsic approach.[51] It should incorporate the dipole moments, topology and physio-chemical characteristics of the natural complex. A few complexes (Figure 2.2) have been prepared to mimic estradiol, progesterone and dihydrotestosterone.[52]

[50] Lattuada, L.,Barge, A., Cravotto, G., Giovenzana, G.B., Tei, L. *Chem. Soc. Rev*. **40** (2011) 3019-3049.
[51] Hom, R.K., Katzenellenbogen, J.A., *Nucl. Med. Biol*. **24** (1997) 485-498.
[52] Chi, D.Y., Oneil, J.P., Anderson, C.J., Welch, M.J., Katzenellenbogen, J.A., *J. Med. Chem*. **37** (1994) 928-937.

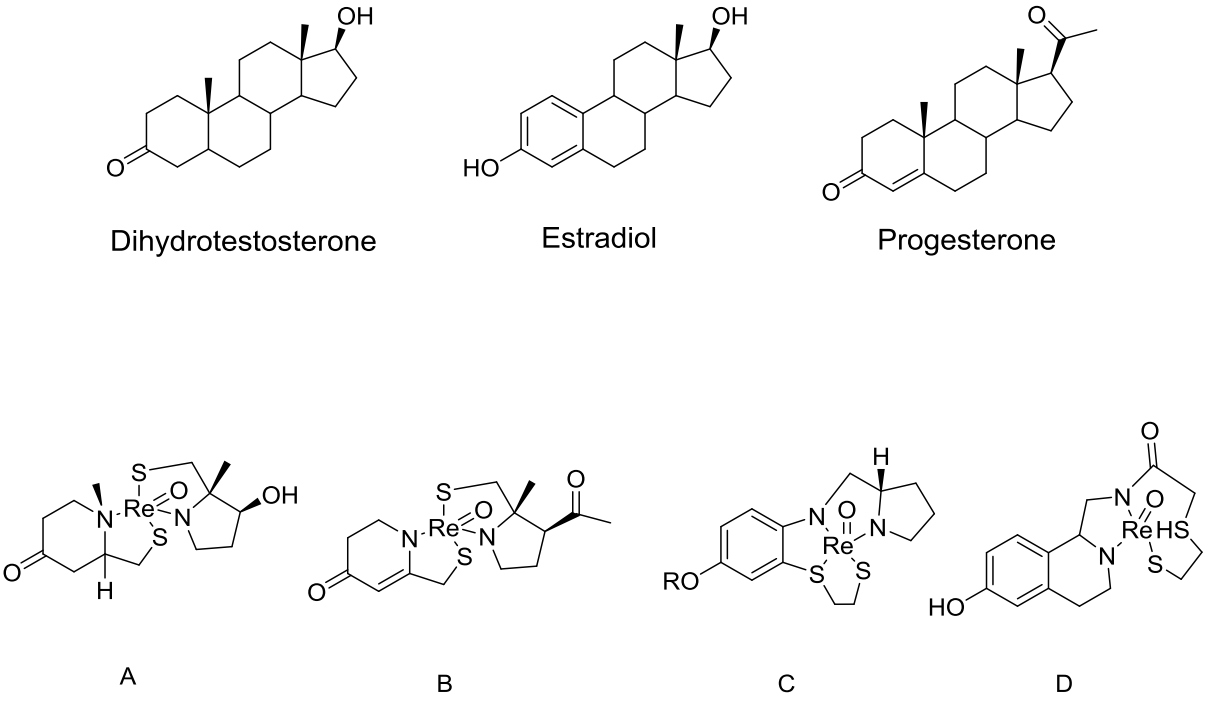

Figure 2.2: Some examples of the intrinsic approach.[50]

For the intrinsic approach, a molecule should have the following properties:

- ❖ High selectivity and specificity for the receptor
- ❖ A low molecular mass, less than 600
- ❖ A well-balanced lipophilicity

Complex A (Figure 2.2) passed all the preclinical tests and has the best receptor binding ability.[53]

2.4 The chemistry of the *fac*-$[Re(CO)_3]^+$ entity

Alberto and his co-workers has contributed substantially toward the coordination chemistry of the M(I) [M = Tc/Re] tricarbonyl complexes containing the *fac*-$[M(CO)_3]^+$

[53] Meegalla, S. K., Plossl, K., Kung, M. P., Stevenson, D. A., Mu, M., Kushner, S., Liable-Sands, L. M., Rheingold, A. L., King, H. H. *J. MEd. Chem*. **40** (1997) 9-17.

moiety.[54,55] This synthon is relevant for the development of new radiopharmaceuticals since it meets all the ideal requirements such as its chemical robust core, high stability and low-spin electron configuration.[56] The M(I) tricarbonyl precursors, *fac*-$[M(CO)_3(X)_3]^{2-}$ and *fac*-$[M(CO)_3(H_2O)_3]^+$ (where X = Br^- or Cl^-) can be easily prepared for the production of different complexes containing the *fac*-$[M(CO)_3]^+$ core. The halide and aqua ligands can be substituted by different functional groups such as amines, phosphines and thiols.[55,57,58]

Many researchers have shifted their focus to the M(I) (M = Tc/Re) complexes due to the great work provided by Alberto and his co-workers. Some of the favourable properties of this fragment include:[57,58]

- *fac*-$[M(CO)_3]^+$ is highly stable in water and air and has the potential of exchanging the labile solvent ligands with a variety of functional groups including thiols, imines, phosphines and thioethers.
- *fac*-$[M(CO)_3]^+$ exhibit an octahedral low spin d^6-configuration which is kinetically inert and has three *facial* carbonyl donor ligands that are fixed leaving the other three *facial* sites open for substitution.[59,60]
- *fac*-$[M(CO)_3]^+$ has a high affinity for a variety of donor atoms.
- *fac*-$[M(CO)_3]^+$ is flexible in the labelling of various biomolecules.
- *fac*-$[M(CO)_3]^+$ has unique photophysical properties allowing for its unequivocal detection in cells with its low luminescence.
- *fac*-$[M(CO)_3]^+$ is small and therefore allows for the labelling of low molecular weight biomolecules.[59,60]
- *fac*-$[M(CO)_3]^+$ complexes are resistant to oxidation.[61]

[54] Alberto, A.,Schibli, R., Waihel, R., Schubiger, P.A. *Coord. Chem. Rev*. **190-192** (1999) 190-192.
[55] Schutte, M., Kemp, G.,Visser, H.G., Roodt, A*. Inorg. Chem*. **50** (2011) 12486-12498.
[56] Alberto, R., Schibli, A., Egli, A., Schubiger, P.A., Abram, U., Kanden,. T.A. *J. Am. Chem. Soc*. **120** (1998) 7987-7988.
[57] Brink. A., Visser, H.G., Roodt, A. *Inorg. Chem.* **52** (2013) 8950-8961.
[58] Fuks, L., Gniazdowska, E., Kozminski, P. *Polyhedron*. **29** (2010) 634-638.
[59] Bertrand, H.C., Clede, S., Guillot, R., Lambert, F., Policar, C. *Inorg. Chem*. **53** (2014) 6204-6223.
[60] Wei, L., Babich, J.W., Oullette, W., Zubeita, J. *Inorg. Chem* **45** (2006) 3057-3066.
[61] Coogan, M.P., Doyle, R.P., Valliant, J.F., Babich, J.W., Zubeita, *J. Label Compd. Radiopharm*. **57** (2014) 255-261.

2.5 Coordination chemistry aspects of rhenium(I)

2.5.1 Introduction

Rhenium metal is a reliable choice for therapeutic purposes and its chemistry has been widely reported. The coordination chemistry of rhenium (I) tricarbonyl complexes provides potential application to the development of radiopharmaceuticals. Complexes with rhenium in oxidation state -1 to +7 exhibit considerable chemical diversity.[62] Rhenium chemistry has a wide range of applications that is reflected in the number of robust chemical cores.[63,64] A large amount of research has been done on the rhenium oxo core, $[Re^{v}O]^{3+}$.[65,66] The most recent organometallic approach in radiopharmacy has resulted in the development of the *fac*-$[M(CO)_3]^+$ (M = Tc/Re) core.[67]

The *fac*-$[M(CO)_3]^+$ core is an attractive low spin d^6 M(I) center and is available as the air-stable species *fac*-$[M(CO)_3(X)_3]^n$ (M =Tc/Re, X= Br/H_2O, n = -2/+1). A variety of functional groups such as amines, thiols, thioethers, phosphines and imines can react with this synthon to substitute the labile aqua or bromido ligands.

2.5.2 S,S'-bidentate ligands

Much research has been done on Re(I) tricarbonyl complexes with N,O and O,O' bidentate ligands, but only a few studies of thioester bidentate ligands (S,S' ligands) have been investigated using the Re(I) precursor prepared by Alberto.[68] Pietzsch[69] and co-workers reported the crystal structure of *fac*-$[Re(CO)_3BrL]$, where L = 4,7-dithia-1-octyne (Scheme 2.3). The organometallic precursor *fac*-$[NEt_4]_2[Re(CO)_3Br_3]$ was reacted with the bidentate dithioester to form the stable complex.

[62] Wei, L., John W Babich,J. W., Ouellette, W., zubieta, J. *Inorg. Chem*. **45** (2006) 3057-3066.
[63] Kohlickova, M., Jedinakova-Krizova, V., Melichar, F. *Chem. Listy*. **94** (2000) 151-158.
[64] Banerjee, S. R.; Francesconi, L.; Valliant, J. F.; Babich, J. W.; Zubieta, *J. Nucl. Med. Biol*. **32** (2005) 1-20.
[65] Latapie, L., Le Gal, J., Hamaoui, B., Jaud, Gressier, M., Benoist, E. doi:10.1016 /j.poly.2007.07.032
[66] Dizio, J. P., Andreson, C. J., Davison, A., Ehrhardt, G, J., Carlson, K. E., Welch, M. J., Katzenellenbogen, J. A. *J. Nucl. Med*. **33 (**1992) 558-569.
[67] Chen, W., Zhai, H., Huang, X., Wang, L. *Chemical Physics Letters*. **512** (2011) 49-53.
[68] Alberto, R., Egli, A., Abram, U., Hegestschweiler, K., Gramlich, V., Schubiger, P.A. *J. Chem. Soc. Dalton Trans*. **19** (1994) 2815-2820.
[69] Pietzsch, H.J., Gupta, A., Reisgys, M., Drews, A., Seifert, S., Syhre, S., Spies, H., Alberto, A. Abram, U., Schubiger, A., Johannsens, B. *Bioconjugate Chem*. **11** (2000) 414-424.

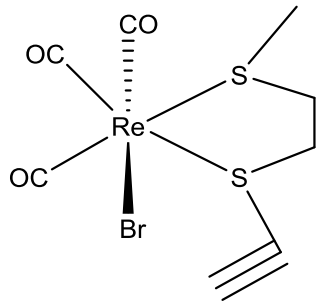

Scheme 2.3: Structure of bromidotricarbonyl(4,7-dithia-1-octyne)rhenium(I).

2.5.3 S,O-bidentate and S,S,O-tridentate ligands

Fuks and co-workers[70] reported a structure with a S,O-bidentate ligand (methyl thiosalicylate) and Pietzsch and co-workers[69] reported two structures with S,S,O-tridentate ligands (1-carboxylato-6-carboxy-2,5-dithiahexane and 1,8-dihydroxy-3,6-dithiaoctane). These structures are reported in Scheme 2.4 as A, B and C respectively. These complexes were also prepared from the precursor reported by Alberto.

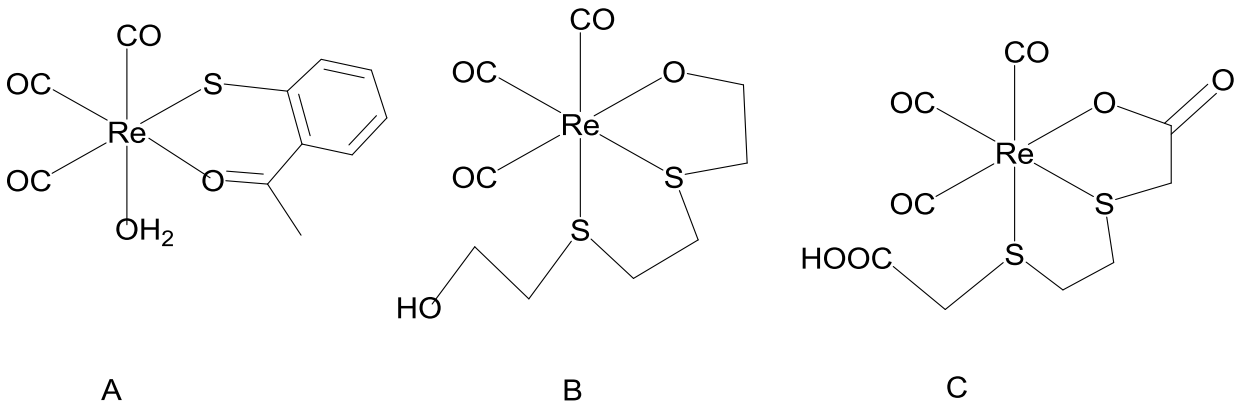

Scheme 2.4: Structure of tricarboblyrhenium(I) methylthiosalicylate complex (A), (1-carboxylato-6-carboxy-2,5-dithiahexane-O,S,S)tricarbonylrhenium(I) (B) and (1,8-Dihydroxy-3,6-dithiaoctane-O,S,S)tricarbonylrhenium(I) nitrate (C).

[70] Fuks, L., Gniazdowska, E., Kozminski. *Polyhedron*. **29** (2010) 634-638.

2.6 Kinetic study of aqua complexes

Elements in group 7 can form complexes of the type *fac*-$[M(CO)_3(H_2O)_3]^+$ with stable carbonyl groups and labile water molecules. The carbonyl groups and the labile water molecules are very attractive characteristics for applications in nuclear medicine. It was reported earlier that the $^{186/188}$Re compounds have the same labelling techniques as the ^{99m}Tc compounds.[71] It is crucial to know the mechanism and reactivity of the substitution of the labile water molecules when dealing with fast, simple or complicated synthesis of the potential radiopharmaceuticals.

2.6.1 Water exchange of *fac*-$[M(CO)_3(H_2O)_3]^+$

The water exchange rate decreases when moving down group 7 and 6 (Table 2.2). It also decreases from left to right with an increase in charge. Laurenczy and Rapaport reported the same tendency for the $[Ru(H_2O)_6)]^{2+}$ and $[Rh(H_2O)_6]^{3+}$ aqua ions.[72,73,74] The water exchange interchange dissociative, I_d, mechanism that was proposed for the Ru complex changed over to an interchange associative, I_a, mechanism for the corresponding reaction on the Rh complex due to the meta-water bond length.[75] Thus, the metal-water bond is influenced by the electrostatic interaction that is observed in the increase of activation enthalpies (Table 2.2).

Table 2.2: The selected kinetic data and mechanisms of water exchange for the aqua complexes of Cr(0), W(0), Mn(I), Tc(I), Re(I) and Ru(II) at 298 K.[73,76,77,78]

Group 6 metal complex	k_{ex}^{298} (S^{-1})	$\Delta H^{\ddagger}$ (KJ mol^{-1})	$\Delta S^{\ddagger}$ (JK^{-1} mol^{-1})	$\Delta V^{\ddagger}$ (cm^3 mol^{-1})	pKa
***fac*-$[Cr(CO)_3(H_2O)_3]$**	1.1×10^5	50	+20		<8
***fac*-$[W(CO)_3(H_2O)_3]$**	3.1×10^1	58	-22		<4.5
Group 7 metal complex					
***fac*-$[Mn(CO)_3(H_2O)_3]^+$**	23	72.5	+24.4	7.1	9-10
***fac*-$[Tc(CO)_3(H_2O)_3]^+$**	4.9×10^{-1}	78.3	+11.7	+3.8	
***fac*-$[Re(CO)_3(H_2O)_3]^+$**	5.4×10^{-3}	90.3	+14.5		7.5
***fac*-$[Re(CO)_3(H_2O)_2(HO)]^+$**	2.7×10^1				
***fac*-$[Ru(CO)_3(H_2O)_3]^{2+}$**	10^{-4}-10^{-3}				-0.14
***fac*-$[Ru(CO)_3(H_2O)_2(HO)]^+$**	5.3×10^{-2}				

[71] Kluba, C. A., Mindt, T. L. *Molecules.* **18** (2013) 3206-3226.
[72] Rapaport, I., Helm, L., Merbach, A.E., Bernhard, P., Ludi, A. *Inorg Chem*. **27** (1988) 873-879.
[73] Grundler, P.V., Helm, L., Alberto, R., Merbach, A.E. *Inorg. Chem*. **45** (2006) 10378-10390.
[74] Laurenczy, G., Rapaport, I., Zbinden, D., Merbach, A.E. *Magn. Reson. Chem*. **27** (1991) S45-S51.
[75] De Vito, D., Sidorenkova, E., Rotzinger, F.P., Weber, J., Merbach, A.E. *Inorg. Chem*. **39** (2000) 5547-5552.
[76] Prinz, U., Ph.D. Thesis, RWTH Aachen, Aachen, Germany, 2000.
[77] Meier, U.C., Scopelliti, R., Solari, E., Merbach, A.E. *Inorg. Chem*. **39** (2000) 3816-3822.
[78] Salignac, B., Grundler, P.V., Cayemittes, S., Frey, U., Scopelliti, R., Merbach, A. *Inorg. Chem*. **42** (2003) 3516-3522.

Salignac *et al*.[78] reported the first thermodynamic and kinetic data for water exchange on *fac*-$[Re(CO)_3(H_2O)_3]^+$ in 2003 where the water exchange rate constant (K_{ex}) for *fac*-$[Re(CO)_3(H_2O)_3]^+$ and the monohydroxo species *fac*-$[Re(CO)_3(H_2O)_2(OH)]$ were calculated as $6.3 \pm 0.1 \times 10^{-3}$ s^{-1} and 2.7 ± 1 s^{-1} respectively. However, at a pH higher than 2.5, the acidity dependence was noted accordingly and at lower pH the *fac*-$[Re(CO)_3(H_2O)_3]^+$ species was found to be in solution. The activation parameters' values that suggested a dissociative activation mode for the water exchange process were calculated as $\Delta H^{\ddagger} = 90 \pm 3$ kJ mol^{-1} and $\Delta S^{\ddagger} = +14 \pm 10$ JK^{-1} mol^{-1}. Helm[79] introduced Tc and Mn by NMR techniques to the work of Salignac, and it was found that the Mn complexes reacted the fastest and the Re complexes the slowest. Helm *et al.* investigated the pH dependency in these complexes. During the study, the water exchange was visible at a pH lower than 2.5, on *fac*-$[M(CO)_3(H_2O)_3]^+$ only, while at a pH higher than 4, *fac*-$[Re(CO)_3(H_2O)_2(OH)]$ is also involved in the water exchange reactions.

2.6.2 Water substitution reactions of *fac*-$[M(CO)_3(H_2O)_3]^+$

Paragraph 2.6.1 reports the importance of investigating the kinetic behaviour and mechanism of these *fac*-$[Re(CO)_3(H_2O)_3]^+$ complexes with different ligands. The half-life of the radionuclide has a great influence on the preparation time of the complex which must be a complete and fast reaction. The three labile water molecules can be replaced by monodentate ligands and can be fully characterized. The kinetic mechanism below shows the water molecules' substitution by a monodentate ligand, with equilibrium constants K_1, K_2 and K_3. (L = Ligand).

$$fac\text{-}[Re(CO)_3(H_2O)_3]^n + L \underset{k_{-1}}{\overset{k_1}{\rightleftharpoons}} fac\text{-}[Re(CO)_3(H_2O)_2(L)]^n + H_2O \quad \text{where} \quad K_1 = \frac{k_1}{k_{-1}} \qquad (1)$$

$$fac\text{-}[Re(CO)_3(H_2O)_2(L)]^n + L \underset{k_{-2}}{\overset{k_2}{\rightleftharpoons}} fac\text{-}[Re(CO)_3(H_2O)(L)_2]^n + H_2O \quad \text{where} \quad K_2 = \frac{k_2}{k_{-2}} \qquad (2)$$

$$fac\text{-}[Re(CO)_3(H_2O)(L_2)]^n + L \underset{k_{-3}}{\overset{k_3}{\rightleftharpoons}} fac\text{-}[Re(CO)_3(L)_3]^n + H_2O \quad \text{where} \quad K_3 = \frac{k_3}{k_{-3}} \qquad (3)$$

Scheme 2.5: The kinetic mechanism of the water molecules' substitution by mondentate ligands to form a positively charged (n) complex.

[79] Helm, L. *Coord. Chem. Rev*. **252** (2008) 2346-2361.

Helm *et al.* found that the rates of the above mentioned substitution reactions are in the same order of magnitude as the water exchange rates and therefore predicted a dissociative type mechanism in both cases. In Table 2.3, 2.4 and 2.5 the kinetic data for the water substitution reactions with the incoming ligands CH_3CN (acetonitrile), DMS (dimethyl sulfide), Py (pyridine) and H_2O (water) are reported.

Table 2.3: Kinetic parameters for the water substitution reaction of *fac*-$[Mn(CO)_3(H_2O)_3]^+$.[73]

	CH_3CN	DMS	H_2O
K_1^{298} (M^{-1})	4.5	2.52×10^1	-
$k_{f,1}^{298}$ ($M^{-1}s^{-1}$)	1.75	5.34	-
$k_i'^{298}$ (M^{-1})	2.9×10^1	8.9×10^1	2.3×10^1
$\Delta H_{f,1}^{\ddagger}$ (KJ mol^{-1})	83.9	71.2	72.5
$\Delta S_{f,1}^{\ddagger}$ (JK^{-1} mol^{-1})	+41.3	+8.1	24.4
$\Delta V_{f,1}^{\ddagger}$ (cm^3 mol^{-1})	+4.2	+11.3	+7.1

K_1 = equilibrium constant , $k_{f,1}$ = formation rate constant , k_i = equilibrium constant , $\Delta H_{f,1}^{\ddagger}$ = enthalpy of activation , $\Delta S_{f,1}^{\ddagger}$ = entropy of activation , $\Delta V_{f,1}^{\ddagger}$ = volume of activation.

Table 2.4: Kinetic parameters for the water substitution reaction of *fac*-$[^{99m}Tc(CO)_3(H_2O)_3]^+$.[73]

	CH_3CN	DMS	H_2O
K_1^{298} (M^{-1})	2.9	1.49 x 101	-
$k_{f,1}^{298}$ ($M^{-1}s^{-1}$)	3.99×10^{-2}	6.65×10^{-1}	-
$k_i'^{298}$ (M^{-1})	6.08×10^{-2}	1.01	4.90×10^{-1}
$\Delta H_{f,1}^{\ddagger}$ (KJ mol^{-1})	7.78	70.6	78.3
$\Delta S_{f,1}^{\ddagger}$ (JK^{-1} mol^{-1})	-10	-31.1	+11.7
$\Delta V_{f,1}^{\ddagger}$ (cm^3 mol^{-1})	-	-	+3.8

Table 2.5: Kinetic parameters for the water substitution reaction of *fac*-$[Re(CO)_3(H_2O)_3]^+$.[73]

	Py	CH_3CN	DMS	H_2O
K_1^{298} (M^{-1})	237	4.8	8.3	-
$k_{f,1}^{298}$ ($M^{-1}s^{-1}$)	1.06×10^{-3}	7.6×10^{-4}	1.18×10^{-3}	-
$k_i'^{298}$ (M^{-1})	1.77×10^{-2}	1.27×10^{-2}	2.0×10^{-2}	5.4×10^{-3}
$\Delta H_{f,1}^{\ddagger}$ (KJ mol^{-1})	-	98.6	-	90.3
$\Delta S_{f,1}^{\ddagger}$ (JK^{-1} mol^{-1})	-	+26.6	-	+14.5
$\Delta V_{f,1}^{\ddagger}$ (cm^3 mol^{-1})	+5.4	-	-12	-

The low chemical attraction of the metal for the N-binding CH_3CN compared to the S-binding DMS is seen in the fast water substitution rate of DMS compared to CH_3CN. Table 2.6 below reports the equilibrium and rate constants for the aqua substitution reaction with different ligands for *fac*-$[Re(CO)_3(H_2O)_3]^+$.[80]

[80] Grundler, P.V., Salignac, B., Cayemittes, S., Alberto, R., Merbach, A.E., *Inorg. Chem*. **43** (2004) 865-873.

Table 2.6: The equilibrium and rate constants of the water substitution reaction of *fac*-$[Re(CO)_3(H_2O)_3]^+$ (water exchange rate K_{ex} = 6.3 x 10^{-3} s^{-1}, Pyz = pyrazine, DMS = dimethylsulfide, THT = tetrahydrothiophene, TU = thiourea).[80]

	$10^3k_{f,1}$ ($M^{-1}s^{-1}$)	$10^5k_{f,1}$ (s^{-1})	$10^3k'_i$ (s^{-1})[II]	K_1 (M^{-1})
N-bonded				
CH_3CN	7.6 x 10^{-1}	1.6 x 10^1	1.27 x 10^1	4.8
Pyz	1.06	4.5 x 10^{-1}	1.77 x 10^1	2.37 x 10^2
S-bonded				
DMS	1.18	1.42 x 10^1	2.0 x 10^1	8.3
THT	1.28	3.05	2.1 x 10^1	4.1 x 10^1
TU	2.49	1.6	4.15 x 10^1	1.60 x 10^2
Anionic				
Br^-	1.6	2.30 x 10^2	5.8	7.0 x 10^{-1}
Cf_3COO^-	8.1 x 10^{-1}	9.9 x 10^1	2.9	8.2 x 10^{-1}

k_1 = forward rate constant, k_{-1} = reverse rate constant, $k_{i'}$ = interchange rate constant and K_1 = equilibrium rate constant.

Grundler[80] *et al*. showed interest in the formation of *fac*-$[Re(CO)_3(H_2O)_3]^+$ from the reverse reaction rate constants, k_{-1} and it was found that k_{-1} increases in 3 orders of magnitude from Pyz to Br^- (Table 2.6). The change in nucleofugal ability of each species and the basic character can explain this phenomenon. Pyz has a pk_a value of 0.6 that shows it is the slowest leaving group compared to Br^- which is the fastest leaving group with a pk_a value of -4.7. The stability constants K_1 (from $K_1 = k_1/k_{-1}$) differ for the different reactions.

Langford *et al*.[81] stated that when the product is almost similar to the nature of the leaving group in the transition state, a straight line is observed with a gradient of 1 from a graph of log k_1 *vs*. –log K_1. Grundler observed the same trend and an I_d type mechanism was proposed. Since the substitution rate constants are close to the water exchange rates (k_{ex}), this also confirms the statement above. The activation volumes of the different reactions were found to be negative for S-bonded ligands (DMS, $\Delta V^{\ddagger}$ = -12; THF, $\Delta V^{\ddagger}$ = -6.6 $cm^3\,mol^{-1}$) and positive for N-bonded ligands (Pyz, $\Delta V^{\ddagger}$ = +5.4 $cm^3\,mol^{-1}$).[73,80] These oppose the previous results by Helm, and a changeover mechanism from an I_d to a I_a is observed in the complex formation.

2.6.3 Substitution kinetics of *fac*-$[Re(CO)_3(L,L'\text{-Bid})X]$ type complexes

Schutte[82] studied complexes of the type *fac*-$[Re(CO)_3(L,L'\text{-Bid})(X)]^n$ (n = 0,+1, L,L'-Bid = various bidentate ligands, X = H_2O/CH_3OH). These complexes were investigated and the reactivity evaluated by substituting the sixth H_2O/CH_3OH ligand by different

[81] Langford, C.H., Gray, H.B. Ligand Substitution Processes. Benjamin, W. A Inc., New York. 1965
[82] Schutte, M., M.Sc. Dissertation, University of the Free State, Bloemfontein, South Africa, 2008

incoming monodentate ligands. Stable N,N'-, N,O- and O,O'-bidentate chelating ligands were used and a variety of monodentate entering ligands.

According to the results obtained the incoming ligand Br^- is approximately 5 to 7 times faster than the neutral ligands. When looking at the neutral ligands, k_1 (4-dimethylaminopyridine) is larger than the other rate constants. From these results and the pK_a value of DMAP (9.8), imidazole (6.99), pyridine (5.25) and pyrazole (2.49) one can expect an associative activated mechanism.[83] The negative values of $\Delta S^{\ddagger}$ obtained by Schutte lead to the conclusion of an I_a mechanism type even though one would expect an I_d mechanism for these octahedral complexes. It was stated that high pressure studies must be performed in future to unambiguously determine the mechanism of these reactions.

The results obtained indicated that the N,O bidentate ligands' rate constants, k_1, are smaller than that of the O,O' bidentate ligands and the first order rate constant decreased from Br^- > 4-dimethylaminopyridine > pyridine > pyrazole > imidazole. This was found to be consistent with the nucleophilicity of the different entering ligands and the negative values obtained for $\Delta S^{\ddagger}$ support these results.

Schutte-Smith[84] then continued and expanded the range of bidentate and monodentate ligands. The following bidentate ligands were used: 2,5-pyridinedicarboxylic acid (2,5-PicoH_2), isatin (Isa) and tropolone (Trop). The *fac*-[Re(Trop)$(CO)_3(OH_2)$] complex were found to be soluble in water and the aqua substitution were followed in water as solvent as well as methanol.[85,86] The rate constant for all the methanol substitution reactions are illustrated in Table 2.7.

[83] Perrin, D.D.(1965). Dissociation Constants of Organic Bases in Aqueous Solution. Butterworths. London. Supplement. 1972.
[84] Schutte, M., Ph.D. Dissertation, University of the Free State, Bloemfontein, South Africa, 2011.
[85] Schutte, M., Roodt, A., Visser, H. G. *Inorg. Chem*. **51** (2012) 1996-12006.
[86] Vd Westhuizen, H.J., Meijboom, R., Schutte, M., Roodt, A. *Inorg. Chem*. **49** (2010) 9599-9608.

Table 2.7: Summary of the rate constants of the methanol substitution reactions between three studied *fac*-Re(I) tricarbonyl complexes with different entering ligands at 25 °C. [84]

Ligands	Constant	[Re(2,5-PicoH)]	[Re(Trop)]	[Re(Isa)]
Br^-	$(10^3)k_1$ (M^{-1} s^{-1})	10.52 (9)	505 (4)	-
	$(10^3)k_{-1}$ (s^{-1})	0.910 (3)	477 (1)	-
	K_1 (M^{-1} s^{-1})	11.6 (1)	1.059 (9)	-
	$\Delta H^{\neq}_{(k1)}$ (kJ mol^{-1})	79.7 (5)	76.1 (6)	-
	$\Delta S^{\neq}_{(k1)}$ (Jk^{-1} mol^{-1})	5 (2)	5 (2)	-
I^-	$(10^3)k_1$ (M^{-1} s^{-1})	11.53 (9)	765 (2)	**-**
	$(10^3)k_{-1}$ (s^{-1})	0.437 (3)	674 (1)	**-**
	K_1 (M^{-1} s^{-1})	26.4 (3)	1.136 (3)	**-**
	$\Delta H^{\neq}_{(k1)}$ (kJ mol^{-1})	77(1)	75.3 (9)	**-**
	$\Delta S^{\neq}_{(k1)}$ (Jk^{-1} mol^{-1})	-22 (4)	6 (3)	**-**
Pyridine	$(10^3)k_1$ (M^{-1} s^{-1})	1.281 (7)	263.2 (1)	17.7 (2)
	$(10^3)k_{-1}$ (s^{-1})	0.032 (2)	0.07 (1)	2.44 (5)
	K_1 (M^{-1} s^{-1})	40 (3)	3760 (537)	7.3 (2)
	$\Delta H^{\neq}_{(k1)}$ (kJ mol^{-1})	82 (1)	64.7 (9)	79.0 (5)
	$\Delta S^{\neq}_{(k1)}$ (Jk^{-1} mol^{-1})	-25 (4)	-39 (3)	-13 (2)
Imidazole	$(10^3)k_1$ (M^{-1} s^{-1})	1.192 (2)	287 (3)	-
	$(10^3)k_{-1}$ (s^{-1})	0.0293 (6)	0.46 (9)	-
	K_1 (M^{-1} s^{-1})	40.7 (8)	624 (122)	-
	$\Delta H^{\neq}_{(k1)}$ (kJ mol^{-1})	84 (2)	61.8 (7)	-
	$\Delta S^{\neq}_{(k1)}$ (Jk^{-1} mol^{-1})	-19 (6)	-48 (2)	-
NCS^-	$(10^3)k_1$ (M^{-1} s^{-1})	2.104 (3)	268 (2)	18.7 (1)
	$(10^3)k_{-1}$ (s^{-1})	0.0921 (3)	4.4 (2)	0.48 (4)
	K_1 (M^{-1} s^{-1})	22.84 (8)	61 (3)	39 (3)
	$\Delta H^{\neq}_{(k1)}$ (kJ mol^{-1})	82.5 (5)	62 (2)	78.7 (7)
	$\Delta S^{\neq}_{(k1)}$ (Jk^{-1} mol^{-1})	-19 (2)	-48 (6)	-14 (2)
Thiourea	$(10^3)k_1$ (M^{-1} s^{-1})	19.19 (7)	556 (3)	36.5 (2)
	$(10^3)k_{-1}$ (s^{-1})	0.116 (2)	0.95 (10)	1.709 (6)
	K_1 (M^{-1} s^{-1})	165 (3)	585 (62)	21.4 (1)
	$\Delta H^{\neq}_{(k1)}$ (kJ mol^{-1})	70 (1)	58.0 (7)	78.9 (5)
	$\Delta S^{\neq}_{(k1)}$ (Jk^{-1} mol^{-1})	-44 (4)	-55 (2)	-8 (2)
1-Methyl-2-thiourea	$(10^3)k_1$ (M^{-1} s^{-1})	21.93 (7)	626 (2)	50.9 (1)
	$(10^3)k_{-1}$ (s^{-1})	0.056 (2)	1.84 (5)	2.190 (3)
	K_1 (M^{-1} s^{-1})	392 (14)	340 (9)	23.24 (6)
	$\Delta H^{\neq}_{(k1)}$ (kJ mol^{-1})	68 (1)	59.0 (4)	77.67 (7)
	$\Delta S^{\neq}_{(k1)}$ (Jk^{-1} mol^{-1})	-49 (4)	-51 (1)	-9 (2)

[Re(2,5-PicoH)]= [Re(2,5-PicoH)$(CO)_3$(MeOH)], [Re(Trop)] = [Re(TropBr$_3$)$(CO)_3$(MeOH)] and [Re(Isa)] = [Re(Isa)$(CO)_3$(MeOH)].

The following trends were observed from the studies by Schutte-Smith:[84,84] k_1 increases from the least electron donating to the most electron donating bidentate ligand complexes: Re(N,N'Bid) < Re(N,O-Bid) < Re(O,O'-Bid) and k_1 increases from pyridine to 1-methyl-2-thiourea as entering ligand and from pyridine to I^- as entering ligand: k_1 (N-donating) < k_1 (S-donating) and k_1 (N-donating) < k_1 (halides). The reactivity of the *fac*-$[Re(CO)_3(H_2O)_3]^+$ complex was tuned to up to 20 000 times more with these bidentate ligand systems. [87]

Brink[88, 89, 90] studied the axial methanol substitution reaction in neutral *fac*-[Re(N,O-Bid)$(CO)_3(HOCH_3)$] complexes. Five complexes were used in the kinetic reaction study

[87] Schutte, M., Kemp, G., Visser, H.G., Roodt, A. *Inorg. Chem*. **50** (2011) 12486-12498.

[88] Brink. Ph.D. Thesis, University of the Free State, South Africa, 2011.
[89] Brink, A., Visser, H. G., Roodt, A. *Inorg. Chem*. **52** (2013) 8950-8961.
[90] Brink, A., Visser, H. G., Roodt, A. *Inorg. Chem*. **53** (2014) 12480-12488.

with different monodentate entering ligands - 3-chloropyridine (3-ClPy), pyridine (Py), 4-picoline (4-Pic) and 4-dimethylaminopyridine (DMAP).

Table 2.8: The kinetic data for the reaction of *fac*-[Re(Sal-mTol)(CO)$_3$(HOCH$_3$)] with different entering ligands at 25 ºC.

Ligands	3-ClPy	Pyridine	4-Picoline	DMAP
k_1 (M^{-1} s^{-1})	2.33 (1)	1.29 (2)	1.27 (5)	-
k_{-1} (M^{-1} s^{-1})	0.026 (3)	0.019 (5)	0.05 (2)	-
k_1 (M-1 s^{-1})	91 (11)	67 (18)	25 (10)	-
k_3 (s^{-1})	9 (2)	5.5 (9)	3.9 (3)	1.15 (2)
K_2 (M^{-1})	0.30 (8)	0.27 (5)	0.44 (4)	1.88 (7)
K_4 (M^{-1})	9 (2)	5.5 (9)	3.9 (3)	1.15 (2)
K_4/k_5	0.13 (4)	0.15 (3)	0.093 (9)	0.0215 (8)
pKa	2.81	5.23	5.99	9.8

Sal-mTol = 2-(m-tolyliminomethyl)phenolato.

When considering the *p*K$_a$ values, the kinetic reaction rate of *fac*-[Re(Sal-mTol)(CO)$_3$(HOCH$_3$)] with the different monodentate entering ligands decrease as the *p*K$_a$ value increase: DMAP > 4-Pic >Py > 3-ClPy. The observed results are contrary to what was expected for an associative (A) or interchange associative (I$_a$) mechanism. The positive value of activation entropy $\Delta S^{\ddagger}$ propose a dissociative or I$_d$ type mechanism. The rate constant, k$_1$, of *fac*-[Re(Sal-mTol)(CO)$_3$(HOCH$_3$)] with pyridine (1.29 (2)) were found to be faster than the values that was obtained by Schutte[86] and Kemp[91] for the analogous N,O- bidentate ligands as shown in Table 2.9.

Table 2.9: Comparison of the k_1 rate constant values for various bidentate complexes with pyridine.

N,O- bidentate complexes	10^{-3} k_1 ($M^{-1}s^{-1}$)
***fac*-[Re(Pico)(CO)$_3$(MeOH)]**[a]	1.6 (1)
***fac*-[Re(Quin)(CO)3(MeOH)]**[a]	3.9 (1)
***fac*-[Re(2,4-PicoH)(CO)$_3$(MeOH)]**[b]	1.641 (8)
***fac*-[Re(2,4-Quin)(CO)$_3$(MeOH)]**[b]	3.31 (2)
***fac*-[Re(Sal-mTol)(CO)$_3$(MeOH)]**[c]	1.29 (2)
***fac*-[Re(Sal-pTol)(CO)$_3$(MeOH)]**[c]	1.393 (3)
***fac*-[Re(Sal-Ph)(CO)$_3$(MeOH)]**[c]	1.26 (2)
***fac*-[Re(Sal-CylHexl)(CO)$_3$(MeOH]**[c]	2.03 (6)
***fac*-[Re(Sal-3MeBu)(CO)3(MeOH)]**[c]	1.79 (2)

[a] Schutte *et al*[84], [b] Schutte *et al*[84], [c]Brink *et al*[88].

According to the previous studies, there is still much that need to be explored and learned regarding the mechanism of substitution reactions of *fac*-[M(CO)$_3$(OH$_2$)(L,L'-bid)] and *fac*-[M(CO)$_3$(MeOH)(L,L'-bid)] type complexes. This study intend to investigate the potential reactivity of these type of complexes with S,O and S,S' bidentate ligands.

[91] Kemp. Ph.D. Thesis, University of Johannesburg, Johannesburg, South Africa, 2006.

2.7 Dithiolate complexes of Re(I) and Mn(I)

A few years ago, the chemistry of transition-metal complexes with sulfur-rich thiolate ligands has been a fascinating focus area due to their interesting catalytic properties and crystal structures. Liaw and co-workers synthesized an air-stable neutral dinuclear Mn(I)-bismercaptophenyl disulphide complex (Scheme 2.6).[92] The compound was synthesized by treating the anionic pentacoordinated complex with HBF_4 in THF solvent at room temperature, under a nitrogen atmosphere. The dinuclear structure was assumed to form via the protonation of the thiolate ligand, the elimination of two hydrogen atoms (H_2) and the formation of a S-S bond as demonstrated in Scheme 2.6. However, the reverse of this reaction results in an anionic pentacoordinate structure when *fac*-[$(Mn(CO)_3)_2(\mu\text{-}SC_6H_4\text{-}o\text{-}S\text{-}S\text{-}C_6H_4\text{-}o\text{-}\mu\text{-}S\text{-})$] is treated with [PPN][$BH_4$] in THF solvent at room temperature. The anionic pentacoordinate complex and the neutral dinuclear Mn(I)-bismercaptophenyl disulphide complex are considered chemically interconvertible.

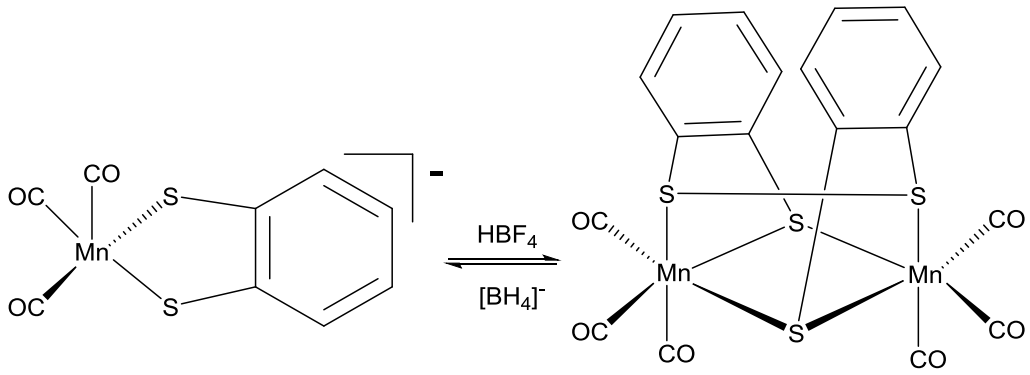

Scheme 2.6: Illustration of the synthetic procedure of the formation of *fac*-[$(Mn(CO)_3)_2(\mu\text{-}SC_6H_4\text{-}o\text{-}S\text{-}S\text{-}C_6H_4\text{-}o\text{-}\mu\text{-}S\text{-})$] by Liaw *et al.*

Begum *et al.* expanded this work by synthesizing the *fac*-[$Re_2(CO)_6(\mu\text{-}\eta^4\text{-}m\text{-}TolBSPh\text{-}S\text{-}S\text{-}m\text{-}TolBSPh)$] complex (Scheme 2.7).[93] This complex was synthesized by the reaction of $Re_2(CO)_{10}$ with 3,4-toluenedithiol that resulted in the formation of the dirhenium complex *fac*-[$Re_2(CO)_6(\mu\text{-}\eta^4\text{-}SC_6H_3(CH_3)S\text{-}SC_6H_3(CH_3)S)$] with the formation of the S-S bond as previously obtained by Liaw *et al*.

[92] Liaw, W.-F., Hsieh, C.-K., Lin, G.-Y., Lee, G.-H. *Inorg. Chem*. **40** (2001) 3468-3475.

[93] Begum, N., Hyder, M.I., Kabir, S.E., Hossain, G.M.G., Nordlander, E., Rokhsana, D., Rosenberg, E. *Inorg. Chem.* **44** (2005) 9887-9894.

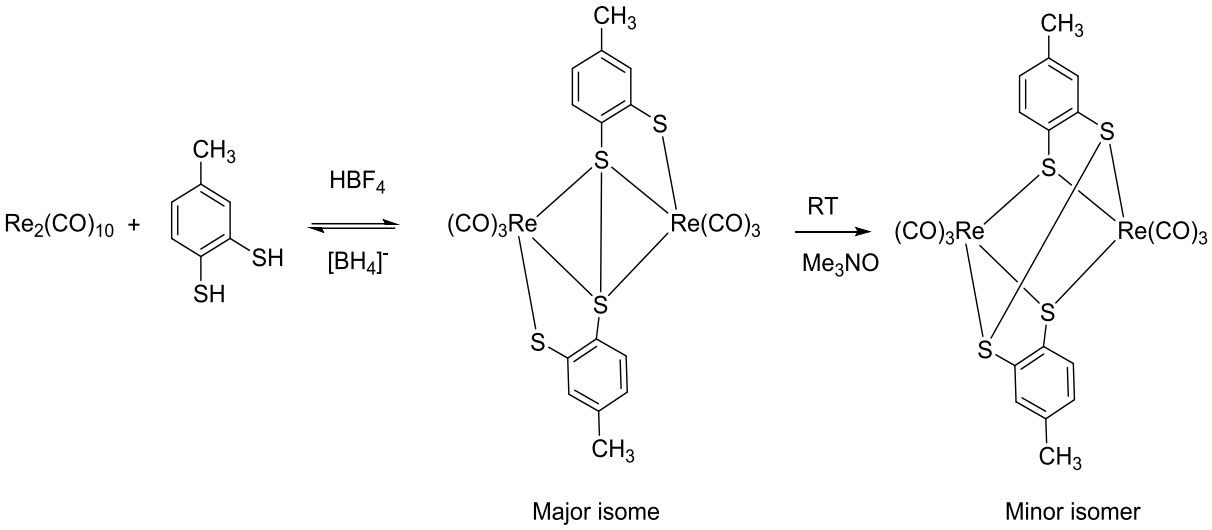

Scheme 2.7 Illustration of the synthetic procedure of the formation of of *fac*-[$Re_2(CO)_6$(μ-η^4-$SC_6H_3(CH_3)S$-$SC_6H_3(CH_3)S$)] by Begum *et al*.

However, the NMR spectrum of *fac*-[$Re_2(CO)_6$(μ-η^4-$SC_6H_3(CH_3)S$-$SC_6H_3(CH_3)S$)] contains two isomers in solution in a 3:1 ratio. The major isomer spectrum shows the following peaks in ^{1}H NMR: two doublets at δ 7.98 and 7.23 (d, *J* = 7.9 Hz) and a singlet at δ 7.50. The minor isomer shows the following peaks in ^{1}H NMR: two doublets at δ 7.54 and 7.18 (d, *J* = 7.9 Hz) and a singlet at δ 7.94. The methyl peak for the major and minor isomers appear as two singlets at δ 1.50 and 1.24 respectively. The only difference in the isomers is the formation of the disulphide bond. In the major isomer the S-S bond formed between the sulphur atoms para to the methyl group while in the minor isomer the S-S bond formed between the sulphur atoms meta to the methyl group. It was expected that a third isomer can be formed with the disulphide bond between the sulphur atoms of one meta and one para to the two methyl groups. This isomer was reported to form in concentrations too low to be detected by NMR. The interpretation of the results obtained by Begum *et al.* was that the isomers are in equilibrium and is presented by the 1:3 ratio. The inductive effect of the methyl group causes the slight preference for the para-para linkage in the crystal structure.

It is clear from the preceding paragraphs that there is a lack in knowledge of the coordination of S,O; S,S' and S,S',S'' type ligands to the rhenium (I) tricarbonyl core (mononuclear as well as dinuclear compounds), the mechanistic characteristics of

these complexes as well as its reactivity, solubility and biological activity. This illustrates the importance of the data presented in this study.

3 THEORETICAL ASPECTS OF INSTRUMENTAL TECHNIQUES AND METHODS

3.1 Introduction

The rhenium (I) tricarbonyl complexes synthesized in this study was characterized by different methods namely Nuclear Magnetic Resonance spectroscopy (NMR), Infrared spectroscopy (IR), Ultraviolet-Visible spectroscopy (UV/VIS) and some complexes by single crystal X-ray diffraction, ICP-MS, LECO. The theory on chemical kinetics is briefly discussed even though no chemical reactions were performed on these complexes at this stage. These different characterization methods and the theory behind them are discussed in this chapter.

3.2 Nuclear Magnetic Resonance Spectroscopy

NMR is a commonly used technique that is specifically used to determine the detailed molecular structure of a compound, compared to other analytical techniques like mass spectrometry and Infrared spectroscopy.[1] This technique is similar to Magnetic Resonance Imaging (MRI) that is used in the field of medical radiology to characterize soft tissue in the human body. NMR uses the nuclei of atoms that have magnetic properties and then applies it to yield chemical information. One can imagine protons, electrons and neutrons spinning on their axes. Isotopes with even numbered protons and/or neutrons such as ^{12}C, ^{16}O and ^{32}S have a total spin of zero. Therefore nuclei of isotopes like ^{1}H, ^{15}N, ^{15}F, ^{31}P and ^{13}C have an overall non-zero spin. In order to

[1] Jacobsen, N.E. *NMR Spectroscopy Explained*, Wiley and Sons, New Jersey. 2007.

determine the spin quantum number (*I*) of a nucleus, the following rules must be considered:

- The nucleus has no spin if the number of protons and neutrons are both even.
- The nucleus has a half-integer spin i.e. 1/2, 3/2, 5/2 etc. if the number of protons plus the number of neutrons give an odd number.
- The nucleus has an integer spin i.e. 1, 2, 3 etc. if the number of protons and the number of neutrons are both odd.

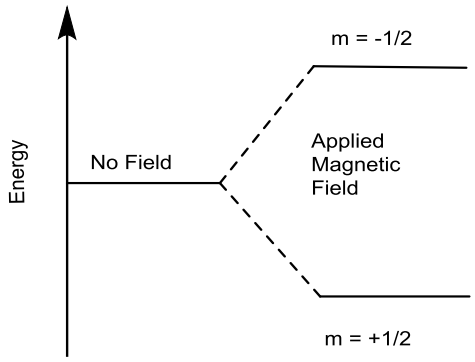

Figure 3.1: The energy levels of a nucleus with spin quantum number 1/2.

The nuclear magnetic moment of a nucleus can align with an external magnetic field (strength B_o) in (2*I* + 1) possible orientations. A nucleus with spin *I* = 1/2 will have two possible orientations i.e. +1/2 which is parallel to the applied magnetic field (lower energy) and is given the notation α whereas the spin of -1/2 is aligned in the opposite direction to the applied magnetic field (higher energy) and is denoted β. The applied magnetic field will split the energy levels (Figure 3.1) but if no external magnetic field is applied the orientations will have equal energies. It is not possible for the rotational axis of the spinning nucleus to be orientated exactly parallel (or anti-parallel) to the direction of the applied field but it processes at an angle with and angular velocity given by Equation 3.1.

$$\boldsymbol{\omega_o = \gamma B_o} \qquad \textbf{3.1}$$

ω_o is the Larmor frequency and the constant γ denotes the magnetogyric ratio. The magnetogyric ratio includes the magnetic moment (μ) and the spin quantum number (*I*) for a nucleus as shown in Equation 3.2.

$$\boldsymbol{\gamma = 2\pi\mu/hI} \qquad \textbf{3.2}$$

All nuclei have a γ value that is characteristic to that nucleus and is a constant of proportionality between the nuclear angular momentum and magnetic moment. An electric field with a frequency of ω_o is generated when the nucleus is spinning. If the sample is then irradiated with radio waves, the proton can absorb that energy and get excited to the higher energy state. The energy that is absorbed is called resonance due to the frequency of the applied radiation and resonate (Figure 3.2).

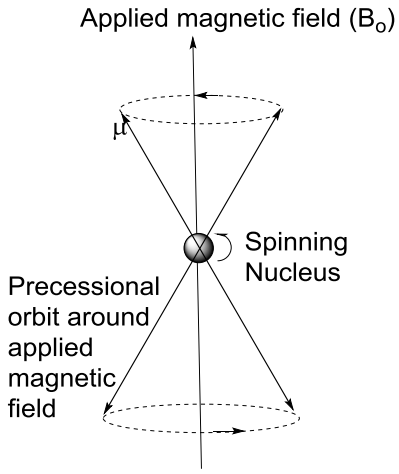

Figure 3.2: The axis of rotation processing around the magnetic field.

The orientations of a nucleus against an external magnetic moment are of unequal energy. The spin states parallel to the external field have lower energies than in the absence of an external field and the spin states opposing the external field are higher in energy than in the absence of an external field (Figure 3.3). When different energies exist, transition between the different spin states can be observed. A nucleus with a low energy state can be 'excited' to the higher energy state by irradiation of the correct energy. This absorption of energy is the foundation of NMR. Other techniques i.e. UV/Vis and IR spectroscopy also depend on the absorption of energy during a transition but the nature and the energy of these transitions vary significantly. The energy difference between spin states is denoted by ΔE and is influenced by the strength of the magnetic field and the nuclear magnetic moment. The energy difference

(ΔE) is characterized by the frequency of the radiation necessary to allow the excitation from the low to the high energy state ($\Delta E = h\nu$).[2]

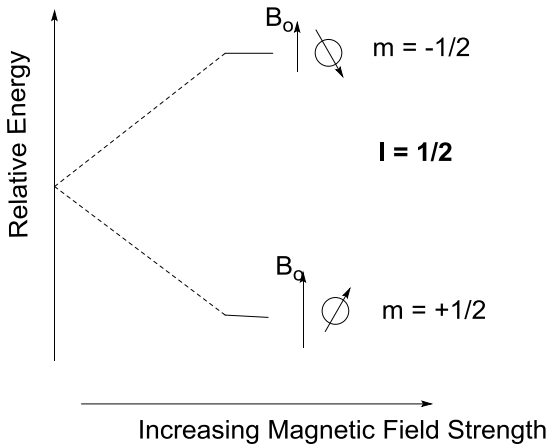

Figure 3.3: The energy levels for a nucleus with spin quantum number 1/2.

The surrounding electrons that are part of sigma bonds shield the protons of the nucleus and therefor lower the effective magnetic field and the resonance frequency is then lower than expected. The difference in resonance frequency results in different signals which are called nuclear shielding or chemical shifts. There are many factors that may influence the nuclear shielding of protons such as hydrogen bonding, geometry, stereochemistry and polar functional groups.

3.3 Infrared Spectroscopy

Infrared spectroscopy (IR) is an important analytical technique. One of the advantages is that any sample in any state can be studied or examined.[3] Species such as powders, fibres, solutions, films, liquids, surfaces and gases can be examined by different sampling techniques. The IR technique is based on the vibrations of atoms of a molecule. In order to obtain an infrared spectrum, the infrared radiation is allowed to pass through a sample and the fraction of the incident radiation absorbed at a certain energy value is determined. The frequency of a vibration of a part of a molecule

[2] Pavia, D.L., Lampman, G.M., Kriz, G.S., Vyvyan, J.R. *Introduction to Spectroscopy*, 4th Edition. Brooks/Cole Cengage Learning. United States of America. 2009.
[3] Stuart, B. *Infrared Spectroscopy: Fundamentals and Applications*. Wiley and Sons. 2004.

corresponds to an energy value in an absorption spectrum. Electromagnetic radiation is synchronized oscillating magnetic and electric fields, perpendicular to each other and perpendicular to the direction of energy and the wave propagation. However, the radiation can also be seen as a stream of particles whereby the energy (E) can be determined as shown in Equation 3.3, where h is Planck's constant with a value of 6.626 x 10^{-34} J.s.

$$\boldsymbol{E = hv} \qquad \textbf{3.3}$$

The infrared spectrum measured by the percentage transmittance or absorbance placed on the y-axis and wavelength (nm) or wavenumber (cm^{-1}) placed on the x-axis. Most of compounds has a characteristic absorption fingerprint in the infrared region. Simple demonstration of an idealized band is shown below (Figure 3.4).

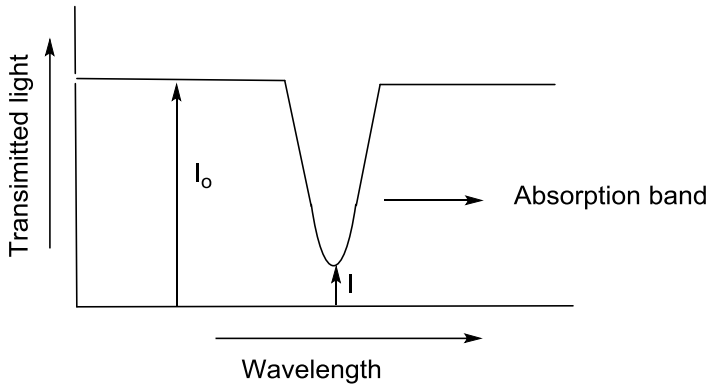

Figure 3.4: A simple illustration of an idealized infrared spectrum band.

The general presentation of IR absorption is in the form of a spectrum with wavelength as the x-axis and transmitted light as the y-axis (Figure 3.4). Absorption is the logarithm to the base ten of the reciprocal of the transmittance (*T*) and the transmittance (*T*) is the ratio of radiant power transmitted by the sample (*I*) to the radiant power incident on the sample (I_o) (Equation 3.4).[4]

$$\boldsymbol{A = \log\frac{1}{T} = \log(\frac{I_o}{I})} \qquad \textbf{3.4}$$

Infrared light forms part of the electromagnetic spectrum and are found between the microwave and visible regions. The electromagnetic spectrum covers a wide range of wavelengths and are divided into a near infrared (12 500 - 4000 cm^{-1}), mid infrared

[4] Sherman Hsu, C. P. *Infrared Spectroscopy: Handbook of Instrumental Techniques for Analytical Chemistry*. Prentice Hall. 2000.

(4 500 – 400 cm^{-1}) and far infrared (400 - 12.5 cm^{-1}) region. The main region IR is based on is the mid infrared region since it is based on the vibrations of the atoms of the molecules. The parameters that are crucial in this technique are the wavelength (λ), wave number ($\bar{\upsilon}$, number of waves per unit length) and frequency (v). The relationship of these parameters is given in Equation 3.5.

$$\bar{\upsilon} = \frac{v}{(\frac{c}{n})} = \frac{1}{\lambda} \qquad \textbf{3.5}$$

The radiation frequency and the molecular dipole moment (μ) are important characteristics in IR. The resonance condition is involved in the interaction of radiation with molecules where the specific oscillating radiation frequency relates with the natural frequency of a certain normal mode of vibration. The energy is transferred from the IR photon to the molecule due to the change in the dipole moment of the molecule caused by the molecular vibration.[5]

An infrared spectrum depends on the frequencies of chemical bond's rotation and/or vibration. If the IR radiation is of the same frequency as one of the vibrational modes of the molecule, the bond will absorb energy and move to a higher vibrational energy state. The energy difference of these two vibrational modes is equal to the energy associated with the wavelength of the radiation that was absorbed. Four bending vibrations exist: rocking, twisting, wagging and scissoring, while stretching vibrations can be classified as symmetrical or asymmetrical. Stretching vibrations have higher frequencies and require higher energies than bending vibrations; and the bonds of heavier atoms vibrate at a lower energy than the bonds of lighter atoms.[6]

3.4 Ultraviolet-visible Spectroscopy (UV/Vis)

Ultraviolet-Visible spectroscopy is an important analytical technique that is used to analyse or identify compounds in the ultraviolet (UV) (190 - 380 nm) and visible (Vis) (380 – 750 nm) region of the electromagnetic spectrum. It can determine the content

[5] Sathyanarayana, D.N. *Vibrational Spectroscopy: Theory and Applications*. New Age International. New Delhi. 2004.
[6] Field, L. D., Sternhell, S., Kalman, J. R. *Organic Structures from Spectra*, 4th Ed, Wiley and Sons, New York, 2007.

of a substance and can identify certain functional groups.[7] When IR and UV/Vis are compared, the most significant difference is that in UV/Vis electronic transitions are responsible for the signals while in IR spectroscopy the vibrational motions are responsible for the observations. One can determine the maximum absorbance of a compound at a specific wavelength. The absorbance of a compound contains significant information and can be defined by Beer`s Law in Equation 3.6,

$$\boldsymbol{A = \varepsilon l C} \qquad \textbf{3.6}$$

where absorbance is denoted by *A* the molar extinction coefficient by ε, the path length by *l* and the concentration by C. The energy of the compound can be calculated by using Equation 3.7 (where E = energy, λ = wavelength, h = Planck`s constant and c = speed of light).

$$\boldsymbol{E = \frac{hc}{\lambda}} \qquad \textbf{3.7}$$

Ultraviolet and visible radiation causes electronic transition when it interacts with atoms. The following transitions are possible:

- π → π*
- n → n*
- σ → σ*
- n → σ*

UV/Vis spectroscopy is based on electrons absorbing energy. When electrons absorb UV or visible light, the electrons get excited from the ground state (highest occupied molecular orbital - HOMO) to the excited state (lowest unoccupied molecular orbital-LUMO). The strength of the bond between the valence electrons and the atom determine the wavelength where the molecules absorb energy. The electrons in double and triple bonds are not strongly bound and are easily excited, therefor useful absorption peaks are obtained.

[7] Rouessac, F., Rouessac, A. *Chemical Analysis: Modern Instrumentation Methods and Techniques*. 2nd Ed. Wiley and Sons. New York, 2007.

3.5 Some theoretical considerations of X-ray Crystallography

3.5.1 History

In 1669 the first experiment was performed to investigate crystal symmetry and up until 1912 the nature of X-rays was unknown.[8] The fact that crystals could diffract X-rays by X-ray diffraction, confirmed that X-rays were a form of electromagnetic radiation.[9] In 1922 the doubt about the nature of X-rays was resolved when the photon model was confirmed.[10]

3.5.2 Introduction

X-rays are electromagnetic radiation with a wavelength between 0.01 to 10 nm, which are longer than gamma rays but shorter than those of UV rays. In 1912, Bragg and co-workers provided a good understanding of crystallography.[10] It has been two years after the celebration of the 100th year of existence of X-ray crystallography in 2013/2014 and that year was announced as the International Year of Crystallography by the United Nations.[11] This simply highlights the great importance of X-ray crystallography in the field of science and in the world development.

3.5.3 Bragg's Law

According to Bragg and his son, an X-ray that enters a crystal at a certain angle of incidence, θ, will reflect back with the same angle of reflection, θ. Constructive interference is observed when the path difference, d is equal to a whole number, n."[12] All the X-rays reflected from a given plane are in-phase resulting in constructive interference. Reflections from adjacent planes travel different path lengths and result

[8] Clegg, W. *Crystal Structure Determination*, New York: Oxford University Press, Inc., 1998.
[9] Friedrich, W., Knipping, P., von Laue, M. *Interferenz-Erscheinungen bie Röntgenstrahlen*. 1912.
[10] Compton, A. H. *Phy. Rev*. **21** (1923) 483-502.
[11] Website: http://www.iycr2014.org/ accessed on 21/12/2015.
[12] Bragg, W.L. *The Crystalline State: Volume I.* New York: The Macmillan Company, 1934.

in 'out-of-phase' reflections, therefor destructive interference is observed. However, if the distance between two adjacent planes is an integral number of wavelengths (nλ), constructive interference will also be observed. Bragg's law can be defined by Equation 3.8 below,

$$n\lambda = 2d_{hkl}sin\theta \qquad \textbf{3.8}$$

where λ is the wavelength of the scattered radiation, n is an integer, d_{hkl} is the path length between two adjacent parallel planes and θ is the angle of incidence and reflection. In Figure 3.5 Bragg's law is explained by means of an illustration.

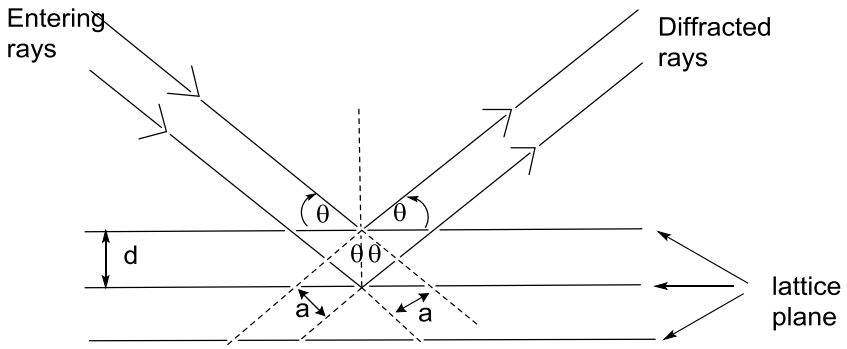

Figure 3.5 : Diffraction of X-rays according to Bragg.[13]

Within a crystal there are an infinite number of sets of atom planes. Bragg's law is used to correct the difference in phase because of the reflections from the different planes.[12]

3.5.4 X-rays

X-ray crystallography is an analytical tool, used to analyse and determine how atoms are arranged in a single crystal. In the early 20th century it was discovered that X-rays could be used to observe the structure of a molecule in a non-intrusive manner.[14] X-ray crystallography allows researchers to study the chemical bonds between atoms, atomic positions *etc*. and this knowledge can be used to modify a structure and thus change its behaviour and properties. William Henry Bragg and W. Lawrence Bragg were the first scientists to start using X-ray crystallography in 1912/1913 since the

[13] Tilley, R. J. D. *Crystals and Crystal Structures*, Wiley and Sons, New York. 2006. 114.
[14] http://www.iycr2014.org/__data/assets/pdf_file/0010/78544/220914E.pdf accessed on 21/12/2015.

discovery of X-rays and radioactivity between 1880 and the First World War.[15] With the help of the Braggs the arrangement of atoms in a crystal can now be determined accurately.

In X-ray crystallography the primary target is a single crystal. This target is classified as a solid, three dimensional structure with unit cells repeating in all three dimensions. The unit cell can be defined by its three edge lengths (*a, b, c*) and it's three bond angles (α, β, γ) (Figure 3.6). The Miller indices denoted by (*hkl*) describe the planes and the direction in a crystal lattice while the crystal's space group (230 different types) describe the symmetry of a unit cell.[16]

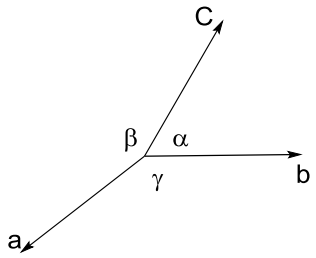

Figure 3.6: Illustration of unit cell parameters.

Significant knowledge of crystal structures is obtained from X-ray diffraction. X-ray diffraction is defined as the scattering of a wave as it passes through an obstacle. When crystalline structures are exposed to X-rays, electrons in the crystals diffract these X-rays and this result in a diffraction pattern. From the diffraction patterns a three dimensional picture of the electronegativity of the electrons is obtained.

3.5.5 Structure factor

The primary data of X-ray crystallography is the intensities and relative positions of the reflections. Three indices identifies each reflection, *h*, *k* and *l* which specify the specific orientation in the reciprocal lattice. The intensity of a reflection is written as *I(hkl)*The phase, denoted by $Ø_J$, present the horizontal shift which correspond to a certain origin and the amplitude, denoted by $|F(hkl)|$, present the height of the wave and it is

[15] Anders, L. *Acta Cryst*. **A69** (2013) 10–15.
[16] Hahn, T. *International Tables for Crystallography*, A, 5th Ed., Kluwer Academic Publishers, Springer, 2002.

determined by the number of electrons that are present. In order to obtain the resultant beam, the scattering for each atom within a unit cell should be added in order.

The structure factors, *F(hkl)*, gives the scattering of all the atoms (j) in the unit cell and compare them to a single electron. Therefore the resultant wave of the unit cell is defined by Equation 3.9 below.

$$\boldsymbol{F_{hkl} = \sum_{j=1}^{N} f_j \exp[i2\pi(hx_j + ky_j + Iz_j)]} \qquad \textbf{3.9}$$

In Equation 3.9, f_j denotes the scattering factor for N atoms and the position of each individual atom in the unit cell is represented by (x_j, y_j, z_j). According to this equation, the magnitude of the structure factor depends on the atoms' relative position and the atoms' scattering factors. Each term present a wavelet with a magnitude f_j and a phase of $\emptyset_j = i2\pi(hx_j + ky_j + Iz_j)$ which present the path length of each scattered wavelet. Therefore the structure factor *F(hkl)* is the effect of the wavelet that are scattered by the N atoms present within the cell unit.[17,18] By manipulating Equation 3.9 the following equation is obtained (Equation 3.10).

$$\boldsymbol{F_{hkl} = \sum_{j=1}^{N} f_j \exp[i2\pi(hx_j + ky_j + Iz_j) + isin2\pi(hx_j + ky_j + Iz_j)]} \qquad \textbf{3.10}$$

F^2 is proportional to the intensity of the diffracted X-rays due to the energy related to the cosine wave, which is proportional to the square of the magnitude of the wave. An X-ray diffraction can be expressed in terms of the strength of the scattered wave ($I_o(hkl)$) and from Equation 3.11 $|F(hkl)|^2$ is referred to the ideal intensity.

$$\boldsymbol{I_o(hkl) \propto |F(hkl)|^2} \qquad \textbf{3.11}$$

The relationship in Equation 3.11 is ideal since it allows to directly link the experimental ($I_o(hkl)$) values to the structure by $|F(hkl)|^2$. Low electron concentrations are observed for atoms with low atomic numbers while atoms with high atomic numbers are known to yield higher electron concentrations. Electron density $\rho\,(x, y, z)$ is a function of position and can be presented in terms of the structure factor $|F(hkl)|$ (Equation 3.12).[18]

[17] Azaroff, L. V. *Elements of X-ray Crystallography*, McGraw-Hill, Inc., New York, 1968.
[18] Waseda, Y., Matsubara, E., Shinoda, K. *X-Ray Diffraction Crystallography: Introduction, Examples and Solved Problems*, Springer, New York. 2011.

$$F_{hkl} = \int \rho(x, y, z) \exp[i2\pi(hx_n + ky_n + Iz_n)]\, dV \qquad \textbf{3.12}$$

3.5.6 The 'Phase Problem' in Crystalography

Although the modulus $|F(hkl)|$ can be directly obtained from the intensity data, the phase corresponding to *F(hkl)* cannot be directly measured. The amplitude and the phase must be known for all reflections in order to determine the crystal structure. X-ray diffraction has a big disadvantage in that it cannot determine the complete sectorial structure factor. However, the structure factor can be obtained from the intensity data (Equation 3.11), but not directly with the corresponding phase.[19] It is crucial to know both the phase and the amplitude to determine the structure. This inability to determine the phase is referred to as the phase problem and two known methods can be used to solve this problem, namely the Patterson function and the Direct Method.[20]

3.5.7 Patterson Function

This function is used for molecules with heavy atoms and where the other part of the structure is already known. It contains a set of peaks presenting intramolecular vectors for each molecular orientation found in the unit cell.[21] The Patterson Function which is defined by Equation 3.13, looks like an electron density map with positive electron density peaks in different positions, but these electron density peaks are not the positions of the atoms in the crystal but rather an indication of the position of the atoms relative to one another thus interatomic metals.

$$P(u, v, w) = V^{-1} \sum_h \sum_k \sum_l (F_{hkl})^2 \exp[-i2\pi(hu + kv + lw)] \qquad \textbf{3.13}$$

The volume of the unit cell is presented by V and u, v and w are the difference in coordinates of two atoms represented by each peak.[22]

[19] Hauptman, H. *Rep. Prog. Phys*. **54** (1991) 1427-1454.
[20] Rhodes, G. *Crystallography Made Crystal Clear: A Guide For Users Of Macromolecular Models*. 3rd Edition. Elsevier Inc. Canada. 2006.
[21] Terwilliger, T. C., Kim, S. H. *Acta Cryst*. **A43** (1987) 1-5.
[22] Lunger, P. *Modern X-ray Analysis on Single Crystals*, Walter de Gruyter and Co. Germany. 1980.

3.5.8 Direct Method

This method is referred to as the 'Direct Method' because the phases are determined directly from the observed diffraction pattern. It uses the mathematical relationship between the structure factors to determine the initial and expanding phases from the measured X-ray intensities. Small and intermediate sized atoms are normally well defined in this method and as a result structure factors are measured to very high diffraction angles which yield more precise data.[23]

3.5.9 Least Square Refinement

The least square refinement is a method used to compare the experimental diffraction pattern and calculated diffraction pattern in order to get a degree of similarity between them. The comparison of the experimental structure factor (F_o) and the calculated structure factor (F_o) is denoted in terms of the residual index (R-factor). Equation 3.14 below defines the R-factor.

$$\boldsymbol{R} = \frac{\sum ||\boldsymbol{F_o}| - |\boldsymbol{F_c}||}{\sum |\boldsymbol{F_o}|} \qquad \textbf{3.14}$$

A well-defined, complete and correct structure is usually defined by an R-factor that ranges between 0.02 and 0.07. In order to obtain a better refinement, the weighting factor (w) must be incorporated for each reflection. Equation 3.15 illustrates the R factor in terms of the weighting factor.[24]

$$\boldsymbol{wR_2} = \frac{\sum \boldsymbol{w}(\boldsymbol{F_0^2} - \boldsymbol{F_c^2})^2}{\sum \boldsymbol{w}(\boldsymbol{F_0^2})^2} \qquad \textbf{3.15}$$

[23] Giacovazzo, C. *Direct Phasing in Crystallography: Fundamentals and Applications*. Oxford University Press. New York. 1998.

[24] Muller, P., Herbst-Irmer, R., Spek, A. L. Schneider, T. R. Sawaya, M.R. *Crystal Structure Refinement: A Crystallographer`s Guide To SHELXL*. Oxford University Press. New York. 2006.

3.6 Selected theory behind Chemical Kinetics

3.6.1 Introduction

Chemical kinetics, also known as reaction kinetics, is the study of the behaviour of chemical reactions like the rates and mechanisms of the reaction as well as the effect of various variables on the system like the re-arrangement of atoms, intermediate formation etc. Reaction kinetics is based on the change of a system from one state to another. The measurement of kinetics is often obtained for light absorbing species by using spectrophotometry, since there is a unique absorption spectrum for every molecule. Reaction kinetics relate to the Beer-Lambert law, which states that the absorbance is directly proportional to the concentration of every molecule as presented in Equation 3.16 below,

$$\boldsymbol{A = -Log_{10}(T) = -Log_{10}\frac{I_t}{I_o} = \varepsilon Cl} \qquad \textbf{3.16}$$

Where the light intensity is denoted by I_t, the transmitted intensity by I_t, l is the path length, C is the concentration, ε is the molarextinction coefficient and A is the absorbance. Equation 3.17 below illustrates the total absorbance of a solution (sum of individual absorbance of each substance).

$$\boldsymbol{A = \sum_i \varepsilon Cl} \qquad \textbf{3.17}$$

During the process of reaction kinetics, there are several factors that influence the reaction mechanism and rate constants namely, concentration, pressure, temperature, homogeneity and the sensitivity to light or air or to a radiofrequency (NMR). However, when the pressure, temperature and volume are kept constant, the rate constant of the reaction is simply the rate of change in time (of any of the reactants or products).

3.6.2 The reaction rate and rate laws

The reaction rate changes as the concentration of the reactants change per unit time in a chemical reaction as shown in Equation 3.18 below.

$$\boldsymbol{iI + nN \xrightarrow{k} pP} \qquad \textbf{3.18}$$

The increase in the concentration of the product is denoted by $\Delta[C]$ and the decrease in reactants by $\Delta[I]$ and $\Delta[P]$. Therefore the rate of the generic reaction could be determined by Equation 3.19 as follows,

$$\boldsymbol{Rate} = \frac{-\Delta[\boldsymbol{I}]}{\Delta \boldsymbol{t}} = \frac{-\Delta[\boldsymbol{P}]}{\Delta \boldsymbol{t}} = \frac{\Delta \boldsymbol{C}}{\Delta \boldsymbol{t}} \qquad \textbf{3.19}$$

Where the units is given by moles per litre per time $(\mathrm{mol\ L^{-1}\ s^{-1}})$. The negative signs in Equation 3.19 illustrate the decrease of the reactants. The relationship of the substances in the reaction and the rate of a reaction is called the rate law and the general rate law is given by Equation 3.20,

$$\boldsymbol{Rate} = \boldsymbol{k}[\boldsymbol{I}]^{\boldsymbol{a}}\,[\boldsymbol{P}]^{\boldsymbol{b}} \qquad \textbf{3.20}$$

Where k is called the rate constant and the order of the reaction is represented by the overall sum of the two exponents a and b. Every reaction has its unique rate constant that is independent on the concentration of that reactant. The rate constant changes when the solvent and temperature change. The order of a reaction is defined by the way the rate changes when the concentration of one or both of the reactants change. It is not easy to determine the order of a reaction experimentally; however there is one way to deal with this problem and this is to use *pseudo* first-order conditions. *Pseudo* first-order conditions occur when one of the reactants' concentration is kept constant while the other one changes ($[\mathrm{P}] >> [\mathrm{I}]$). Equation 3.21 illustrates the rate of a *pseudo* first-order reaction.

$$\boldsymbol{Rate} = \boldsymbol{k_{obs}}[\boldsymbol{I}]^{\boldsymbol{a}} \text{ , where } \boldsymbol{k_{obs}} = \boldsymbol{k}[\boldsymbol{P}]^{\boldsymbol{b}} \qquad \textbf{3.21}$$

The new constant is called k_{obs}, which is the observed *pseudo* first-order rate constant. The rate constant, k, of the reaction can be determined by varying the concentration of P and calculating each observed rate constant. For a second order reaction, where $\mathrm{a} = \mathrm{b} = 1$, the rate law is given by Equation 3.22.

$$a[I] + b[P] \underset{k_2}{\overset{k_1}{\rightleftharpoons}} c[C]$$

$$\boldsymbol{Rate = k_1[I][P] + k_2[I]} \quad \textbf{3.22}$$

From the above equation for *pseudo*-first order conditions ([P] >> [I]), k_{obs} is given by Equation 3.23.

$$\boldsymbol{k_{obs} = k_1[P] + k_2} \quad \textbf{3.23}$$

In this equation k_1 represents the forward reaction and k_2 represents the reverse reaction. The equilibrium constant for equilibrium reactions is given by Equation 3.24.

$$\boldsymbol{K_{eq} = \frac{k_1}{k_2}} \quad \textbf{3.24}$$

When Equation 3.21 is integrated from t = 0 to t = t, Equation 3.25 is obtained.

$$\boldsymbol{In \frac{[C]_t}{[C]_0} = k_{obs}} \text{ or } \boldsymbol{[C]_t = [C]_0 e^{k_{obs}}} \quad \textbf{3.25}$$

$[C]_o$ and $[C]_t$ are the concentration of the reactant at time = 0 and t respectively. Beer`s law express absorbance in terms of the concentration of a solution and are shown in Equation 3.26 below,

$$\boldsymbol{A_t = A_\infty - (A_\infty - A_0) e^{k_{obs}}} \quad \textbf{3.26}$$

Where A_t is the absorbance after time t and is the absorbance at infinite time. The k_{obs} of the reaction can be obtained for a pseudo first-order reaction from the absorbance *versus* time data by using Equation 3.26, and the observed rate constant (k_{obs}) can be evaluated further as a function of temperature and concentration etc. Equation 3.26 was used to fit all the data in this study. The half-life of the reaction can be obtained from the following equation (Equation 3.27).

$$\boldsymbol{t_{1/2} = \frac{In2}{k_{obs}} = \frac{0.6932}{k_{obs}}} \quad \textbf{3.27}$$

3.7 Inductively Coupled Plasma Optical Emission Spectrometry (ICP-OES)

ICP-OES was developed by Geenfield *et al*.[25] in the 1960s. ICP-OES is one of the most popular analytical tools used by researchers to determine the trace elements in different samples. This technique is mainly used by researchers due to its sensitivity and ability to quantify the different elements in complicated material. The main advantage of ICP-OES is its ability for effective and reproducible vaporization, atomization, excitation and ionization for a broad range of elements in a variety of compound matrices. This is due to the high temperature of the observation zones of ICP; it is in the range of 6 000 – 7 000 K and much higher than the maximum temperature of open flames and furnaces (3 300 K).[26] In addition, ICP-OES is an electrodeless source, therefore no contamination can occur *via* the electrodes, it is easy to build an ICP assembly and it is an inexpensive analytical tool when compared to other sources such as laser-induced plasma (LIP). The advantageous characteristics of the ICP-OES source are listed below:[26]

- Low background emission and low chemical interference.
- Excellent detection limits for most elements (0.1 - 100ng mL^{-1}).
- Applicable to the refractory elements.
- Cost-effective analyses.
- Wide liner dynamic range (LDR) (4 to 6 orders of magnitude).
- Significant degree of ionization for most elements.
- High electron density (10^{14} - 10^{16} cm^{-3}).
- Simultaneous multi-element capability (over 70 elements including phosphorus and sulphur).
- High temperature range (7 000 – 8 000K).
- High stability leading to excellent accuracy and precision.

[25] Greenfield, S., Jones, I.L., Berry, C.T. *Analyst*. **89** (1964) 713-720.
[26] Hou, X., Jones., B.T. *Inductively Coupled Plasma/Optical Emission Spectrometry*, Wake Forest University, Winston-Salem, USA, 2000

3.8 CHNS micro-analyser (elemental analyser)

A CHNS micro-analyser for combustion analysis is an analytical tool used by researchers. A CHNS micro-analyser is an elemental analyser that is used in the determination of oxygen, hydrogen, nitrogen and sulphur in a sample. It is used mainly to analyse a variety of the following material:

- Protein measurement in food,[27]
- glow discharge emission in metals,[27]
- sulphur in coal emission,[27]
- multi-dimensional gas chromatograph mass spectrometry,[27]
- environmental monitoring,[27]
- air quality[27]
- and it has diverse medical and pharmaceutical applications.[27]

CHNS micro-analysis is a very fast and accurate method that is capable of handling a very wide variety of sample types such as liquids, solids, volatile and viscous samples in the field of polymers, the environment, chemicals, pharmaceuticals, food and energy.[27,28]

[27] http://www.leco.com. Accessed on 17January2016.
[28] Thopson M. *Analytical Methods Committee*. AMC technical briefs. ©The Royal Society of Chemistry 2008.

4 SYNTHESIS OF RHENIUM (I) TRICARBONYL COMPLEXES

4.1 Introduction

The nuclear properties and environments of metal centres are important when designing new radiopharmaceuticals. In the past, the study of designing radiopharmaceuticals using rhenium (I) and technetium (I) metal complexes have been investigated and are still under development.[1] Initially the research was focused on the $[M^{v}O]^{3+}$ core (M = Tc or Re) due to its easy preparation from the permetalate. After the discovery of the cardiac imaging agent $[^{99m}Tc(MIBI)_6]^{+}$ (MIBI = 2-methoxy-2-methylpropylisocyanide) (Scheme 4.1) and the easy preparation of the starting material *fac*-$[M(CO)_3(H_2O)_3]^{+}$ and *fac*-$[M(CO)_3(X)_3]^{+}$ (X = Cl or Br), researchers moved their focus to the oxidation state M (I).

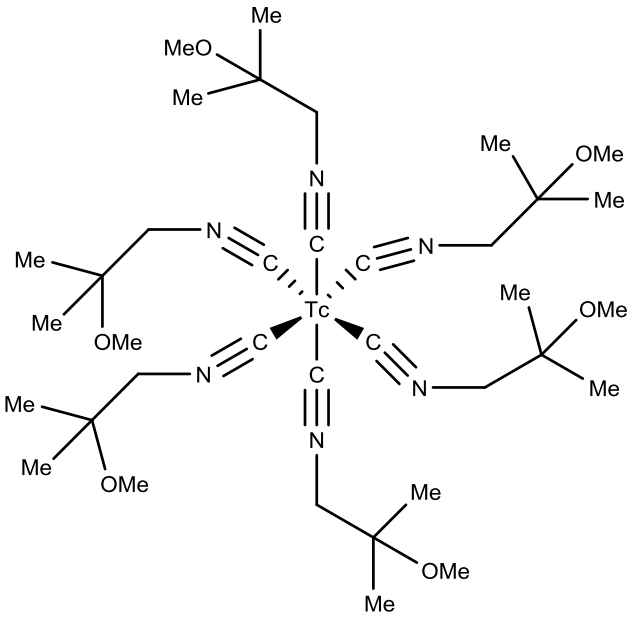

Scheme 4.1: The structure of $[^{99m}Tc(MIBI)_6]^{+}$ (MIBI = 2-methoxy-2-methylpropylisocyanide).

[1] Yorke, E. D., Beaumier, P., Wessels, A., Fritzberg, A., Morgan, C. *Nucl. Med. Biol*. **18** (1991) 827-835.

The starting material, *fac*-$[M(CO)_3(H_2O)_3]^+$ is stable in aqueous solution in the pH range 2 to 12 for several hours. Three carbonyl ligands are strongly coordinated to the rhenium metal and form the stable *fac*-$[Re(CO)_3]^+$ core. The three water molecules can easily be substituted by several functional groups i.e thioethers, thiols, phosphines and amines. This substitution can be done by the [2+1] mixed ligand approach (one bidentate and one monodentate ligand) and the [3+1] mixed ligand approach (one tridentate ligand and one monodentate ligand).[2,3,4] The substitutions would ideally not influence the biological properties of the biomolecule used in the radiopharmaceuticals due to the small size and the charge of the *fac*-$[Re(CO)_3]^+$ synthon.

According to the previous studies, little evidence of kinetic studies is present compared to the large amount of synthetic work that was performed on technetium and rhenium tricarbonyl systems.[4] However, the pH dependence of the di-rhenium and tri-rhenium complexes was investigated by Alberto *et al*.[5] with some substitution kinetics performed with different monodentate ligands.[6,7]

In this study, several promising and compatible N,O; S,S'; S,O bidentate and S,S',S" tridentate ligand systems were investigated. One of the aims of the study was to investigate the ability of the chosen N,O; S,S'; S,O bidentate and S,S',"S tridentate ligands to coordinate to *fac*-$[Re(CO)_3]^+$. The results were compared to previous studies of N,O and O,O' bidentate ligand systems to observe the variation in coordination behaviour and a possible difference in reactivity. The ligands used are listed in Table 4.1 together with the abbreviations that are used. A schematic representation of the ligands is given in Scheme 4.2.

[2] Schibli, R., Bella, R., Alberto, R., Garcia-Garayoa, E., Ortner, K., Ubram, U., Schubiger, P. A. *Bioconjugate Chem*. **11** (2000) 345-351.
[3] Development of ^{99m}Tc agent for imaging central neutral system receptors, IAEA Technical Report TRS46, Vienna, 2004.
[4] Mundwiler, S., Kunding, M., Ortner, K., Alberto, R. *Dalton Trans*. **9** (2004) 1320-1328.
[5] Alberto, R., Egli, A., Abram, U., Hegetschweiler, K., Gramlich, V., Schubiger, P.A. *J. Chem. Soc. DaltonTrans.* **19** (1984) 2815-2820.
[6] Salignac, B., Grundler, P.V., Cayemittes, S., Frey, U., Scopelliti, R., Merbach, A.E. *Inorg. Chem*. **42** (2003) 3516-3526.
[7] Helm, L., *Coord. Chem. Rev*. **252** (2008) 2346-2361.

Table 4.1: List of the chosen ligand systems and the abbreviations used.

Ligand Name	Abbreviation
N,O bidentate ligand systems	
5-Phenylazo-8-hydroxyquinoline	ANAOXH
5-(m-Tol)azo-8-hydroxyquinoline	m-TolANAOXH
5-(2,3-diMephenyl)azo-8-hydroxyquinoline	2,3-diMeANAOXH
5-(2,6-diMe phenyl)azo-8-hydroxyquinoline	2,6-diMeANAOXH
5-(3,4-diMe phenyl)azo-8-hydroxyquinoline	3,4-diMeANAOXH
S,O bidentate ligand systems	
Methyl benzo[b]thiophene-2-carboxylate	BSOC
2-Mercaptoethanol	$BSOH_2$
2-Mercaptophenol	$BSOPhH_2$
2-Methoxythiophenol	BSOPhCH
S,S' bidentate ligand systems	
5-Bromo-2,2`-bithiophene	BSBr
2,2'-bithiophene-5-carboxylic acid	BSCH
Benzene-1,2-dithiol	$BSPhH_2$
Toluene-3,4-dithiol	$m\text{-}TolBSPhH_2$
S,S',S" tridentate ligand system	
2,2`-Thiodiethanethiol	TSH_2

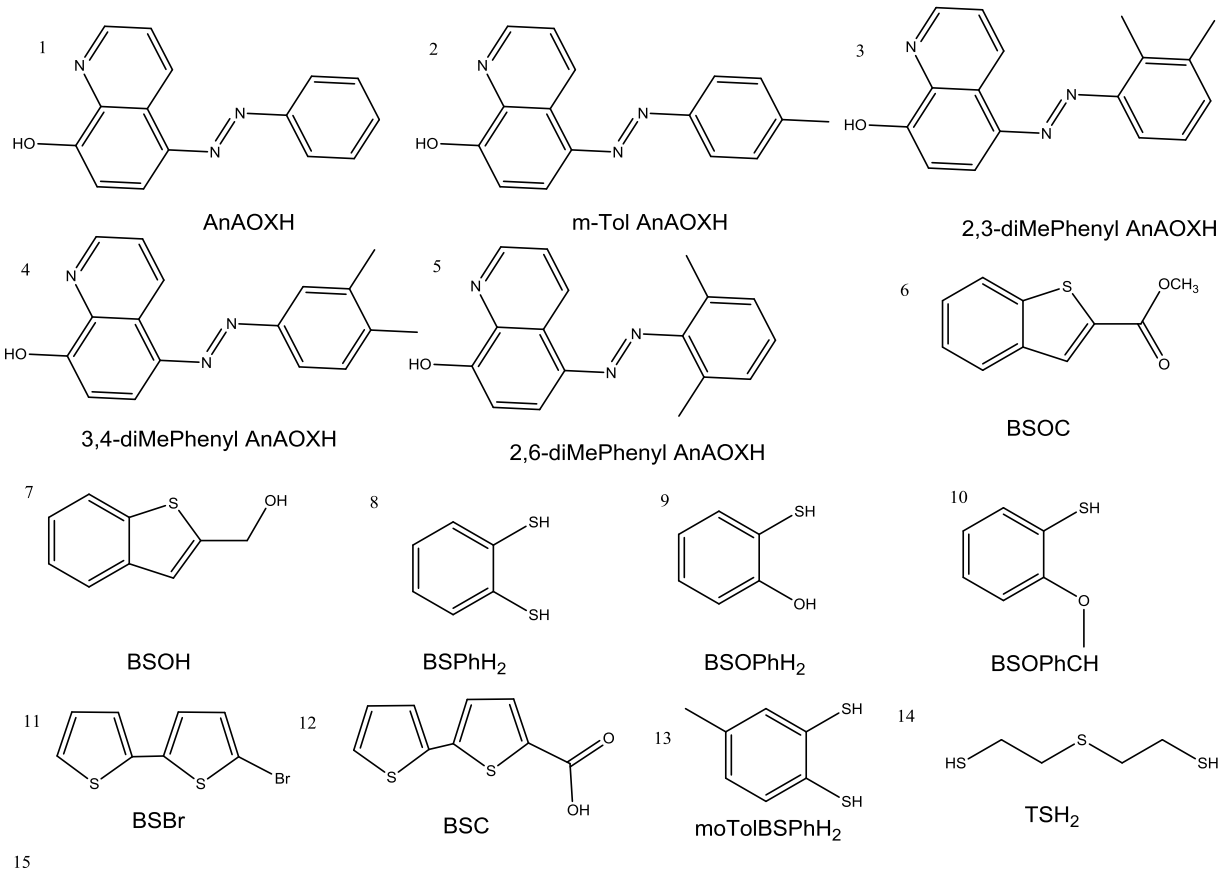

Scheme 4.2: Schematic illustration of the chosen ligands and the respective abbreviations.

The general synthetic pathway that was proposed for this study is illustrated in Scheme 4.3. However, the S,O and S,S' bidentate and S,S',S'' tridentate ligand systems did

not follow the expected pathway. The results obtained from this study indicated these ligand systems to follow the synthetic pathway presented in Scheme 4.4 below.

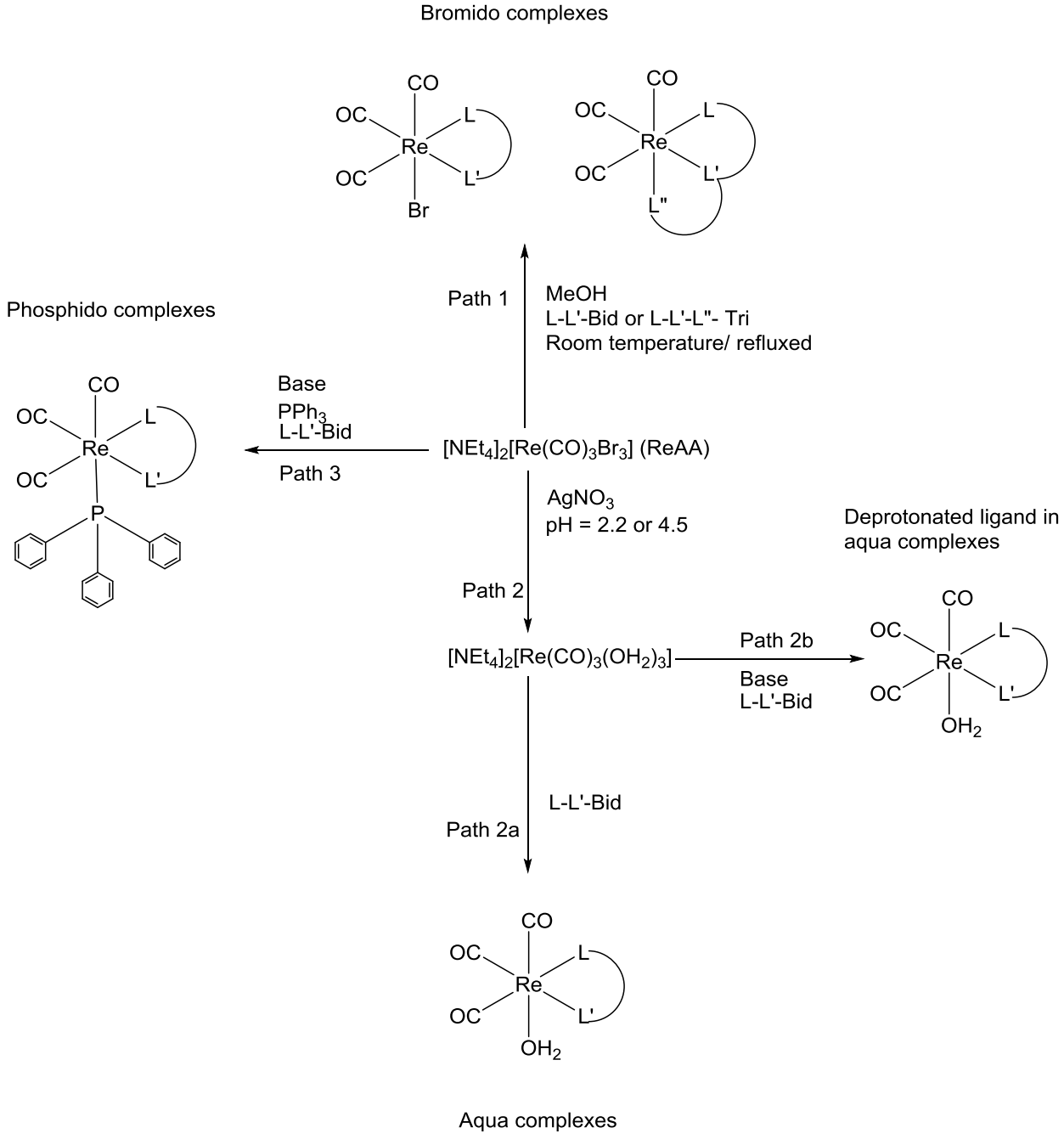

Scheme 4.3: The proposed general synthetic approach.

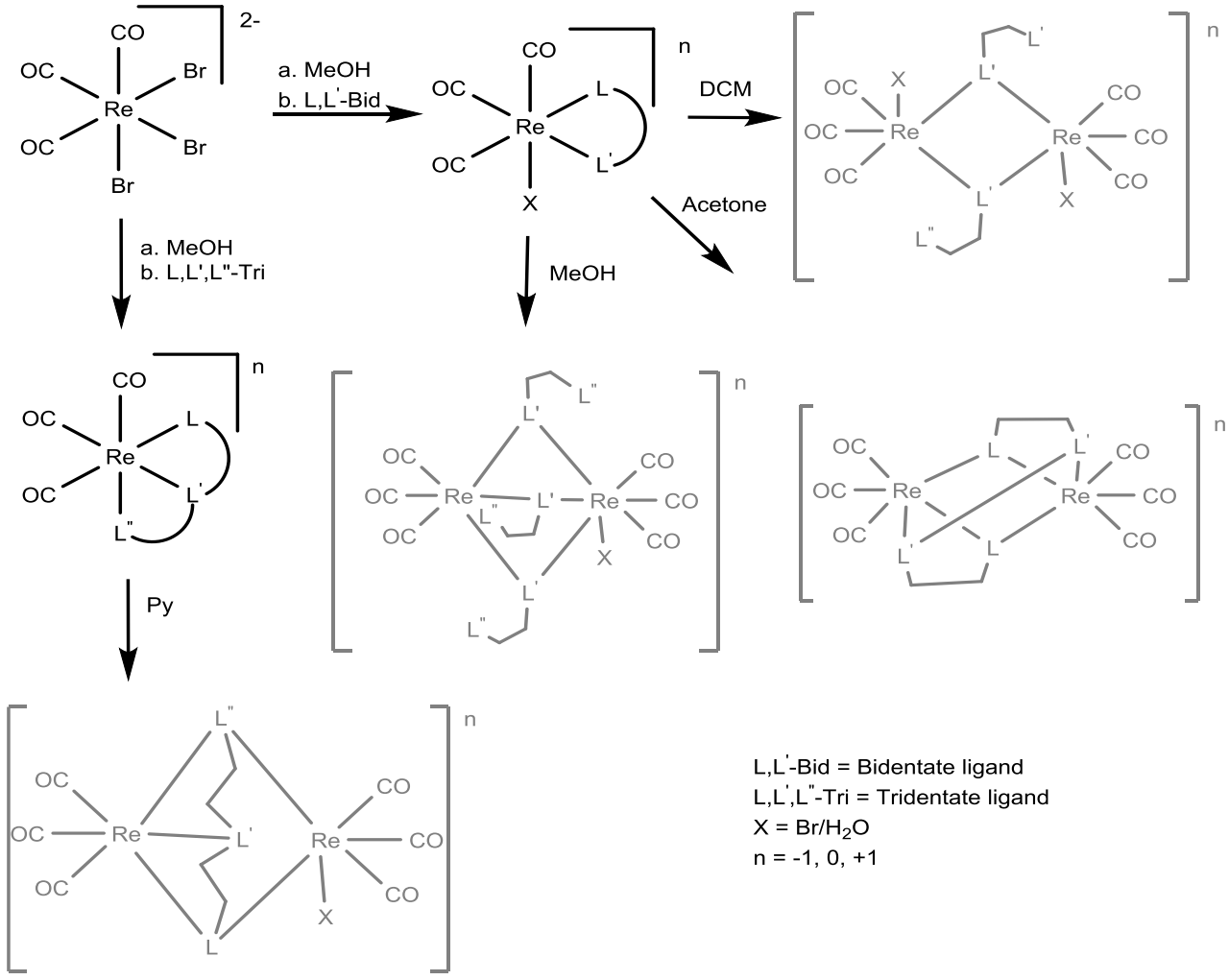

Scheme 4.4: The synthetic procedure for the specific complexes with S,O; S,S' and S,S',S'' tridentate ligand systems in this study.

4.2 Chemicals and Materials

All the chemicals used for the synthesis and characterisation were of reagent grade and were used without further purification. Chemicals were purchased from Sigma-Aldrich, South Africa, unless stated otherwise. For drying conditions, all solvent used were purified and dried by following the procedure prescribed by Perrin.[8, 9] Schlenk line methods were used for all reactions that were either moisture or air sensitive. Rhenium

[8] Perrin, D.D., Armarego, W.L.F. *Purification of laboratory chemicals*, 3rd Ed, Great Britain: Butterworth-Heinemann Publishers, 1988.
[9] Perrin, D.D., Armarego, W.L.F. *Purification of laboratory chemicals*, 5th Ed, Great Britain: Butterworth-Heinemann Publishers, 2003.

pentacarbonyl bromide was bought from Strem Chemicals, Newburyport (US). The precursor used for aqua complexes were synthesised according to the procedure provided by Roger Alberto, Switzerland.[10] All the ligands were bought from Sigma-Aldrich and will be abbreviated as shown in Table 4.1. Nitric acid (HNO_3) is used to adjust the pH during the synthesis of the aqua complexes.

The UV/Vis spectra were performed on a Varian Cary 50 Conc UV/Visble Spectrophotometer, equipped with a Julabo F12mV temperature cell regulator (accurate within 0.1 ºC) in a 1.000 ± 0.001 cm quartz cuvette cell. The infrared spectra of the complexes were recorded on a Bruker Tensor 27 Standard System Spectrophotometer with a laser range of 4000- 370 cm^{-1} which is coupled to a computer. The IR spectrometer was equipped with a temperature cell regulator accurately within 0.3 ºC. KBr pellets was used for solid samples. All Nuclear Magnetic Resonance (NMR) data were performed on a Bruker 300 MHz NMR spectrometer operating at 300 MHz using deuterated solvents or samples spiked with deuterated solvent. All the chemical shifts, δ, are reported in ppm (part per million) using TMS (tetramethylsilane) as internal standard of ^{1}H NMR. Coupling constants, *J*, are reported in Hertz (Hz).

4.3 Synthetic Methods

The synthesis of the starting synthon, *fac*-$[NEt_4]_2[Re(CO)_3Br_3]$ (ReAA), was strictly performed under Schlenk conditions. Different methods were used for the synthesis of the bromido and aqua complexes, as illustrated in Scheme 4.2. Two dinuclear structures with a S,S',S'' tridentate ligand, three dinuclear structures with a S,O bidentate ligand and one dinuclear structure with a S,S' bidentate ligand were successfully synthesized. Five bromido complexes with N,O bidentate ligands were successfully synthesized and characterized. Unfortunately the aqua complexes could not be isolated at this stage.

The synthesis of nine rhenium (I) complexes is presented in Appendix E. IR, NMR and UV/Vis characterization was performed but the exact structure of the complexes could not be conclusively determined as an in depth NMR study and suitable crystals for

[10] Albert, R., Schibli, R., Waihle, R., Schubiger, P. A. *Coord. Chem. Rev*. **190** (1999) 190-192.

single crystal XRD is imperative (see Chapter 6 for a complete discussion). Elemental analysis was performed but at the time of the study the results were not yet available. We present here the synthetic methods of the eleven successfully characterized and confirmed structures.

4.3.1 Synthesis of the starting synthon

4.3.1.1 Synthesis of *fac*-$[NEt_4]_2[Re(CO)_3Br_3]$ (ReAA)

$$ReBr(CO)_5 + 2(NEt_4)Br \xrightarrow{Ar,diglyme} \textit{fac}\text{-}[NEt_4]_2[ReBr_3(CO)_3] + 2CO$$

$(NEt_4)Br$ (5.00 g, 0.024 mol) was grounded to a fine powder with a mortar and pestle and left to dry overnight in a vacuum desiccator. 2,5,8-Trioxanone diglyme (150 ml) was added to the $(NEt_4)Br$ under a dry argon atmosphere and slurried in a preheated oil bath of 80 °C, for 30 minutes. The system was evacuated and purged with argon several times. $Re(CO)_5Br$ (5 g, 12.3 mmol) was added as a solid to the mixture and stirred at 115 °C for 15 hours. Good stirring and ventilation is necessary because of the continuous evolution of CO. The mixture was cooled down to room temperature and the precipitate was filtered off (colourless solid) and dried. The precipitate was stirred in a small amount of cold ethanol for 5 minutes, filtered and washed with cold dichloromethane. The product is slightly soluble in ethanol. Yield: 8.1296 g, 86 %).

IR (KBr, cm^{-1}): ν_{CO} = 1996, 1846.

4.3.2 Syntheses of complexes with S,O; S,S' and S,S',S'' ligands

4.3.2.1 Synthesis of *fac*-$[Re_2(CO)_6(TS)(Py)]$ (1)

ReAA (100 mg, 0.130 mmol) was dissolved in methanol (10 ml). TSH_2 (17.1 µL, 0.130 mmol) was added to the mixture as a liquid and stirred at room temperature for 2 hours. The product was collected by vacuum and recrystallized from a 100% pyridine solution. Yield: 75 %

IR (KBr, cm^{-1}): ν_{CO} = 1985, 1864.

^{1}H NMR (300 MHz, Methanol-*d_4*): δ (ppm) **=** 9.26 (dd, *J* = 7.7, 1.5 Hz, 1H), 8.61 (dd, *J* = 6.6, 1.6 Hz, 2H), 8.35 (t, 2H), 3.99 (t, 4H), 3.89 (t, 4H).

ICP-OES: Re – Cald: 48.26, Found: 47.85.

CHNS micro-analysis: C – Cald: 23.33, Found: 23.09, H – Cald: 1.68, Found 1.11, N – Cald: 1.81, Found: 1.59, S – Cald: 12.48, Found: 12.29.

Yield of crystals: 21 %

4.3.2.2 Synthesis of *fac*-[NEt_4][$Re_2(CO)_6(TS)(Br)$] (1a)

ReAA (100 mg, 0.130 mmol) was dissolved in methanol (10 ml). TSH_2 (17.1 µL, 0.130 mmol) was added to the mixture as a liquid and stirred at room temperature for 2 hours. The product was collected by vacuum. Yield: 86 %.

IR (KBr, cm^{-1}): ν_{CO} = 1989, 1871.

UV/Vis: λ_{max} = 311 nm, ε = 1854 M^{-1} cm^{-1}.

^{1}H NMR (300 MHz, Methanol-*d_4*): δ (ppm) = 3.31 (q, 8H (NEt_4)), 2.77 (t, 4H), 2.70 (t, 4H), 1.17 (q, 12H (NEt_4)).

^{13}C NMR (150 MHz, Methanol-*d_4*): δ (ppm) = 36.84, 25.49, 53.31 (NEt_4), 7.69 (NEt_4).

ICP-OES: Re – Cald: 41.33, Found: 41.58.

CHNS micro-analysis: C – Cald: 23.97, Found: 23.80, H – Cald: 3.11, Found: 3.18, N – Cald: 1.55, Found: 1.34, S – Cald: 10.69, Found: 10.23.

4.3.2.3 Synthesis of *fac*-[$Re_2(CO)_6(PPh_3)(BSOPhC)_2(Py)$] (2)

ReAA (100 mg, 0.130 mmol) and triphenylphosphine (34 mg, 0.130 mmol) were dissolved in 10 mL of methanol. BSOPhCH (15.8 µL, 0.130 mmol) and sodium bicarbonate (10.9 mg, 0.130 mmol), mixed in 10 mL of methanol were added to the ReAA solution. The reaction mixture was stirred for 2 hours. The product was filtered off, dried and weighed. The product was crystallized from dichloromethane and a drop of pyridine by solvent evaporation. Yield: 67 %.

IR (KBr, cm^{-1}): ν_{CO} = 2090, 2011, 1974.

^{1}H NMR (300 MHz, DMSO-*d_6*): δ (ppm) = 7.89 - 6.77 (PPh_3, Py and $(BSOPhC)_2$ peaks, 28H), 3.83 (methyl peaks, s, 6H).

ICP-EOS: Re – Cald: 32.10, Found: 31.87, P – Cald: 2.67, Found: 2.39.

CHNS micro-analysis: C – Cald: 44.48, Found: 44.87, H – Cald: 2.93, Found: 2.81, N - Cald: 1.21, Found: 1.18, S – Cald: 5.53, Found: 5.43.

Yiels of crystals: 70 %

4.3.2.4 Synthesis of *fac*-[$Re_2(CO)_6(PPh_3)_2$(BSOPhC)] (2a)

ReAA (100 mg, 0.130 mmol) and triphenylphosphine (34 mg, 0.130 mmol) were dissolved in 10 mL of methanol. BSOPhCH (15.8 µL, 0.130 mmol) and sodium bicarbonate (10.9 mg, 0.130 mmol) mixed in 10 mL of methanol were added to the ReAA solution. The reaction mixture was stirred for 2 hours. The product was filtered off, dried and weighed. Yield: 60 %

IR (KBr, cm^{-1}): ν_{CO} = 2087, 2004, 1968.

UV/Vis: λ_{max} = 302 nm, ε = 2641 M^{-1} cm^{-1}.

^{1}H NMR (300 MHz, Dichloromethane-*d_2*): δ (ppm) = 7.76 - 6.70 (2 x PPh_3 and 2 x BSOPhC, 38H), 3.56 (methyl peaks), s, 6H).

ICP-EOS: Re – Cald: 27.70, Found: 27.89, P – Cald: 4.61, Found: 4.85.

CHNS micro-analysis: C – Cald: 50.04, Found: 49.97, H – Cald: 3.27, Found: 3.21, S – Cald: 4.78, Found: 4.73.

4.3.2.5 Synthesis of *fac*-[NEt_4][$Re_2(CO)_6$(BSOPhC)$_3$] (3)

ReAA (100 mg, 0.130 mmol) was dissolved in 10 ml methanol. BSOPhCH (15.8 µL, 0.130 mmol) was added to the mixture and stirred at room temperature for 3 hours. The product was dried *in vacuo*. The product was crystallized from methanol by solvent evaporation. Yield: 89 %.

IR (KBr, cm^{-1}): ν_{CO} = 2002, 1869.

UV/Vis: λ_{max} = 214 nm, ε = 3853 M^{-1} cm^{-1}.

^{1}H NMR (300 MHz, Methanol-*d_4*): δ (ppm) = 7.42 (dd, *J* = 7.7, 1.6 Hz, 2H), 7.54 (dd,*J* = 7.7, 1.6 Hz, 1H), 7.20 (dtd, *J* = 22.2, 7.8, 1.6 Hz, 3H), 6.83 (d, *J* = 16.0 Hz, 6H), 3.94 (d, *J* = 11.4 Hz, 9H), 2.93 (q, 8H (NEt_4)), 1.13 (tt, 12H (NEt_4)).

^{13}C NMR (150 MHz, DMSO-d6): δ (ppm) = 133.75, 126.77, 121.34, 119.84, 111.34, 110.37, 55.47, 51.39 (NEt_4), 7.12 (NEt_4).

ICP-EOS: Re – Cald: 34.24, Found: 32.31.

CHNS micro-analysis: C – Cald: 38.61, Found: 38.56, H – Cald: 3.77, Found: 3.59, N – Cald: 1.29, Found: 1.13, S – Cald: 8.85, Found: 8.74.

Yield of crystals: 82 %

4.3.2.6 Synthesis of *fac*-[$Re_2(CO)_6$(μ-η^4-m-TolBSPh-S-S-m-TolBSPh)] (4)

ReAA (100 mg, 0.130 mmol) was dissolved in 10 ml methanol. m-TolBSPhH_2 (20.28 mg, 0.130 mmol) was added to the mixture as a liquid and stirred at room temperature for 2 hours. The product was filtered, dried and weighed. The product was crystallized from acetone by solvent evaporation. Yield: 76 %.

IR (KBr, cm^{-1}): ν_{CO} = 2005, 1869.

UV/Vis: λ_{max} = 250 nm, ε = 3621 M^{-1} cm^{-1}.

^{1}H NMR (300 MHz, dichloromethane-*d_2*): δ (ppm) = 7.97 (d, *J* = 8.0 Hz, 2H), 7.46 (s, 2H), 7.17 (d, *J* = 8.0, 2H), 2.41 (d, *J* = 0.7, 6H)

^{13}C NMR (150 MHz, Methanol-*d_4*): δ (ppm) = 131.10, 128.01, 126.15, 125.11, 120.28, 1321.13, 32.12.

ICP-EOS: Re – Cald: 43.81, Found: 43.76.

CHNS micro-analysis: C – Cald: 28.23, Found: 28.21, H – Cald: 1.41, Found: 1.31, S – Cald: 15.11, Found: 15.03.

Yield of crystals = 23 %

4.3.3 Syntheses of bromido complexes with N,O bidentate ligands

The N,O' bidentate complexes synthesized were characterized by IR, UV/Vis and ^{13}C NMR. The ^{1}H NMR data is not reliable in the case of (**7**) and (**9**) and it was decided not to include it. These five complexes were synthesized and compared to the two complexes synthesized by Schutte-Smith *et al*.[11] and a good correlation was found in the NMR and IR data.

4.3.3.1 Synthesis of *fac*- [NEt_4][$Re(CO)_3$Br(AnAOX)] (5)

ReAA (100 mg, 0.130 mmol) was dissolved in 10 ml methanol. 3,4-diMeAnAOXH (36.2 mg, 0.130 mmol) was added to the mixture as a solid and stirred at room temperature for 2 hours. The precipitate was filtered, dried and weighed. Yield: 68 %.

[11] Schutte-Smith, M., Muller, T.J., Visser, H.G., Roodt, A. *Acta Cryst*. **C69** (2013) 1467-1471.

IR (KBr, cm^{-1}): ν_{CO} = 2003, 1869, $\nu_{diazenyl}$ = 1454.

UV/Vis: λ_{max} = 304 nm, ε = 1840 M^{-1} cm^{-1}.

^{1}H NMR (300 MHz, DMSO-*d*$_6$): δ (ppm) = 9.11 (d, *J* = 8.7 Hz, 1H), 8.92 (d, *J* = 4.7 Hz, 1H), 8.02 (d, *J* = 8.9 Hz, 1H), 7.76 – 7.69 (m, 1H), 7.14 (s, 5H), 6.88 – 6.80 (m, 1H). 3.58 (q, 8H (NEt_4)), 1.14 (q, 12H (NEt_4)).

^{13}C NMR (150 MHz, DMSO-*d*$_6$): δ (ppm) = 151.70, 149.50, 148.55, 142.76, 137.26, 134.51, 134.01, 130.52, 129.93, 129.52, 127.67, 124.74, 120.11, 117.97, 115.30, 51.95 (NEt_4), 7.57 (NEt_4).

4.3.3.2 Synthesis of *fac*-[NEt_4][$Re(CO)_3Br$(m-TolAnAOX)] (6)

ReAA (100 mg, 0.130 mmol) was dissolved in 10 ml methanol. m-TolAnAOXH (32.4 mg, 0.130 mmol) was added to the mixture as a solid and stirred at room temperature for 2 hours. The precipitate was filtered, dried and weighed. Yield: 62 %.

IR (KBr, cm^{-1}): ν_{CO}= 2004, 1873, $\nu_{diazenyl}$ = 1499.

UV/Vis: λ_{max} = 310 nm, ε = 1750 M^{-1} cm^{-1}.

^{1}H NMR (300 MHz, DMSO-*d*$_6$): δ (ppm) = 9.45 (d, *J* = 8.6 Hz, 1H), 9.02 (d, *J* = 4.7 Hz, 1H), 8.14 (d, *J* = 8.9 Hz, 1H), 7.55 – 7.46 (m, 2H), 7.34 (d, *J* = 7.3 Hz, 1H), 6.93 (d, *J* = 8.9 Hz, 1H), 2.58 (s, 5H), 3.28 (q, 8H (NEt_4)), 1.23 (q, 12H (NEt_4)).

^{13}C NMR (150 MHz, DMSO-*d*$_6$): δ (ppm) = 152.97, 149.10, 147.52 142.48, 138.67, 133.80, 133.34, 130.16, 129.68, 129.09, 126.71 124.13, 122.06, 119.58, 117.96, 115.09, 21.04, 51.48 (NEt_4), 7.19 (NEt_4).

4.3.3.3 Synthesis of *fac*-[NEt_4][$Re(CO)_3Br$(2,3-diMeAnAOX)] (7)

ReAA (100 mg, 0.130 mmol) was dissolved in 10 ml methanol. 2,3-diMeAnAOXH (36.1 mg, 0.130 mmol) was added to the mixture as a solid and stirred at room temperature for 2 hours. The precipitate was filtered, dried and weighed. Yield: 59 %.

IR (KBr, cm^{-1}): ν_{CO} = 2003, 1863, $\nu_{diazenyl}$ = 1440.

UV/Vis: λ_{max} = 305 nm, ε = 1230 M^{-1} cm^{-1}.

^{13}C NMR (150 MHz, DMSO-*d*$_6$): δ (ppm) = 153.44, 153.25, 149.57, 142.46, 139.56, 139.11, 133.81, 131.59, 130.57, 130.21, 129.64, 124.55, 120.06, 118.49, 115.60, 21.44, 20.10, 51.91 (NEt_4), 7.57 (NEt_4).

4.3.3.4 Synthesis of *fac*-[NEt4][Re(CO)$_3$Br(3,4-diMeAnAOX)] (8)

ReAA (100 mg, 0.130 mmol) was dissolved in 10 ml methanol. 3,4-diMeAnAOXH (36.2 mg, 0.130 mmol) was added to the mixture as a solid and stirred at room temperature for 2 hours. The precipitate was filtered, dried and weighed. Yield: 66 %.

IR (KBr, cm^{-1}): ν_{CO}=2005, 1881, $\nu_{diazenyl}$ = 1457.

UV/Vis: λ_{max} = 304 nm, ε = 2756 M^{-1} cm^{-1}.

^{1}H NMR (300 MHz, DMSO-*d$_6$*): δ (ppm) = 9.36 (d, *J* = 8.5 Hz, 1H), 8.94 (d, *J* = 4.7 Hz, 2H), 8.06 (d, *J* = 8.6 Hz, 1H), 7.79 – 7.60 (m, 2H), 7.30 (d, J = 7.8 Hz, 1H), 6.85 (d, *J* = 8.8 Hz, 1H), 2.31 (d, *J* = 12.4 Hz, 6H), 3.22(q, 8H (NEt_4)), 1.15 (q, 12H (NEt_4)).

^{13}C NMR (150 MHz, DMSO-*d$_6$*): δ (ppm) = 151.12, 149.10, 142.52, 138.22, 137.22, 133.84, 133.26, 130.23, 129.64, 124.04, 122.67, 120.97, 119.73, 117.84, 115.14, 19.56, 19.39, 51.46 (NEt_4), 7.17(NEt_4).

4.3.3.5 Synthesis of *fac*-[NEt$_4$][Re(CO)$_3$Br(2,6-diMeAnAOX)] (9)

ReAA (100 mg, 0.130 mmol) was dissolved in 10 ml methanol. 2,6-diMeAnAOXH (36.5 mg, 0.130 mmol) was added to the mixture as a solid and stirred at room temperature for 2 hours. The precipitate was filtered, dried and weighed. Yield: 64 %.

IR (KBr, cm^{-1}): ν_{CO} = 2004, 1870, $\nu_{diazenyl}$ = 1461.

UV/Vis: λ_{max} = 314 nm, ε = 936 M^{-1} cm^{-1}.

^{13}C NMR (150 MHz, DMSO-*d$_6$*): δ (ppm) = 153.12, 151.19, 148.42, 146.82, 140.02, 137.44, 135.46, 130.89, 127.64, 123.89, 122.12, 120.45, 118.45, 117.02, 116.02, 20.01, 19.45, 51.36 (NEt_4), 7.32(NEt_4).

4.4 Discussion

The syntheses of the *fac*-[NEt_4][Re(CO)$_3$(Br)(N,O-bid)] (N,O-bid = N,O bidentate ligands) type complexes were generally straight forward; the rhenium precursor (ReAA) and the N,O bidentate ligand were dissolved in MeOH and stirred for a certain period of time to result in mononuclear complexes. The five complexes (**5**) to (**9**) were fully characterized and compare well to two similar structures in literature.[11]

The complexes *fac*-[$Re_2(CO)_6(TS)(Py)$] (**1**), *fac*-[NEt_4][$Re_2(CO)_6(TS)(Br)$] (**1a**), *fac*-[$Re_2(CO)_6(PPh_3)(BSOPhC)_2(Py)$] (**2**), *fac*-[$Re_2(CO)_6(PPh_3)_2(BSOPhC)_2$] (**2a**), *fac*-[$Re_2(CO)_6(BSOPhC)_3$ (**3**) and *fac*-[$Re(CO)_3(Br)$(μ-η4-m-TolBSPh-S-S-m-TolBSPh)] (**4**) were fully characterized and suitable crystals for single crystal XRD was obtained for (**1**), (**2**), (**3**) and (**4**). The synthetic procedure and structure determination of complexes with the chosen S,O, S,S' and S,S',S'' proved to be not that easy because of the different bonding modes of these complexes.

In Table 4.1 below, all the v_{CO} stretching frequencies as well as the $v_{diazenyl}$ stretching frequencies for the N,O bidentate complexes are reported. Infrared spectroscopy is used to characterize complexes and the v_{CO} stretching frequencies specifically provide a good fingerprint. The carbonyl group is polarized and the vibrational stretching of the bond influences the dipole moment. The asymmetric stretching of the C=O bond can be found at higher frequencies than the symmetric stretching due to the energy needed. The bending stretching frequencies need less energy than the corresponding stretching frequencies, as discussed in Chapter 3.

Infrared spectroscopy was used in this study to monitor the shift in stretching frequencies (Table 4.1). The carbonyl stretching frequencies for the precursor *fac*-[NEt_4][$Re(CO)_3(Br)_3$] are 1996 and 1846 cm^{-1}.

Table 4.2: The selected stretching frequency of tricarbonyl complexes.

Complexes with N,O ligands	$v_{Diazenyl}$	v_{CO}
fac-[NEt_4][$Re(CO)_3Br$(AnAOX)] (**5**)	1454	2003, 1868
fac-[NEt_4][$Re(CO)_3Br$(m-TolAnAOX)] (**6**)	1499	2004, 1873
fac-[NEt_4][$Re(CO)_3Br$(2,3-diMeAnAOX)] (**7**)	1440	2003, 1863
fac-[NEt_4][$Re(CO)_3Br$(3,4-diMeAnAOX)] (**8**)	1457	2005, 1881
fac-[NEt_4][$Re(CO)_3Br$(2,6-diMeAnAOX)] (**9**)	1461	2004, 1870

Complexes with S,O, S,S' and S,S'',S'' ligands	v_{CO}
fac-[$Re_2(CO)_6(TS)(Py)$] (**1**)	1984, 1864
fac-[NEt_4][$Re_2(CO)_6(TS)(Br)$] (**1a**)	1989, 1871
fac-[$Re_2(CO)_6(PPh_3)(BSOPhC)_2(Py)$] (**2**)	2090, 2004, 1968
fac-[$Re_2(CO)_6(PPh_3)_2(BSOPhC)_2$] (**2a**)	2094, 2008, 1973
fac-[NEt_4][$Re_2(CO)_6Br(BSOPhC)_3$] (**3**)	2007, 1869
fac-[$Re_2(CO)_6$(μ-η4-m-TolBSPh-S-S-m-TolBSPh)] (**4**)	2093, 2014, 1994

The diazenyl frequencies of (**5**) to (**9**) vary between 1440 cm^{-1} and 1499 cm^{-1}. This is in normal range and comparable to the two similar structures reported by Schutte-Smith *et al*., with values reported between 1449 cm^{-1} and 1507 cm^{-1}.[11]

The carbonyl stretching frequencies of the complexes with N,O ligands (**5**) to (**9**) are very similar and are comparable to the two reported structures with values ranging between 1894 cm^{-1} and 2022 cm^{-1}. (**1**) and (**1a**) have very similar stretching

frequencies of 1984 cm^{-1} and 1864 cm^{-1} for (**1**) and 1989 cm^{-1} and 1871 cm^{-1} for (**1a**). This is expected since the only difference is the pyridine and the bromido ligand. The ν_{CO} values for (**2**) and (**2a**) are also comparable at 2090 cm^{-1}, 2004 cm^{-1} and 1968 cm^{-1} for (**2**) and 2094 cm^{-1}, 2008 cm^{-1} and 1973 cm^{-1} for (**2a**). The carbonyl stretching frequency of (**3**) is quite different from the other sulphur bridged complexes and it might be explained by the fact that the dinuclear structure of (**3**) has three sulphur bridges compared to the two sulphur bridges of the other structures. The carbonyl stretching frequency of (**4**) is similar to that of (**2**) and (**2a**). No real trend is observed in the carbonyl stretching frequencies of these complexes.

Nine complexes were synthesized and characterized by IR, NMR and UV/Vis but crystals suitable for single crystal XRD was not yet obtained and the elemental analysis results were not yet available. It was decided to add the synthetic procedure of these complexes in Appendix E since more time need to be spend on these structures to confirm the exact structures.

The crystal structures of four of the synthesized complexes, (**1**), (**2**), (**3**) and (**4**) are discussed in Chapter 5. Overall it was confirmed that the S,O, S,S' and S,S',S'' ligands have a variety of bonding modes and it is imperative to confirm the structure of each compound by means of crystal structures and also by a ^{1}H NMR spectroscopic study. This is addressed in Chapter 5 and Chapter 6 respectively.

5 CRYSTALLOGRAPHIC STUDY OF RHENIUM (I) COMPOUNDS

5.1 Introduction

Crystal structures of rhenium (I) tricarbonyl complexes have been intensively studied and reported in literature as described in Chapter 2.[1,2,3,4] However, only a few reported crystal structures contain S,S' and S,O donor bidentate ligands and S,S',S'' donor tridentate ligands.[5,6,7] In this chapter, four new crystal structures are reported: two with S,O bidentate ligands, one with a S,S' bidentate ligand and one with an S,S',S'' tridentate ligand coordinated to the *fac*-$[Re(CO)_3]^+$ core. The ligands used are:

- 2,2-Thiodiethanthiol (TSH_2)
- 2-Methoxythiophenol (BSOPhCH)
- Toluene-3,4-dithiol (m-TolBSPhH_2)

The general synthetic procedure for rhenium (I) tricarbonyl complexes with either bidentate or tridentate ligands is illustrated in Scheme 5.1. In this scheme the compounds in black is part of the known synthetic route up to date (from previous research) while the compounds in grey form part of this study. The mechanism of formation of the dinuclear complexes is unclear at this stage. It is possible that they form directly or that there is a rearrangement after the mononuclear complexes are formed. The last supposition is certainly the case in the formation of the dinuclear

[1] Schutte-Smith, M., Muller, T.J., Visser, H.G., Roodt, A. *Act Cryst*. **C69** (2013) 1467-1471.
[2] Brink, A., Visser, H.G., Roodt, A. *Polyhedron*. **52** (2013) 416-423.
[3] Ursillo, S., Can, D., Peindy N'Dongo, H.W., Schmuts, P., Spingler, B., Alberto, R. *Organometallics*, **33** (2013) 6945-6952.
[4] Alberto, R., Schibli, R., Waibel, R., Abram, U., Schubiger, A.P. *Coord. Chem. Rev.* **190-192** (1999) 901-919.
[5] Pietzsch, H.J., Gupta, A., Reisgys, M., Drews, A., Seifert, S., Syhre, S., Spies, H., Alberto, A. Abram, U., Schubiger, A., Johannsens, B. *Bioconjugate Chem*. **11** (2000) 414-424.
[6] Gerber, T.I.A., Betz, R., Booyen, I.N., Potgieter, K.C., Mayer, P. *Polyhedron*. **30** (2011) 1739-1745.
[7] Martínez-García, H., Morales, D., Pérez, J., Puerto, M., Río, I.D. *Chem. Eur. J*. **20** (2014) 5821-5834.

complex with the tridentate ligand, (**1**) in this case. Chapter 6 describes the synthesis and characterization of these four complexes in more detail. The crystallographic data of the crystal structures of *fac*-[$Re_2(CO)_6$(TS)(Py)] (**1**), *fac*-[$Re_2(CO)_6(PPh_3)(BSOPhC)_2$(Py)] (**2**), *fac*-[$NEt_4$][$Re_2(CO)_6(BSOPhC)_3$] (**3**) and *fac*-[$Re_2(CO)_6(\mu\text{-}\eta^4$-m-TolBSPh-S-S-m-TolBSPh)] (**4**) are listed in Table 5.1 and Table 5.2, with Py = pyridine and PPh_3 = triphenylphosphine.

Scheme 5.1: General synthetic procedure used for synthesizing Re (I) tricarbonyl complexes.

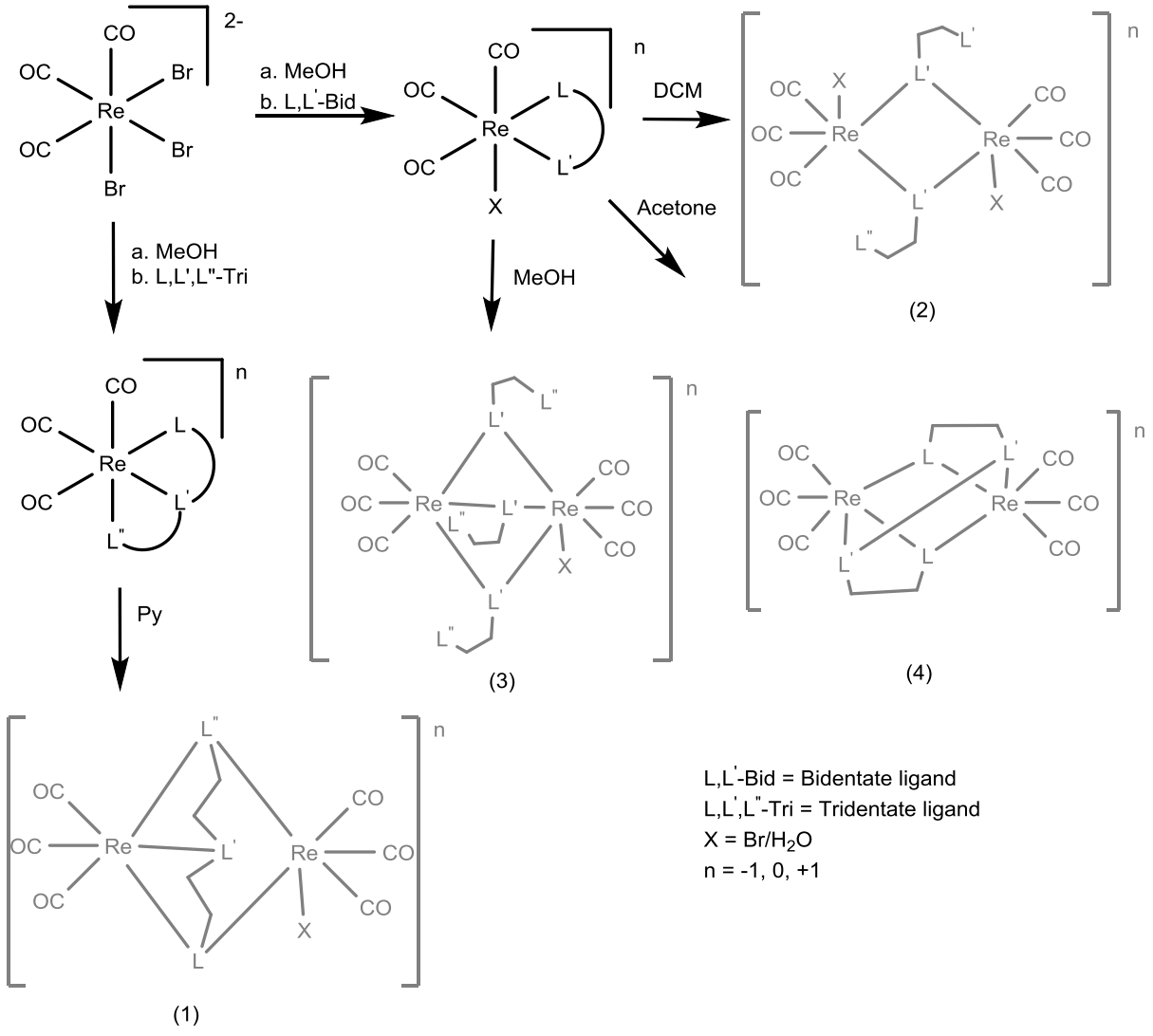

5.2 Experimental

A Bruker X8 Apex II 4K diffractometer equipped with graphite monochromated Mo *K*α radiation with a wavelength of λ = 0.71073 Å and ω- and φ-scans at 100K was used to collect the reflection data of all the structures reported here. The SIR-97[8] package was used to solve all structures while it was refined with WinGX[9] and SHELXL-97.[10] The cell refinement was done with SAINT-Plus[11] and the data reduction with SAINT-plus and XPREP.[11] The SADABS[12] software package with the multi-scan technique was used to obtain absorption corrections, while the molecular graphics and presentation was done with Diamond.[13] All structures are drawn with thermal ellipsoids at a 50 % probability level. All non-hydrogen atoms were anisotropically refined. The methylene, methyl and aromatic hydrogen atoms were placed in geometrically idealized positions and constrained to ride on their parent atoms with C-H = 0.99 Å, 0.95 Å and 0.98 Å and $U_{iso}(H) = 1.5U_{eq}(C)$ and $1.2U_{eq}(C)$ (for methylene and methyl), respectively.

There is an indication of an unresolved solvent molecule within the unit cell as indicated by the elevated electron density peak in (**1**) ($\rho_{max} = 6.821$ and $\rho_{min} = -7.352$ e Å^{-3}). The solvent has not been modelled as illustrated in the current structure as the structure and possible disorder is not fully understood.

[8] Altomare, A., Burla, M.C., Camalli, M., Cascarano, G.L., Giacovazzo, C., Guagliardi, A., Moliterni, A.G.G., Polidori, G., Spagna, R., J. *Appl. Cryst*.**32 (**1999) 115-119.
[9] Farrugia, L.J., *J. Appl. Cryst*. **32** (1999) 837-838.
[10] Sheldrick, G.M., *SHELXL97*, Program for the refinement of crystal structures, University of Göttingen, Germany, 1997.
[11] Bruker, *SAINT-Plus*, Version 7.12 (including XPREP), Bruker AXS Inc., Madison, Wisconsin, USA, 2004.
[12] Bruker, *SADABS*, Version 2004/1, Bruker AXS Inc., Madison, Wisconsin, USA, 1998.
[13] Brandenburg, K., Putz, H., *DIAMOND*, Release 3.0e, Crystal Impact GbR, Bonn, Germany, 2006.

Table 5:1: Crystallographic data of *fac*-$[Re_2(CO)_6(TS)(Py)]$ (1) and *fac*-$[Re_2(CO)_6(PPh_3)(BSOPhC)_2(Py)]$ (2).

Crystallographic data	1	2
Emperical formula	$C_{15}H_{13}NO_6S_3Re_2$	$C_{43}H_{34}NO_8PS_2Re_2$
Formula weight (g mol^{-1})	771.91	1160.22
Crystal system	Triclinic	Monoclinic
Space group	$P\bar{1}$	$P2_1/c$
a (Å)	9.520(5)	12.165(5)
b (Å)	14.951(5)	19.027(5)
c (Å)	16.036(5)	18.848(5)
α (º)	104.677(5)	90
β (º)	106.849(5)	108.735(5)
$_{\gamma}$(º)	104.452(5)	90
Volume ($Å^{-3}$)	1980.4(14)	4131(2)
Z	4	4
P_{calc} (g cm^{-3})	2.834	1.818
Crystal colour	Colourless	Yellow
Crystal morphology	Plate	Cuboid
Crystal size	0.29 x 0.691 x 0.946	0.125 x 0.229 x 0.319
μ (mm^{-1})	12.878	6.029
F (000)	1583	6.029
Θ range (º)	2.27 – 28.43	3.130 – 27.998
Index ranges	-12≤h≤12 -20≤h≤20 -21≤h≤21	-16≤h≤16 -25≤h≤24 -24≤h≤24
Reflections collected	50644	82039
Unique reflections	7731	9939
Reflection with I>2σ	9262	9291
R_{int}	0.0665	0.0921
Completeness to 2 theta (º, %)	7731/0/522	9939/0/514
GooF	1.066	1.037
R[I>2σ(I)]	R_1= 0.1109 wR_2 = 0.3536	R_1= 0.0308 wR_2 = 0.0599
R(all data)	R_1= 0.1238 wR_2 = 0.3631	R_1= 0.0483 wR_2 = 0.0682
ρ_{max} and ρ_{min} (e.$Å^{-3}$)	6.821 and -7.352	1.617 and -1.225

Table 5:2: Crystallographic data of *fac*-[NEt_4][$Re_2(CO)_3(BSOPhC)_3$] (3) and *fac*-[$Re_2(CO)_6(\mu\text{-}\eta^4\text{-m-TolBSPh-S-S-m-TolBSPh})$] (4).

Crystallographic data	3	4
Emperical formula	$C_{35}H_{41}NO_9S_3Re_2$	$C_{20}H_{12}O_6S_4Re_2$
Formula weight (g mol^{-1})	1088.4	849.02
Crystal system	Monoclinic	Triclinic
Space group	*Cc*	$P\bar{1}$
a (Å)	12.712(5)	9.783(5)
b (Å)	17.105(5)	11.128(5)
c (Å)	18.144(5)	12.073(5)
α (º)	90	112.269(5)
β (º)	91.470(5)	102.269(5)
γ(º)	90	97.357(5)
Volume ($Å^{-3}$)	3944(2)	1156(9)
Z	4	4
P_{calc} (g cm^{-3})	1.763	2.621
Crystal colour	Colourless	Red
Crystal morphology	Cuboid	Cuboid
Crystal size	0.124 x 0.166 x 0.303	0.112 x 0.152 x 0.277
μ (mm^{-1})	6.34	14.276
F (000)	2322	832
Θ range (º)	2.975 – 27.991	2.62- 28.22
Index ranges	-16≤h≤16 -22≤h≤22 -23≤h≤23	-12≤h≤12 -14≤h≤14 -15≤h≤15
Reflections collected	37682	19188
Unique reflections	9291	5781
Reflection with I>2σ	8095	6255
R_{int}	0.0848	0.0454
Completeness to 2 theta (º, %)	25.24, 99.8	25.24,99.4
GooF	9291/2/476	5541/0/268
R[I>2σ(I)]	R_1 = 0.0397 wR_2 = 0.0926	R_1 = 0.0340 wR_2 = 0.0913
R(all data)	R_1 = 0.0493 wR_2 = 0.0982	R_1 = 0.0508 wR_2 = 0.1301
ρ_{max} and ρ_{min} (e.$Å^{-3}$)	0.829 and -0.874	1.785 and -2.249

5.3 Crystal structure of *fac*-[$Re_2(CO)_6(TS)(Py)$] (1)

The synthesis of *fac*-[$Re_2(CO)_3(TS)(Py)$] (**1**) is described in Chapter 4. Colourless crystals of this neutral dinuclear sulphide complex were obtained from a 100 % pyridine solution. The compound crystallized in the triclinic $P\bar{1}$ space group with four dinuclear Re_2-units in the unit cell (Z = 4). The two rhenium metal centres are in different coordination environments; Re1 is coordinated to a pyridine ligand and two thiolato sulphur atoms (of the TSH_2 ligand) that bridge to the next rhenium atom (Re2) while Re2 is coordinated to three thiolato sulphur atoms, with two S atoms bridging to Re1. Both the rhenium atoms are also coordinated to three carbonyl ligands. The molecular structure of (**1**) is given in Figure 5.1 below.

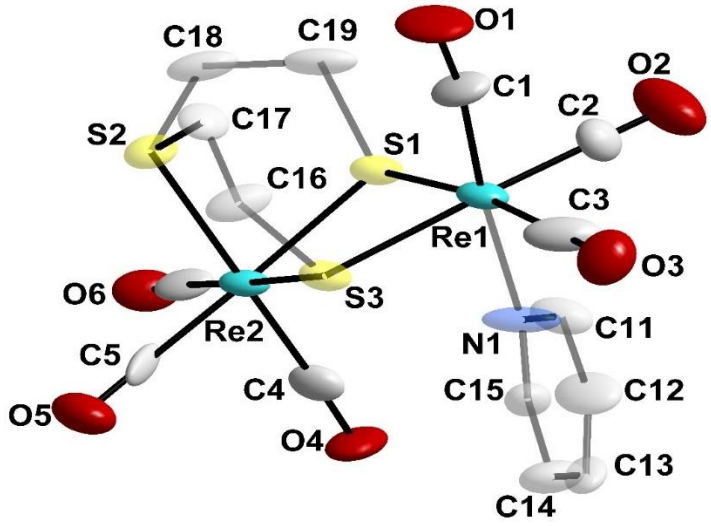

Figure 5.1: Molecular representation of the crystal structure of *fac*-[$Re_2(CO)_6(TS)(Py)$] (1), hydrogen atoms were omitted for clarity. For aromatic rings, the first number represents the ring number and the second number represents the specific C-atom in the ring. For clarity and increased depth perception, certain atoms have been illustrated with higher transparency.

A summary of the general crystal data of (**1**) is given in Table 5.1. Selected bond distances and bond angles are reported in Table 5.3.

Table 5:3: Selected bond distances and bond angles for the structure of (1) (Å, °).

Selected bond distances (Å)			
Re1-C2	1.88(3)	Re1-N1	2.22(2)
Re1-C1	1.90(3)	Re1-S3	2.526(7)
Re1-C3	1.94(4)	Re1-S1	2.562(7)
Re2-C4	1.91(3)	Re2-S2	2.459(7)
Re2-C5	1.92(4)	Re2-S3	2.499(7)
Re2-C6	1.93(3)	Re2-S1	2.513(7)
Selected bond angles (°)			
Re2-S3-Re1	98.1(2)	S3-Re1-S1	80.2(2)
Re2-S1-Re1	96.8(2)	S3-Re2-S1	81.6(2)
C1-Re1-C2	85.4(14)	C4-Re2-C5	87.1(11)
C1-Re1-C3	86.8(14)	C4-Re2-C6	83.5(11)
C2-Re1-C3	86.1(15)	C5-Re2-C6	87.1(12)
C1-Re1-S1	102.1(10)	C4-Re2-S1	96.2(9)
C1-Re1-S3	98.1(10)	C4-Re2-S3	97.5(9)
N1-Re1-S1	82.3(8)	S2-Re2-S1	82.7(2)
N1-Re1-S3	85.4(8)	S2-Re2-S3	85.3(2)
C1-Re1-N1	174.7(14)	C4-Re2-S2	176.8(8)

The non-bonding distance between the two rhenium atoms, Re···Re was determined as 3.796(8) Å. The rhenium to carbon bond distance of the carbonyl ligands vary from 1.88 Å to 1.94 Å and are in range with similar structures.[14,15,16,17,18,19,20,21,22] Each thiolato-bridge is asymmetrical with non-equal Re-S bond distances. The rhenium sulphur bond distances are determined as 2.526(7) Å for Re1-S3, 2.562(7) Å for Re1-S1, 2.459(7) Å for Re2-S2, 2.499(7) Å for Re2-S3 and 2.513(7) Å for Re2-S1. The rhenium to pyridine (N1) distance was determined as 2.22(2) Å. All the bond distances compare well to similar structures reported. [14,15,23,24]

Distorted octahedral geometries around the rhenium centres are evident in the angles of 98.1(2) º for Re2-S3-Re1, 96.8(2) º for Re2-S1-Re1, 80.2(2) º for S3-Re1-S1, 81.6(2)º for S3-Re2-S1, 82.7(2) º for S2-Re2-S1 and 85.3(2) º for S2-Re2-S3. The expected linear angles deviate quite significantly from 180 ° as observed in the coordination of pyridine to Re1 to C1 and in S2-Re2-C4 with determined angles of 174.7(14) º and 176.8(8) º respectively. These angles were compared to similar

[14] Fuks, L., Gniazdowska, E., Kozminski, P. *Polyhedron*. **29** (2010) 634-638.
[15] Makris, G., Karagiorgou, O., Papagiannopoulor, D., Papagiannopoulor, A., Raptopoulou, C.P., Terzis, A., Pyscharis, V., Pelecanou, M., Pirmettis, I., Papadopoulos, M.S. *Eur. J. Inorg. Chem*. **19** (2012) 3132-3139.
[16] Schutte, M., Visser, H.G., Roodt, A. *Acta Cryst*. ***E64*** (2008) m1610-m1611.
[17] Brasey, T., Buryak, A., Scopelliti, R., Severin, K. *Eur. J. Inorg. Chem*. **5** (2004) 964-967.
[18] Schutte, M., Visser, H.G. *Acta Cryst*. ***E64*** (2008) m1226-m1227.
[19] Schutte, M., Visser, H.G., Steyl, G. *Acta Cryst*. ***E63*** (2007) m3195-m3196.
[20] Schutte, M., Visser, H.G., Brink, A. *Acta Cryst*. ***E65*** (2009) m1757-m1576.
[21] Alberto, R., Herrmann, W.A., Kiprof, P., Baumgartner, F. *Inorg. Chem*. ***31*** (1992) 895-899.
[22] Vassiliadis, V., Triantis, C., Catherine P. Raptopoulou, C. P., Vassilis Psycharis, V.,Terzis, A., Ioannis Pirmettis, I., Papadopoulos, M. S., Papagiannopoulou, D. *Polyhedron* **81** (2014) 511–516.
[23] Núñez-Montenegro, A., Carballo, R., Vázquez-López, E.M. *J. Inorg. Biochem* **140** (2014) 53–63.
[24] Herrick, R.S., Ziegler, C.J., Sripothongnak, S., Barone, N., Costa, R., Cupelo, W., Gambella. *J. Organomet.* Chem. **694** (2009) 3929-3934.

reported structures and were found to be in agreement.[14,15,25] The $Re_2(\mu\text{-}S)_2$ unit is non-coplanar with a dihedral angle of 21.728(3) º calculated between the planes through O6..C6..O5..C5..Re2..S1..S3 and O3..C3..O2..C2..Re1..S1..S3. (Figure 5.2). Re1 and Re2 are displaced perpendicular to plane O3..C3..O2..C2..Re1..S1..S3 and plane O6..C6..O5..C5..Re2..S1..S3 by 0.1087 Å and -0.0306 Å. The distance between Re1 and the green plane (O6..C6..O5..C5..Re2..S1..S3) is a bit shorter compared to the distance between Re2 and the red plane (O3..C3..O2..C2..Re1..S1..S3) and was determined as -0.5704 Å and -0.7561 Å respectively.

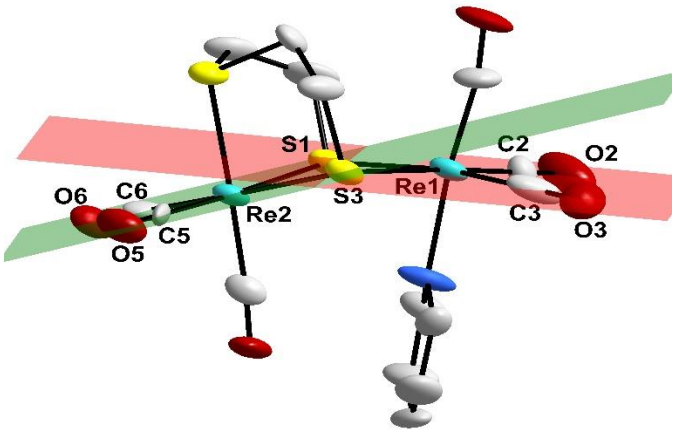

Figure 5.2: Illustration of the planes through O6..C6..O5..C5..Re2..S1..S3 and O3..C3..O2..C2..Re1..S1..S3 with a dihedral angle of 21.728(3) º in the structure of (1). Hydrogen atoms are omitted for clarity.

The observed bending at S1/S3 (dihedral angle of 21.728(3)°) could possibly be due to the pyridine ligand coordinated to Re1 and the steric bulk of the TS ligand (containing three sulphur atoms), coordinated to Re2 that is in a *trans* orientation and also the bending/twisting of the TS ligand to coordinate in a tridentate fashion to Re2.

The crystal structure of (**1**) is stabilized by six C-H…O intermolecular hydrogen interactions. The bonding distances, angles and symmetry operators are presented in Table 5.4. The intermolecular hydrogen interactions contributing to the molecular packing of (**1**) is illustrated in Figure 5.3 (a and b).

[25] Vanitha, A., Sathiya, P., Sangilipandi,S., Mobin, S.M., Manimaran, B. *J. Organomet.* Chem. **695** (2010) 1458-1463.

Table 5:4: Summary of the hydrogen interactions observed in (1) (Å, º).

D-H…A	d (D-H)	d (H…A)	d (D…A)	D-H…A angle
C13-H13...O6[a]	0.93	2.54	3.14(5)	122
C19-H19D…O6[b]	0.96	2.44	3.33(4)	154
C17-H17D...O2[c]	0.97	2.43	3.37(4)	163
C13-H13 ...O4[d]	0.93	2.51	3.29(5)	142’
C11-H11 …O5[e]	0.93	2.56	3.22(4)	128
C18-H18A ...O6[b]	0.97	2.55	3.42(4)	149

Symmetry code, transformations used to generate equivalent atoms: [a]1+x,y,z; [b]1-x,1-y,1-z; [c]x,1+y,z; [d]2-x,1-y,1-z; [e]x,-1+y,z

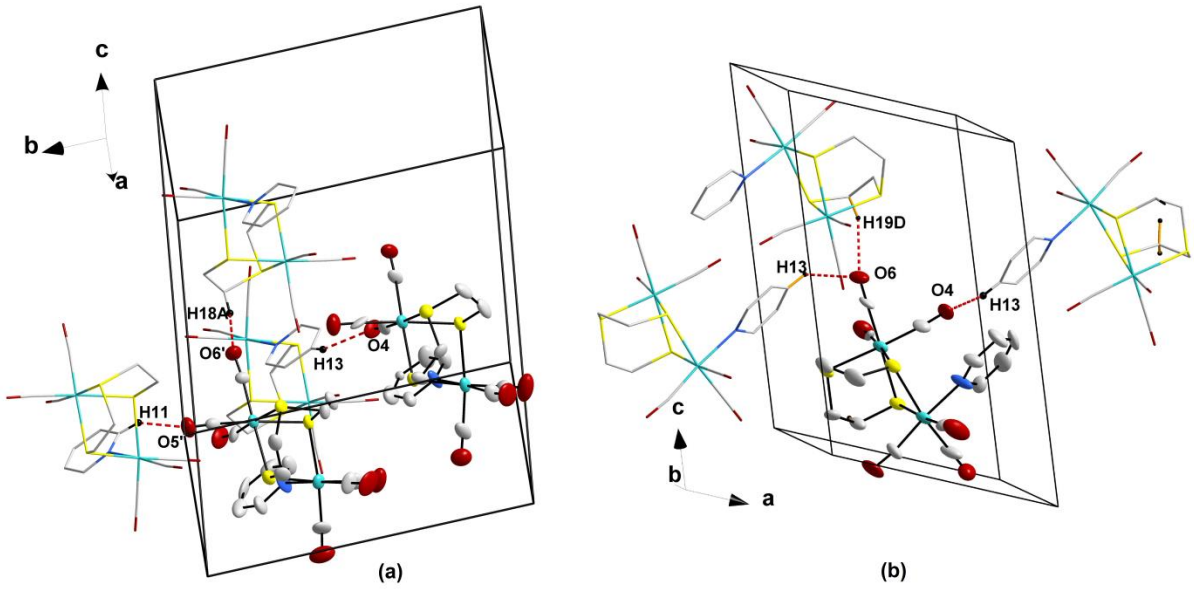

Figure 5.3: The six intermolecular hydrogen interactions observed in the structure of (1) ((a) and (b) for clarity). Hydrogen atoms and numbering of atoms not associated with the hydrogen interactions are omitted for clarity.

The molecules pack in a head-to-head fashion diagonally across the *b,c*-plane as illustrated in Figure 5.4.

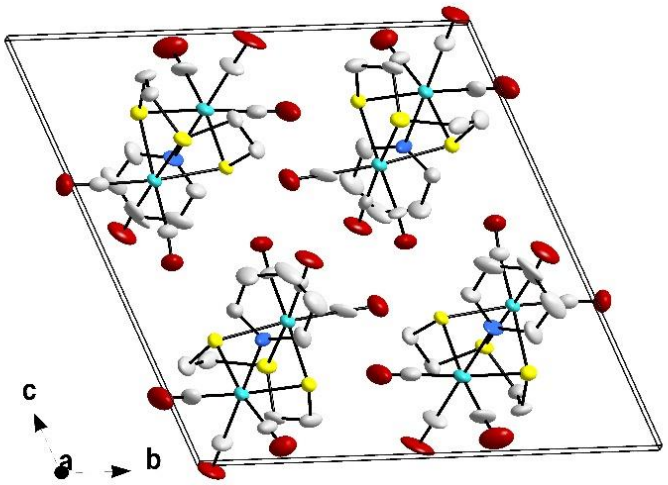

Figure 5.4: Molecular packing of (1) in the unit cell viewed along the *b,c*-plane. Hydrogen atoms and numbering omitted for clarity.

5.4 Crystal Structure of *fac*-[$Re_2(CO)_6(PPh_3)(BSOPhC)_2(Py)$] (2)

The synthesis of *fac*-[$Re_2(CO)_6(PPh_3)(BSOPhC)_2(Py)$] (**2**) is described in Chapter 4. The yellow crystals of this neutral dinuclear disulphide complex were obtained from a methanol:DCM solution (3:1 ratio). The compound crystallized in the monoclinic $P2_1/c$ space group with four dinuclear Re_2 entities in the unit cell (Z = 4). The two rhenium metal centres are in different coordination environments. Re1 and Re2 are coordinated to two 2-methoxythiophenol ligands in a monodentate bridging fashion. Re1 is coordinated to a triphenylphosphine ligand and two sulphur atoms (two 2-methoxythiophenol ligands) that bridge to the next rhenium atom (Re2). Re2 is coordinated to a pyridine ligand and two sulphur atoms (two 2-methoxythiophenol ligands) that bridge to Re1. Both Re1 and Re2 are also coordinated to three carbonyl ligands. The molecular diagram with the numbering scheme for (**2**) is presented in Figure 5.5.

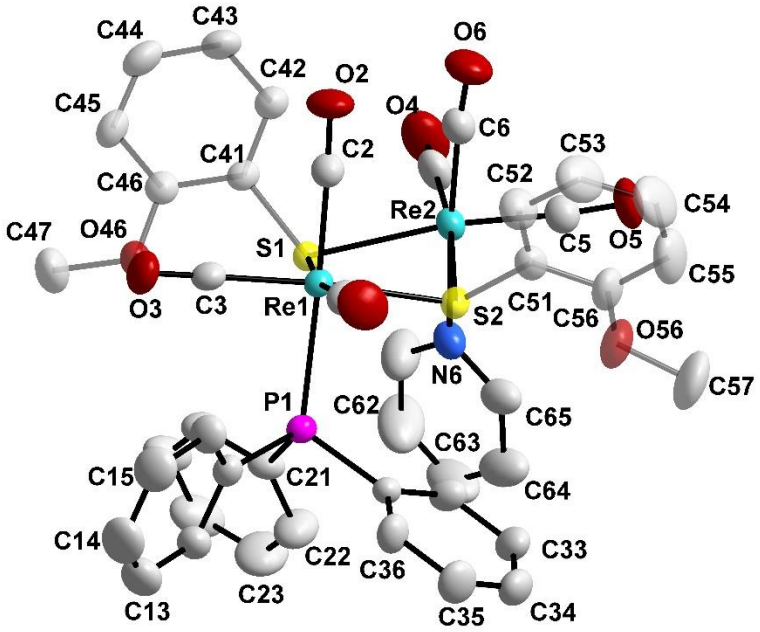

Figure 5.5: Molecular representation of the crystal structure of *fac*-$[Re_2(CO)_6(PPh_3)(BSOPhC)_2(Py)]$ (2). Hydrogen atoms and numbering for certain atoms are omitted for clarity. For aromatic rings, the first number represents the ring number and the second number represents the specific C-atom in the ring. For clarity and increased depth perception, certain atoms have been illustrated with higher transparency.

A summary of the general crystal data of (**2**) is given in Table 5.1. Selected bond distances and bond angles are reported in Table 5.5.

Table 5:5: Selected bond distances and bond angles of the structure of (2) (Å, °).

Selected bond distances (Å)			
Re1-C3	1.922(4)	Re2-C6	1.920(5)
Re1-C1	1.923(5)	Re2-C4	1.919(5)
Re1-C2	1.939(5)	Re2-C5	1.920(5)
Re1-S2	2.5006(13)	Re2-S2	2.497(13)
Re1-P1	2.5103(12)	Re2-N6	2.235(4)
Re1-S1	2.5507(13)	Re2-S1	2.544(15)
Selected bond angles (°)			
C3-Re1-C1	92.23(19)	C3-Re1-S1	96.83(13)
C3-Re1-C2	89.84(18)	C1-Re1-S1	170.34(15)
C1-Re1-C2	90.96(19)	C2-Re1-S1	85.72(14)
C3-Re1-S2	171.01(13)	S2-Re1-S1	76.26(3)
C1-Re1-S2	95.06(14)	P1-Re1-S1	95.06(4)
C2-Re1-S2	95.29(13)	C6-Re2-N6	176.16(16)
C3-Re1-P1	88.00(13)	C4-Re2-N6	91.19(19)
C1-Re1-P1	88.60(14)	C5-Re2-N6	92.47(17)
C2-Re1-P1	177.77(13)	Re2-S1-Re1	98.01(3)
N6-Re2-S2	85.33(11)	S2-Re2-S1	76.44(4)
N6-Re2-S1	83.37(10)	P1-Re1-C2	177.77(13)
Re2-S2-Re1	100.60(4)	C6-Re2-N6	176.16(16)
S2-Re1-P1	86.93(4)		

The non-bonding distance between the two rhenium atoms, Re···Re was determined as 3.845(10) Å. The six rhenium to carbonyl distances of 1.923(5) Å, 1.939(5) Å, 1.922(4) Å, 1.919(5) Å, 1.920(5) Å and 1.920(5) Å (for C1, C2, C3, C4, C5 and C6 respectively) are well within the normal range of similar structures.[14-22] The rhenium sulphur bond distances show a small variation and are reported as 2.5006(13) Å for Re1-S2, 2.5507(13) Å for Re1-S1, 2.497(13) Å for Re2-S2 and 2.544(15) Å for Re2-S1 but are found to be in agreement with other reported structures.[14,15] The rhenium to nitrogen (pyridine) and rhenium to phosphorus (triphenylphosphine) distances are reported as 2.235(4) Å and 2.5103(12) Å respectively. All the bond distances compare well to similar reported structures. [23,24]

Distorted octahedral geometries around the rhenium atoms are evident in the angles of 98.01(3) º for Re2-S1-Re1, 100.60(4) º for Re2-S2-Re1, 76.44(4) º for S2-Re2-S1 and 76.26(3) º for S2-Re1-S1. Two nearly straight line angles are observed in the coordination of pyridine (N6) and triphenylphosphine (P1) to Re2 and Re1 respectively with P1-Re1-C2 reported as 177.77(13) º and C6-Re2-N6 reported as 176.16(16) º. These angles were compared to other reported structures and were found to be in normal range.[14,15,25] The $Re_2(\mu\text{-}S)_2$ unit is non-coplanar with a dihedral angle of 24.39(10) º calculated between the planes through O5..C5..C4..O4..Re2..S1..S2 and O3..C3..O1..C1..Re1..S1..S2 (Figure 5.6). Re1 and Re2 are displaced perpendicular to plane O3..C3..O1..C1..Re1..S1..S2 and O5..C5..C4..O4..Re2..S1..S2 by 0.0122 Å and -0.0534 Å. Very similar distances of -0.8745 Å between Re1 and the green plane (O5..C5..C4..O4..Re2..S1..S2) and 0.9113 Å between Re2 and the red plane (O3..C3..O1..C1..Re1..S1..S2) was determined.

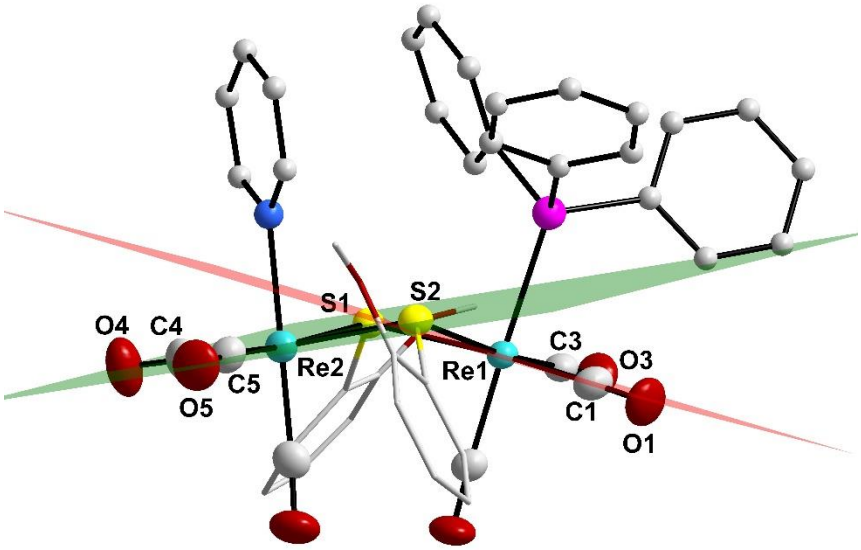

Figure 5.6: Illustration of the planes O5..C5..O4..C4..Re2..S1..S2 and O3..C3..O1..C1..Re1..S1..S2 with a dihedral angle of 24.39(10) º in the structure of (2). Hydrogen atoms and numbering for certain atoms were omitted for clarity.

The bending seen at S1/S2 (dihedral angle of 24.39(10) °) could possibly illustrate the effect of the pyridine and triphenylphosphine ligands on the coordination sphere. The pyridine and triphenylphosphine ligands are coordinated in a *cis* orientation.

No hydrogen interactions or pi-pi interactions are observed in the structure of (**2**). The molecules pack in a head-to-tail fashion along the *b*-axis when viewed along the *b,c*-plane as shown in Figure 5.7.

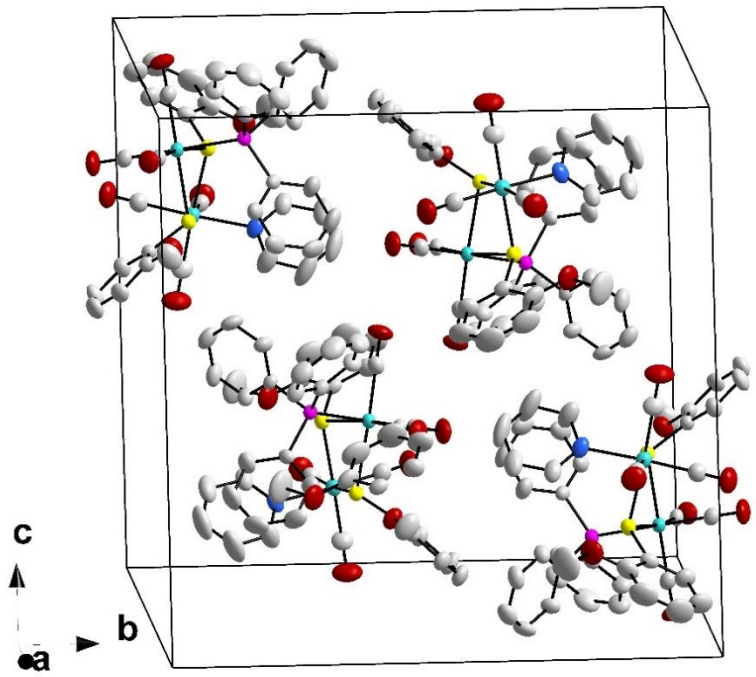

Figure 5.7: Molecular packing of (2) in the unit cell viewed along the *b,c*-plane. Hydrogen atoms and numbering were omitted for clarity.

5.5 Crystal structure of *fac*-[NEt_4][$Re_2(CO)_6(BSOPhC)_3$] (3)

The synthesis of *fac*-[NEt_4][$Re_2(CO)_6(BSOPhC)_3$] (**3**) is described in Chapter 4. Colourless crystals of this dinuclear trisulphide structure were obtained from a methanol solution. The compound crystallized in the monoclinic, *Cc* space group with four dinuclear Re_2-units in the unit cell (Z = 4). The two rhenium metal centres are in similar coordination environments. Re1 and Re2 are coordinated to three sulphur atoms from the 2-methoxythiophenol ligands that form three bridges between the two rhenium atoms and both are coordinated to three carbonyl ligands. The tetraethylammonium cation is positionally disordered in a 0.50:0.50 ratio. The molecular diagram with the numbering scheme for (**3**) is presented in Figure 5.8.

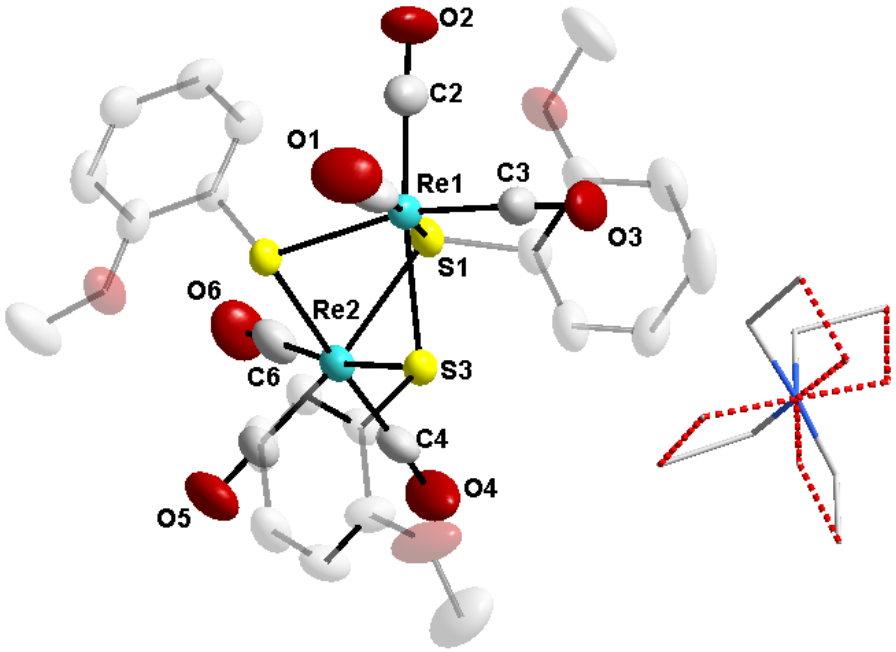

Figure 5.8: Molecular representation of the crystal structure of *fac*-[NEt_4][$Re_2(CO)_6(BSOPhC)_3$] (3) with the disordered tetraethylammonium cation. Hydrogen atoms and numbering for certain atoms were omitted for clarity. For aromatic rings, the first number represents the ring number and the second number represents the specific C-atom in the ring. For clarity and increased depth perception, certain atoms have been illustrated with higher transparency.

A summary of the general crystal data of (**3**) is given in Table 5.2. Selected bond distances and bond angles of (**3**) are reported in Table 5.6.

Table 5:6: Selected bond distances and bond angles for the structure of (3) (Å, °).

Selected bond distances (Å)			
Re1-C1	1.886(15)	Re1-S1	2.511(3)
Re1-C3	1.909(15)	Re1-S2	2.500(3)
Re1-C2	1.924(15)	Re1-S3	2.536(3)
Re2-C4	1.900(15)	Re2-S1	2.511(3)
Re2-C6	1.905(15)	Re2-S3	2.518(3)
Re2-C5	1.910(14)	Re2-S2	2.530(3)
Selected bond angles (º)			
C1-Re1-C3	90.1(7)	C2-Re1-S3	168.3(5)
C1-Re1-C2	87.9(7)	Re2-S1-Re1	87.97(10)
C3-Re1-C2	88.9(6)	Re2-S3-Re1	87.28(9)
C1-Re1-S2	94.9(5)	Re2-S2-Re1	87.78(10)
C3-Re1-S2	165.2(5)	S2-Re1-S1	77.14(10)
C2-Re1-S2	105.2(4)	S2-Re2-S1	76.60(10)
C1-Re1-S1	171.7(5)	S2-Re1-S3	77.51(10)
C3-Re1-S1	98.3(5)	S1-Re1-S3	77.48(10)
C2-Re1-S1	91.9(5)	S1-Re2-S3	77.82(10)
C1-Re1-S3	103.3(5)	S2-Re2-S3	77.32(10)
C3-Re1-S3	87.8(5)		

The non-bonding distance between the two rhenium atoms, Re···Re was determined as 3.488(10) Å. The six rhenium to carbonyl bond distances 1.886(15) Å, 1.924(15) Å, 1.909(15) Å, 1.900(15) Å, 1.910(14) Å and 1.905(15) Å (for C1, C2, C3, C4, C5 and C6) are well within the normal range. [14-22] Each sulfido-bridge is asymmetrical with unequal Re-S distances. The rhenium sulphur bond distances are determined as 2.511(3) Å for Re1-S1, 2.500(3) Å for Re1-S2, 2.536(3) Å for Re1-S3, 2.511(3) Å for Re2-S1, 2.530(3) Å for Re2-S2 and 2.518(3) Å for Re2-S3 and are in agreement with other reported structures.[14,15] All the bond distances of (**3**) are within normal range and agree well with similar reported structures. [23,24]

Distorted octahedral geometries around the rhenium atoms are evident in the angles of 87.97(10) º for Re2-S1-Re1, 87.78(10) º for Re2-S2-Re1, 87.28(9) º for Re2-S3-Re1, 76.60(10) º for S2-Re2-S1 and 77.14(10) º for S2-Re1-S1, 77.51(10) º for S2-Re1-S3, 77.48(10) º for S1-Re1-S3, 77.82(10) º for S1-Re2-S3 and 77.32(10) º for S2-Re2-S3. These angles compare well with other reported structures.[14,15,25] The $Re_2(\mu\text{-}S)_2$ unit is non-coplanar with a dihedral angle of 62.365(3) º calculated between the planes through O3..C3..O1..C1..Re1..S1..S2 and O5..C5..O4..C4..Re2..S1..S2, 62.100(3) º between the planes through O2..C2..O1..C1..Re1..S1..S3 and O6..C6..O5..C5..Re2..S1..S3 and 62.055(3) º between the planes through O3..C3..O2..C2..Re1..S2..S3 and O6..C6..O4..C4..Re2..S2..S3, illustrated in Figure 5.9, Figure 5.10 and Figure 5.11 respectively. Re1 and Re2 are displaced perpendicular to plane O3..C3..O1..C1..Re1..S1..S2 and O5..C5..O4..C4..Re2..S1..S2 by 0.1088 Å and -0.0673 Å (Figure 5.9). The distances between Re1 and the green plane (O5..C5..O4..C4..Re2..S1..S2) and Re2 and the red plane (O3..C3..O1..C1..Re1..S1..S2) are determined as 1.6760 Å and -1.7189 Å respectively.

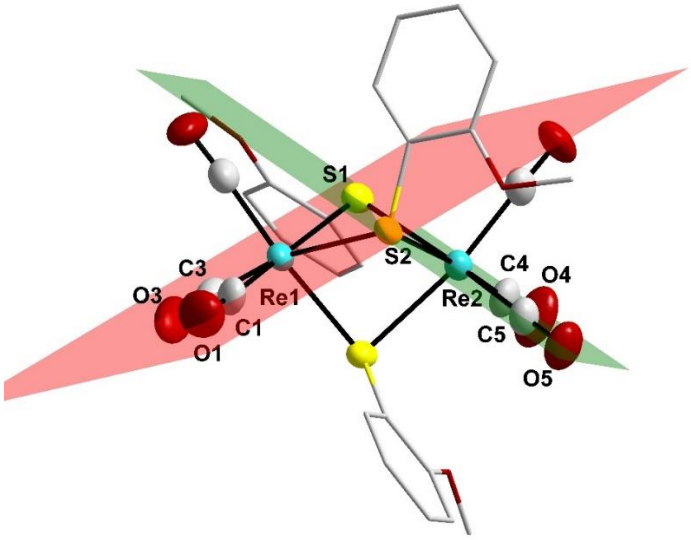

Figure 5.9: Illustration of the dihedral angle of 62.365(3) º between the planes O3..C3..O1..C1..Re1..S1..S2 and O5..C5..O4..C4..Re2..S1..S2.

Re1 and Re2 are displaced perpendicular to plane O2..C2..O1..C1..Re1..S1..S3 and O6..C6..O5..C5..Re2..S1..S3 by 0.0423 Å and -0.1489 Å (Figure 5.10). Similar distances between Re1 and the green plane (O6..C6..O5..C5..Re2..S1..S3) and Re2 and the red plane (O2..C2..O1..C1..Re1..S1..S3) are determined as 1.7495 Å and -1.6447 Å respectively.

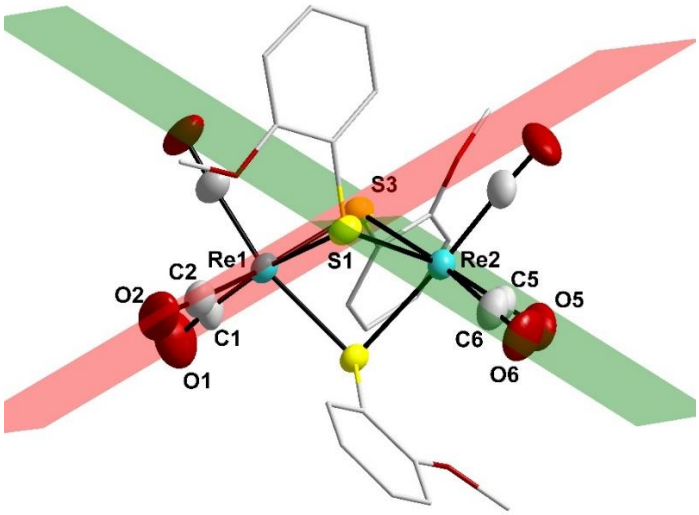

Figure 5.10: Illustration of the dihedral angle of 62.100(3) º between the planes O2..C2..O1..C1..Re1..S1..S3 and O6..C6..O5..C5..Re2..S1..S3.

Re1 and Re2 are displaced perpendicular to plane O3..C3..O2..C2..Re1..S2..S3 and O6..C6..O4..C4..Re2..S2..S3 by 0.1286 Å and -0.0584 Å (Figure 5.11). Similar distances between Re1 and the green plane (O6..C6..O5..C5..Re2..S1..S3) and Re2 and the red plane (O2..C2..O1..C1..Re1..S1..S3) are determined as 1.6584 Å and -1.7491 Å respectively.

The crystal structure of (**3**) is stabilized by one intermolecular hydrogen interaction that is illustrated in Figure 5.12 below. The bond distances and angle are reported in Table 5.7.

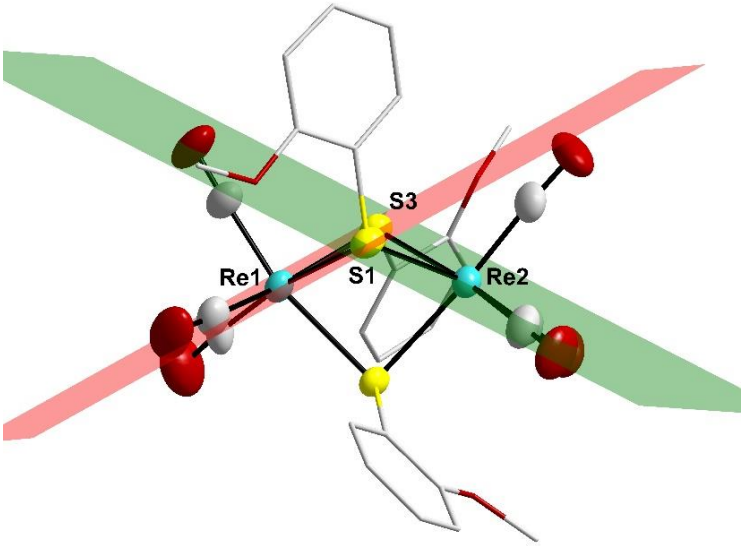

Figure 5.11: Illustration of the dihedral angle of 62.055(3) ° between the planes O3..C3..O2..C2..Re1..S2..S3 and O6..C6..O4..C4..Re2..S2..S3.

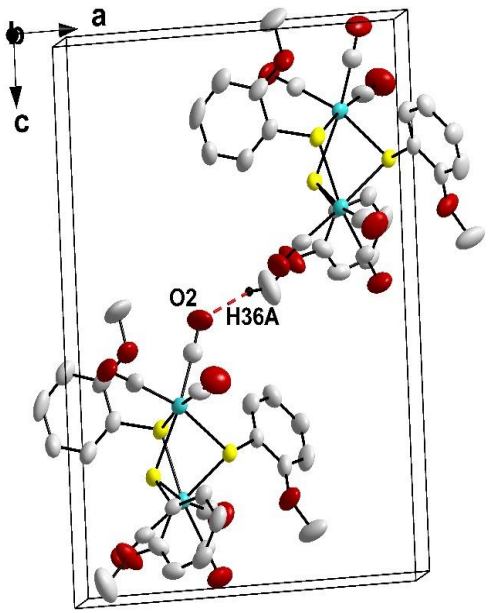

Figure 5.12: Hydrogen interaction observed in the structure of (3), viewed along the *b*-axis. Hydrogen atoms not taking part in the interactions, cations and numbering for certain atoms were omitted for clarity.

Table 5:7: Summary of the hydrogen interaction observed in (3) (Å, º).

D-H…A	d (D-H)	d (H…A)	d (D…A)	D-H…A angle
C36-H36A…O2[a]	0.96	2.42	3.37(3)	167

Symmetry code, transformations used to generate equivalent atoms:[a] -1/2+x, 1/2+y, 1/2+z

Some intramolecular O-π interactions are observed in the structure of (**3**). The oxygen to centroid distances are reported as 3.826 (15) Å for O5 to the centroid Cg6 (ring C21) and 3.695 (17) Å for O6 to the centroid Cg5 (ring C31). Figure 5.13 gives an illustration of the O-π interactions within the structure of (**3**). The bonding distances and angle are reported in Table 5.8.

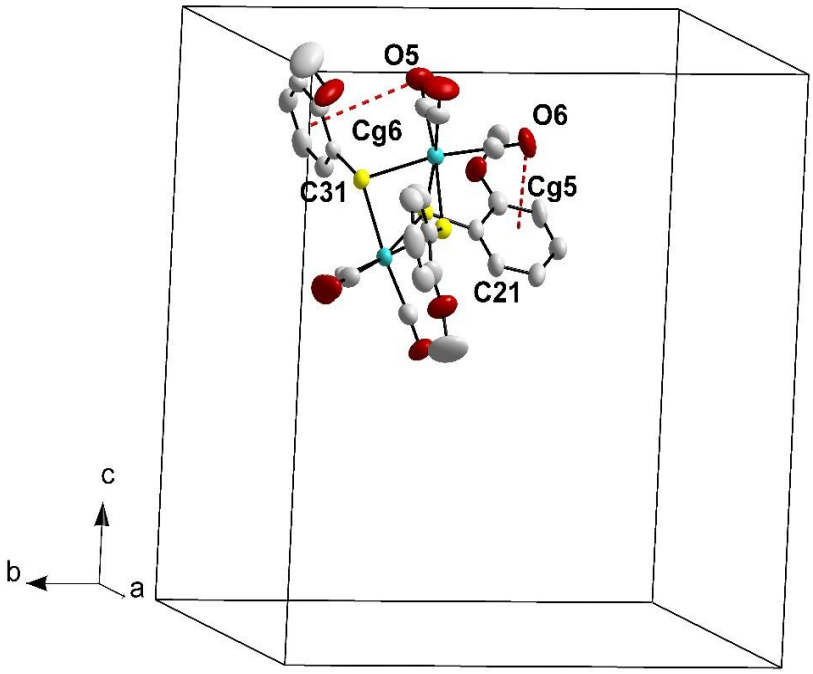

Figure 5.13: O-π interactions observed in the structure of (3), viewed along the *b,c*-plane. Hydrogen atoms, cations and numbering for certain atoms were omitted for clarity.

Table 5:8: The summary of O-π interaction observed in the structure of (3) (Å,º)

Y—X (I)	Res (I) Cg(J)	X..Cg	Y-X…Cg	Y..Cg
C5-O5	[1] → Cg6	3.806 (14)	82.4 (10)	3.826 (15)
C6-06	[1] → Cg5	3.666 (14)	82.6 (10)	3.695 (17)

Symmetry code, transformations used to generate equivalent atoms: x, y, z; Cg5 = centroid atoms of C20, C21, C22, C23, C24, C25; Cg6 = centroid atom of C30, C31, C32, C33, C34, C35.

The molecules pack in a head-to-tail fashion along the *b*-axis in alternating layers when viewed along the *b,c*-plane as shown in Figure 5.14.

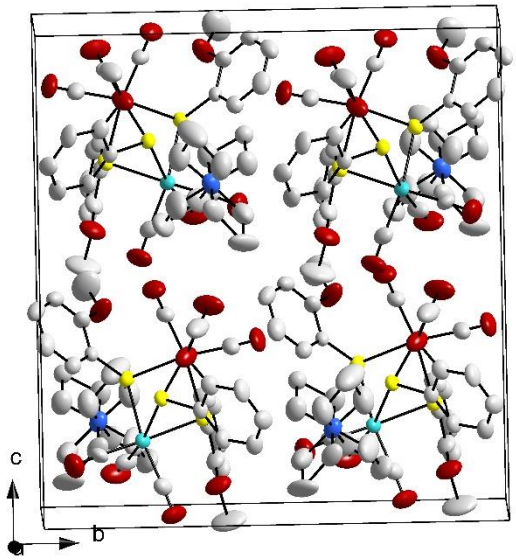

Figure 5.14: Molecular packing of the structure of (3) when viewed along *b,c*-plane. Hydrogen atoms and numbering for atoms were omitted for clarity.

5.6 Crystal structure of *fac*-[$Re_2(CO)_6(\mu\text{-}\eta^4$-m-TolBSPh-S-S-m-TolBSPh)] (4)

The synthesis of *fac*-[$Re_2(CO)_6(\mu\text{-}\eta^4$-m-TolBSPh-S-S-m-TolBSPh)] (**4**) is described in Chapter 4. This structure has been reported before by Begum *et al*.[26] Red crystals of this neutral dinuclear sulphide structure were obtained from an acetone solution. The compound crystallized in the monoclinic, *Cc* space group with four dinuclear Re_2-units in the unit cell (Z = 4). The two rhenium metal centres are in similar coordination environments: Re1 and Re2 are coordinated in a similar way to two toluene-3,4-dithiol ligands in a monodentate bridging fashion followed by the S-S bridging of these two ligands and both are coordinated to three carbonyl ligands. The S-S bridging is an interligand disulphide bond formation between the two dithiolate ligands. This is also observed in the structure reported by Begum *et al*. The molecular diagram with the numbering scheme for (**4**) is presented in Figure 5.15.

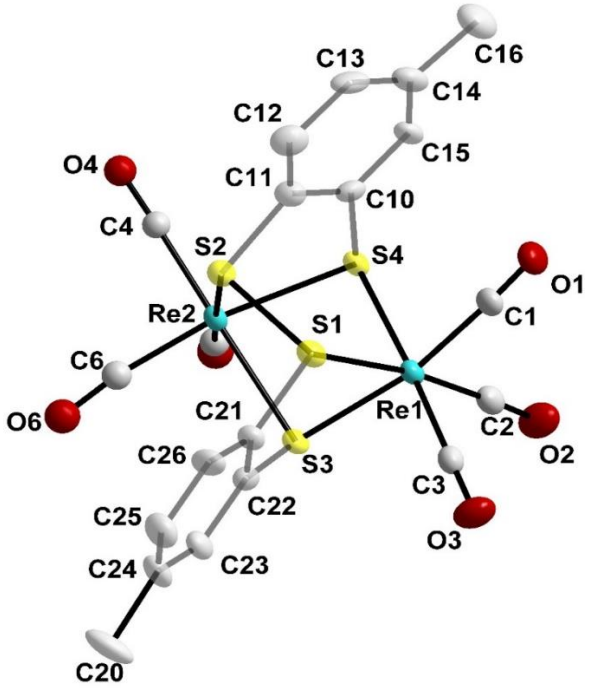

Figure 5.15: Molecular representation of the structure of *fac-[*$Re_2(CO)_6(\mu\text{-}\eta^4$-m-TolBSPh-S-S-m-TolBSPh)] (4). Hydrogen atoms and numbering for certain atoms were omitted for clarity. For aromatic rings, the first number represents the ring number and the second number represents the specific C-atom in the ring. For clarity and increased depth perception, certain atoms have been illustrated with higher transparency.

A summary of the general crystal data of (**4**) is given in Table 5.2. Selected bond distances and bond angles are reported in Table 5.9 below.

Table 5:9: Selected bond distances and bond angles for the structure of (4) (Å, °).

Selected bond distances (Å)			
Re1-C1	1.939(9)	Re1-S1	2.473(2)
Re1-C2	1.949(10)	Re1-S2	2.442(2)
Re1-C3	1.924(9)	Re1-S4	2.543(2)
Re2-C4	1.939(9)	Re2-S1	2.541(2)
Re2-C5	1.917(9)	Re2-S3	2.432(2)
Re2-C6	1.935(9)	Re2-S4	2.490(2)
S3-S2	2.228(3)	Re2-S2	2.431(9)
Selected bond angles (º)			
C3-Re1-C1	93.6(4)	S2-Re2-S3	94.956(12)
C3-Re1-C2	87.2(4)	S3-Re2-S4	80.797(12)
C1-Re1-C2	91.0(4)	S2-Re2-S4	80.850(12)
C3-Re1-S2	86.9(3)	S3-Re1-S4	81.082(12)
C1-Re1-S2	93.2(3)	S2-S3-Re2	102.60(10)
S1-Re1-S4	94.228(12)	Re2-S3-Re1	93.09(8)
S1-Re1-S3	80.884(13)	Re2-S4-Re1	93.11(7)

The non-bonding distance between the two rhenium atoms, Re···Re were found to be 3.654(16) Å. The six rhenium to carbonyl bond distances of 1.939(9) Å, 1.949(10) Å, 1.924(9) Å, 1.939(9) Å, 1.917(9) Å and 1.935(9) Å (for C1, C2, C3, C4, C5 and C6) are well within the normal range. [14-22] Each sulfido-bridge is asymmetrical with unequal Re-

S distances. The rhenium sulphur bond distances are reported as 2.473(2) Å for Re1-S1, 2.442(2) Å for Re1-S2, 2.536(3) Å for Re1-S3, 2.541(2) Å for Re2-S1, 2.431(9) Å for Re2-S2, 2.432(2) Å for Re2-S3 and 2.490(2) Å for Re2-S4 and are found to be in agreement with similar reported structures.[14,15] Sulphur atoms S1 and S2 are coordinated to each other with a bond distance of 2.226(7) Å. All the bond distances are in good agreement with similar reported structures in literature.[23,24,26]

Distorted octahedral geometries around the rhenium atoms are evident in the angles of 93.55(8) º for Re2-S3-Re1, 93.11(7) º for Re2-S4-Re1, 94.228(12) º for S1-Re1-S4, 80.797(12) º for S3-Re2-S4, 94.956(12) º for S2-Re2-S3, 80.884(13) º for S1-Re1-S3, 80.850(12) º for S2-Re2-S4 and 81.082(12) º for S3-Re1-S4. These angles are all within the normal range.[14,15,25] The $Re_2(\mu\text{-}S)_2$ unit is non-coplanar with a dihedral angle of 37.770(3) º between the planes through O3…C3…O1…C1..Re1..S3..S4 and O6…C6…O4…C4..Re2..S3..S4 (Figure 5.16). Re1 and Re2 are displaced perpendicular to the plane O3…C3…O1…C1..Re1..S3..S4 and O6…C6…O4…C4..Re2..S3..S4 by -0.0423 Å and -0.0215 Å respectively. Similar distances between Re1 and the green plane (O6…C6…O4…C4..Re2..S3..S4) and Re2 and the red plane (O3…C3…O1…C1..Re1..S3..S4) are obtained, 1.0765 Å and 1.1261 Å. A definite downward bending of the rhenium (I) tricarbonyl entities are observed at S3 and S4, to accommodate the S-S bond formation between the two bidentate ligands.

[26] Begum, N., Hyder, M.I., Kabir, S.E., Hossain, G.M.G., Nordlander, E., Rokhsana, D., Roserberg, E. *Inorg. Chem*. **44**, (2005) 9887-9894.

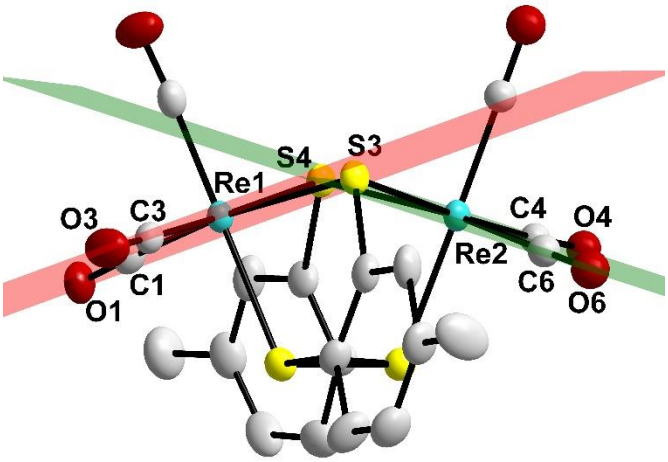

Figure 5.16: Illustration of the dihedral angle between the planes O3…C3…O1…C1..Re1..S3..S4 and O6…C6…O4…C4..Re2..S3..S4 of 37.770(3) ° in the structure of (4). Hydrogen atoms and numbering for certain atoms were omitted for clarity.

The molecules pack in a head-to-tail fashion along the *a*-axis and form one-dimensional encapsulated tunnels when viewed along the *b,c*-plane (Figure 5.17).

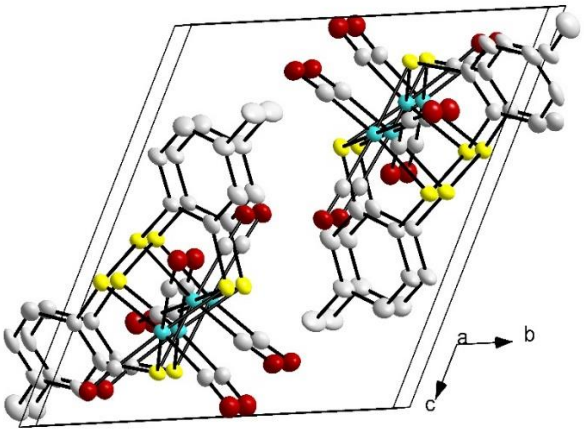

Figure 5.17: Molecular packing of (4) in the unit cell viewed along the *a*-axis. Hydrogen atoms and numbering for atoms were omitted for clarity.

5.7 Discussion

In this chapter four rhenium (I) crystal structures were evaluated, *fac*-[$Re_2(CO)_6$(TS)(Py)] (**1**), *fac*-[$Re_2(CO)_6(PPh_3)$(BSOPhC)(Py)] (**2**), *fac*-[NEt_4][$Re_2(CO)_6$(BSOPhC)$_3$] (**3**) and *fac*-[$Re_2(CO)_6$(μ-η^4-m-TolBSPh-S-S-m-TolBSPh)] (**4**). (**1**) and (**4**) both crystallized in a triclinic crystal system and were refined in the standard space group $P\bar{1}$. (**1**) and (**4**) both have four molecules per unit cell (Z = 4). Complex (**2**) and (**3**) crystalized in a monoclinic crystal system and were refined in a standard space group $P2_1/c$ and *Cc* respectively, with Z = 4 in (**2**) and (**3**). (**1**) and (**3**) were stabilized by a variety of intermolecular hydrogen bonding and (**3**) were also stabilized by two O-π interactions that plays a role in the stabilization of this metal complex.

Table 5.10 below gives a summary of the bond distances and angles of the structures (**1**) - (**4**). The bond distances and bond angles of all four the crystal structures were in agreement with the reported values of similar crystal structures in literature.[1-25] The rhenium carbonyl bond distances vary between 1.88(3) Å (for (**1**)) and 1.95(10) Å (for (**4**)) while the rhenium sulphur distances vary between 2.43(2) Å (for (**4**)) and 2.56(7) Å (for (**1**)). Vassiliadis *et al.*[22] reported a structure similar to that of (**1**) and (**2**) and the Re-P and Re-N bond distances of (**1**) and (**2**) are in good agreement with this. (**1**) has a Re-N bond distance of 2.22(2) Å, (**2**) has a Re-N bond distance of 2.24(4) Å and a Re-P bond distance of 2.51(12) Å.

Table 5:10: Summary of the bond distances (Å) and angles (º) of crystal structures (1), (2), (3) and (4).

	(1)		(2)	
	Unit 1	**Unit 2**	**Unit 1**	**Unit 2**
Re-CO	1.90(3) 1.88(3) 1.93(4)	1.91(3) 1.92(3) 1.93(3)	1.92(5) 1.93(5) 1.92(3)	1.92(5) 1.92(5) 1.92(5)
Dihedral angle between CO-CO-Re-S-S planes[a]	21.728(3) º		24.389(3) º	
Re-S	2.56(7) 2.53(7)	2.51(7) 2.46(7) 2.50(7)	2.55(13) 2.50(13)	2.54(15) 2.50(13)
Re-X	2.22(2)	-	2.51(12) (X = P)	2.24(4) (X = N)
S-Re-S	80.20(2)	85.30(2) 82.70(2) 81.60(2)	76.26(3)	76.44(4)
Re-S-Re	96.80(2)	98.00(2)	98.01(3)	100.60(4)
S- Re-S-Re	14.003(16)		21.962(11)	
Re-S-Re-S	13.975(16)		22.555(12)	
Re···Re	3.796(8)		3.845(10)	

	(3)		(4)	
	Unit 1	**Unit 2**	**Unit 1**	**Unit 2**
Re-CO	1.89(15) 1.92(15) 1.91(15)	1.90(15) 1.91(14) 1.91(15)	1.94(9) 1.95(10) 1.92(9)	1.94(9) 1.92(9) 1.94(9)
Dihedral angle between CO-CO-Re-S-S planes[a]	62.365(3) 62.100(3) 62.055(3)		37.770(3)	
Re-S	2.51(3) 2.50(3) 2.54(3)	2.51(3) 2.53(3) 2.52(3)	2.47(2) 2.44(2) 2.54(2)	2.54(2) 2.43(2) 2.49(2)
Re-X	-	-	-	-
S-S	-	-	-	2.23(3)
S-Re-S	77.16(10) 77.52(10) 77.48(10)	77.82(10) 76.60(10) 77.31(10)	80.98(8) 94.23(8)	80.86(7) 94.99(8) 80.78(7)
Re-S-Re	87.97(10) 87.28(9)	87.77(10)	93.55(8)	93.11(7)
S- Re-S-Re	39.439(11)		25.675(13)	
Re-S-Re-S	39.696(11)		25.620(13)	
Re···Re	3.488(10)		3.654(16)	

[a] for (1) plane O6..C6..O5..C5..Re2..S1..S3 and plane O3..C3..O2..C2..Re1..S1..S3; (2) plane O5..C5..C4..O4..Re2..S1..S2 and plane O3..C3..O1..C1..Re1..S1..S2; (3) plane O3..C3..O1..C1..Re1..S1..S2 and plane O5..C5..O4..C4..Re2..S1..S2, plane O2..C2..O1..C1..Re1..S1..S3 and plane O6..C6..O5..C5..Re2..S1..S3, plane O3..C3..O2..C2..Re1..S2..S3 and plane O6..C6..O4..C4..Re2..S2..S3; (4) plane O3..C3..O1..C1..Re1..S3..S4 and plane O6..C6..O4..C4..Re2..S3..S4.

Two of the coordinating ligands in (**4**) are bonded through a S1-S2 bond. The S1-S2 bond distance of 2.23(3) Å in (**4**) is almost identical to the reported structures by Begum *et al.*[26] of 2.2234(8) Å and 2.235(2) Å and Liaw *et al*.[27] of 2.222(1) Å. The same 'twisting' effect through the S1-S2 bond is seen in all these structures.

The Re-S bond distances in dinuclear crystal structures are longer than the Re-O and Re-N bond distances in similar dinuclear structures where distances of approximately

[27] Liaw, W.-F., Hsieh, C.-K., Lin, G.-Y., Lee, G.-H. *Inorg. Chem*. **40** (2001) 3468 – 3475.

2.1 Å and 2.2 Å are reported respectively.[28] The S-Re-S bite angles of these four complexes vary significantly from 76.26(3) ° in (**2**) to 94.99(8) ° in (**4**). This is comparable to other nitrogen and oxygen bridging dinuclear structures reported in literature as well as other sulphur bridging dinuclear structures.[28,29,30] The large variation in bite angle might be due to the severe twisting of the ligands in (**1**) and (**4**) and the possibility of limited space in (**2**) and (**3**) due to the bulky ligands in (**2**) and the fact that there are 3 sulphur bridges in (**3**).

The angle of the bridging atoms Re-S-Re increase from (**3**) with values of 87.97(10) °, 87.28(9) ° and 87.77(10) ° to (**4**) with values of 93.55(8) ° and 93.11(7) ° to (**1**) with values of 96.80(2) ° and 98.00(2) ° to (**2**) with values of 98.01(13) ° and 100.60(4) °. Although these angles vary substantially, this is within normal range and compare well with Re-N-Re and Re-O-Re values reported.[25,28,29] This same trend is observed in the Re···Re non-bonding distances. An increase from 3.488(10) Å for (**3**), 3.654(16) Å for (**4**), 3.796(8) Å for (**1**) and 3.845(10) Å for (**2**) is observed. This means that the closer the two rhenium atoms are, the smaller the Re-S-Re angles. This correlation is seen from (**3**) to (**4**) to (**1**) to (**2**).[29,25]

Three similar Re (I) tricarbonyl sulphido bridged metallacycles have been reported before.[31,32,33] The reported structures have Re-S and S-Re-S bond distances and angles that vary between 2.49 Å and 2.55 Å and 76.0 °and 80.7 °. This compares well to (**3**) with bond distances between 2.500 Å and 2.536 Å and bond angles of 76.60 ° to 77.82 °.

The dihedral angles (planes calculated as stated in Table 5.10) also show a significant variation. The smallest dihedral angle is found in (**1**) (21.728(3) º) followed by (**2**) (24.389(3) º) and (**4**) with 37.770(3)° and the largest angles in (**3**) with dihedral angles of 62.365(3), 62.100(3) and 62.055(3). The largest dihedral angles is (**3**) could be due to the three sulphur bridges in the structure. In (**4**) the dihedral angle is quite large possibly because of the bending of the two ligands to one another in order for the S-S

[28] Czerwieniec, R., Kapturkiewicz, A., Nowacki, J. *Inorg. Chem. Commun*. **8** (2005) 34-37.
[29] Gerber, T.I.A., Bertz, R., Booysen, I.N., Potgieter, K.C., Mayer, P. *Polyhedron*. **30** (2011) 1739-1745.
[30] Wilberger, R., Piotrowski, H., Mayer, P., Lorenz, I.-P. *Inorg. Chem. Commun*. **5** (2002) 897-902.
[31] Calhorda, M.J., Carrondo, M.A.A.F. de C.T., Dias, A.R., Félix, V., Galvão, A.M., Garcia, M.H., Matias, P.M., Villa de Brito, M.J. *J. Organomet. Chem*. **453** (1993) 231-240.
[32] Mattes, R., Weber, H. *J. Organomet. Chem*. **178** (1979) 191-196.
[33] Nefedov, S.E., Pasynskii, A.A., Eremenko, I.L., Papoyan, G.A., Rubinshtein, L.I., Yanovsky, A.I., Struchkov, Y.T. *Zh.Neorg.Khim.(Russ.)(Russ.J.Inorg.Chem.)* **38** (1993) 76.

bond to form. In (**2**) the PPh_3 and pyridine ligands are in a *cis* orientation, increasing the bulkiness on the one side of the rhenium atoms and therefore causing the twisting effect at the sulphur atoms. The smallest dihedral angle in (**1**) is within normal range of similar structures. The trend for the dihedral angles ((**1**) < (**2**) < (**4**) < (**3**)) is repeated in the torsion angles S-Re-S-Re and Re-S-Re-S, where (**1**) has the smallest torsion angles of 14.003(16) ° and 13.796(8) ° and (**3**) has the largest torsion angles 39.439(11) ° and 39.696(11) ° respectively.

The bond distances and bond angles of the two *fac*-$[Re(CO)_3]^+$ units in all of these dinuclear structures compare well (Table 5.10) and the only significant difference is seen in the bite angles S-Re-S in (**1**). This can be explained since Re1 is coordinated to two of the sulphur atoms in the TS ligand and a pyridine ligand complete the octahedral environment while Re2 is coordinated to three of the sulphur atoms in the TS ligand.

When comparing the structural data of (**1**), (**2**), (**3**) and (**4**) with the data reported by Schutte and Brink[34,35,36] (Table 5.11) of *fac*-$[Re(CO)_3(L,L'\text{-bid})(X)]^n$ type complexes (L,L'-bid = N,O and O,O' bidentate ligands, X = Br-, H_2O, CH_3OH and n = 0, -1), a few observations can be made.

Overall, the rhenium carbonyl distances of the dinuclear structures reported here and that reported in Table 5.11 are in good agreement. No significant differences are seen in the dinuclear (S,O, S,S' and S,S',S' ligands) *vs* mononuclear structures (N,O and O,O' ligands).

[34] Schutte, M. MSc dissertation. University of the Free State, Bloemfontein, South Africa, 2008.
[35] Schutte, M. Thesis. University of the Free State, Bloemfontein, South Africa, 2008.
[36] Brink, A. Thesis. University of the Free State, Bloemfontein, South Africa, 2008.

Table 5:11: Summary of crystal structures reported by Schutte and Brink.

	Re-CO	Re-N	Re-O	Re-X	Bite Angle
O,O' bidentate ligands					
***fac*-[NEt_4][$Re(CO)_3(TropBr_3)(Br)$]**[34]	1.897(3) 1.894(3) 1.898(3)	-	2.1411(18) 2.1322(17)	2.6270(3)	73.56(6)
***fac*-[$Re(CO)_3(Flav)(CH_3OH)$].CH_3OH**[34]	1.894(5) 1.905(5) 1.906(5)	-	2.147(3) 2.141(3)	2.204(4)	76.24(11)
***fac*-[NEt_4][$Re(CO)_3(Trop)(Br)$]**[35]	1.906(5) 1.903(5) 1.861(7)[a] 1.923(18)[b]		2.126(3) 2.135(3)	2.6334(9)[a] 2.467(16)[b]	74.88(12)
***fac*-[NEt_4] [$Re(CO)_3(Trop)(H_2O)$].NO_3.H_2O**[35]	1.894(8) 1.886(8) 1.890(7)		2.121(5) 2.108(4)	2.213(5)	74.82(17)
N,O bidentate ligands					
***fac*-[NEt_4][$Re(CO)_3$(2,5-PicH)(Br)].H_2O**[35]	1.906(7) 1.904(7) 1.963(7)	2.182(5)	2.152(15)	2.6188(13)	74.38(18)
***fac*-[$Re(CO)_3(CH_3OH)$(Sal-mTol)]**[36]	1.913(6) 1.919(6) 1.890(6)	2.157(4)	2.179(3)	2.179(3)	84.6(1)
***fac*-[$Re(CO)_3(CH_3OH)$(Sal-Ph)]**[36]	1.920(7) 1.909(7) 1.895(7)	2.164(6)	2.121(5)	2.188(9)	84.4(2)
***fac*-[$Re(CO)_3(CH_3OH)$(Sal-*p*Tol]**[36]	1.90(3) 1.95(2) 1.89(2)	2.15(2)	2.133(16)	2.42(10)a 2.170(3)[b]	84.8(7)
***fac*-[$Re(CO)_3(CH_3OH)$(Sal-CyHex)]**[36]	1.896(11) 1.894(3) 1.869(10)	2.202(9)	2.131(7)	2.172(8)	84.6(3)

[a] and [b] are disordered atoms

The Re-S bond distances are significantly longer than the Re-N and Re-O bond distances with distances determined between 2.43(2) Å and 2.56(7) Å for Re-S, 2.15(2) Å and 2.202(9) Å for Re-N and 2.108(4) Å and 2.179(3) Å for Re-O as expected for these particular donor atoms. The S-Re-S bite angles vary significantly between 76.26(3) ° and 94.99(8) °. The N-Re-O bite angles vary between 74.38(18) ° and 84.8(7) ° while the O-Re-O bite angles vary from 73.56(6) ° and 74.88(12) °. The following trend is seen in the bond distances: Re-O ≤ Re-N <Re-S with the Re-S bond distances significantly longer than the Re-N and Re-O distances and the average Re-N bond distances are slightly longer than the average Re-O distances. The same trend is seen in the bite angles of these complexes: O,O' complexes < N,O complexes < S,O/S,S'/S,S',S'' complexes. This can be explained by the atomic radius of these donor atoms: O < N < S, with sulphur having the largest atomic radius. The Re-S bond distances and S-Re-S bond angles are therefore expected to be longer and larger, followed by Re-N and O-Re-N and with the Re-O distances and O-Re-O angles the shortest and smallest respectively. The steric bulk which must be accommodated by the Re-thio complexes would also significantly affect the range of the S-Re-S bite angles.

5.8 Conclusion

The four reported structures have bond distances and angles that compare well to each other and to other similar structures in literature. A correlation is found in the Re…Re non-bonding distance and the Re-S-Re angle, both following the trend: (**3**) < (**4**) < (**1**) < (**2**). Another correlation is found in the dihedral angle and the torsion angles S-Re-S-Re and S-Re-S-Re - ((**1**) < (**2**) < (**4**) < (**3**). More research will be required to fully understand the bonding modes of these type of ligand systems.

A comparison between N,O, O,O' (from previous studies), S,O, S,S' and S,S',S'' coordinated complexes could not really be made since all the complexes obtained from the S,O, S,S' and S,S',S'' ligands were dinuclear structures. But nevertheless the same expected trend is found, that follows the atomic radius trend of these donor atoms: Re-O ≤ Re-N < Re-S for the bond distances and O,O' complexes < N,O complexes < S,O/S,S'/S,S',S'' complexes for the bite angles. It is therefore imperative to investigate the synthetic process, bonding modes and coordination chemistry of these complexes in order to potentially obtain the mononuclear structures in future.

Only a few rhenium (I) tricarbonyl structures with S,S', S,S',S'' and S,O ligands have been reported before, so these structures contribute significantly to the available knowledge. In the following chapter a complete discussion is presented on the dinuclear structures obtained in this study and how it was identified and characterized.

6 ^{1}H NMR STUDY of RHENIUM (I) COMPOUNDS IN SOLUTION

6.1 Introduction

The crystal structures of four dinuclear rhenium (I) compounds were reported in Chapter 5. These dinuclear structures formed in spite of every effort on our side to synthesize mononuclear complexes. From the initial IR and NMR data it was assumed that mononuclear structures were synthesized, but the crystals obtained from recrystallization for all four these compounds were found to be dinuclear structures. Therefore it was decided to investigate the possibility of an equilibrium between the mononuclear and dinuclear structures in solution by using ^{1}H NMR spectroscopy.

In order to determine whether a mononuclear or dinuclear compound is present in solution, the use of a reference solvent was employed in each case. By integrating and comparing the number of hydrogen atoms of the added reference to that of the complex, one would easily determine whether the complex is a dinuclear or mononuclear complex in solution. It is imperative for the screening tests for anti-cancer activities as well as future cell studies to confirm the structure and also the stability of these complexes in solution.

6.2 *fac*-$[Re_2(CO)_6(TS)(Py)]$ (1) and *fac*-$[NEt_4][Re_2(CO)_6(TS)(Br)]$ (1a)

The Re (I) tricarbonyl complex synthesized in Chapter 5, *fac*-$[NEt_4][Re_2(CO)_6(TS)(Br)]$ (**1a**) was prepared from the *fac*-$[Re(CO)_3]^+$ precursor and TSH_2 (2,2-thiodiethanethiol) as tridentate ligand. The structure of (**1a**) and the expected structure (mononuclear) are presented in Scheme 6.1. It was impossible to confirm the structure of (**1a**) with ^{1}H

NMR since (**1a**) and the mononuclear (expected) complex have an equal amount of protons.

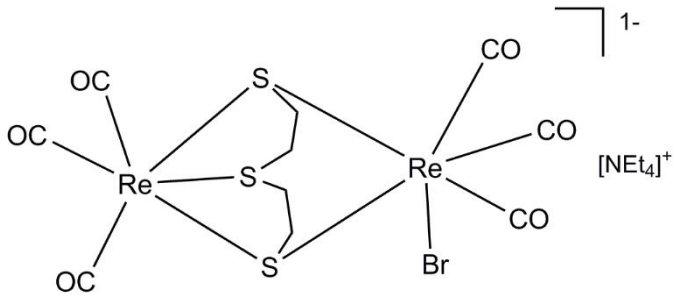

(**1a**)

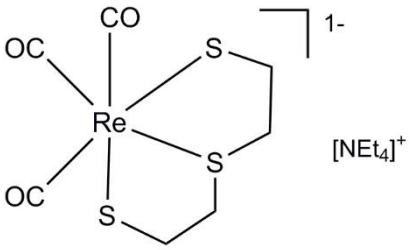

Expected mononuclear structure

Scheme 6.1: Schematic presentation of the structure of (1a) and the expected mononuclear structure of *fac*-[NEt_4][$Re(CO)_3(TS)$].

However, the crystal structure obtained from the recrystallization of (**1a**) in a 100% pyridine solution yielded the dinuclear structure *fac*-[$Re_2(CO)_6(TS)(Py)$] (**1**), illustrated in Scheme 6.2. Obviously pyridine reacted with the synthesized complex to yield the dinuclear complex (**1**). Pyridine was the only solvent in which suitable crystals were obtained and gave the added advantage that it is able to coordinate to rhenium in some cases.

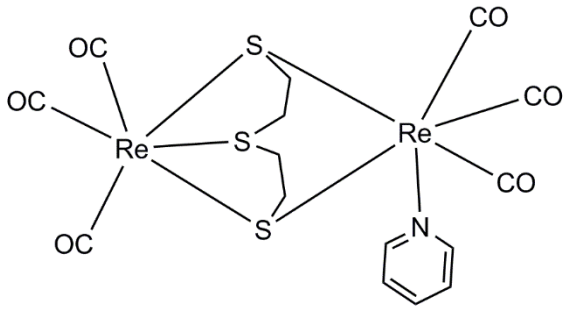

Scheme 6.2: Schematic representation of the obtained dinuclear structure (1).

The question remains whether the substitution process (entering pyridine ligand) involved a mononuclear or dinuclear rhenium (I) complex.

The ^1H NMR of (**1a**) [2.77 (t, 4H), 2.70 (t, 4H), 3.31 (q, 8H (NEt_4)), 1.17 (q, 12H (NEt_4)] was different to that obtained for (**1**) [9.26 (dd, 1H), 8.61 (dd, 2H), 8.35 (t, 2H), 3.99 (t,

4H), 3.89 (t, 4H)] in that the aromatic protons (pyridine contribution) were obviously not present. There was however, a similarity in the rest of the proton signals referring to the tridentate ligand. In order to confirm that the dinuclear complex (**1**) remains structurally intact in solution the following experiment was conducted.

A 1:1 mol ratio of (**1**) and benzene was dissolved in deuterated methanol and the ^{1}H NMR spectrum was obtained. The resulting integration and correlation between the hydrogen atoms of the complex *versus* that of the benzene reference was in a 13:6 ratio as expected. This does not exclude the possibility that the dinuclear compound did not dissociate to (a) and (b) illustrated in Scheme 6.3. However, we did not observe coordinated methanol hydrogen signals in the 2.5 to 3.8 ppm range as expected and conclude that the dinuclear complex probably remains stable in solution.

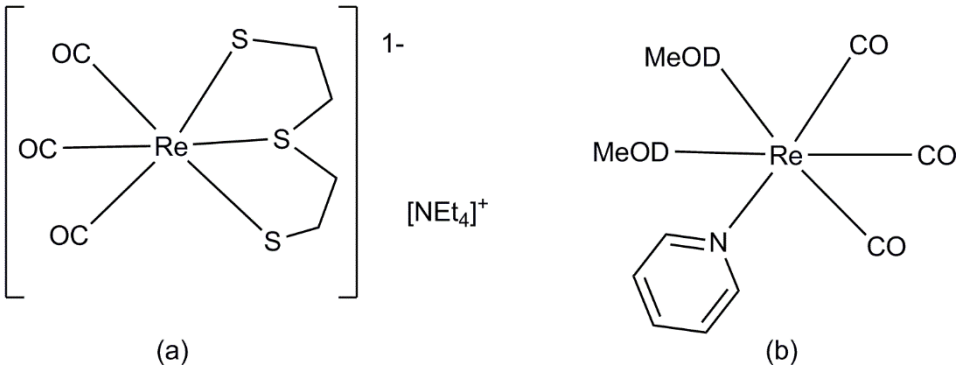

Scheme 6.3: Schematic representation of possible dissociation products of (1).

A literature search revealed that there are zero reports of dinuclear rhenium (I) tricarbonyl structures with a S,S',S'' tridentate ligands coordinated *via* two sulphido bridges.[1] ICP-OES and CHNS micro-analysis also confirmed the dinuclear nature of (**1a**). All the characterization data is presented in Chapter 4.

[1] *Cambridge Structural Database* (CSD), Version 5.36, Nov 2015 update. Allen, F.H. *Acta Cryst*. **B58** (2002**)** 380-388.

6.3 *fac*-$[Re_2(CO)_6(PPh_3)(BSOPhC)_2(Py)]$ (2) and *fac*-$[Re_2(CO)_6(PPh_3)_2(BSOPhC)_2]$ (2a)

The Re (I) tricarbonyl complex *fac*-$[Re_2(CO)_6(PPh_3)_2(BSOPhC)_2]$ (**2a**) synthesized in Chapter 5 was prepared from the *fac*-$[Re(CO)_3]^+$ precursor, BSOPhCH (2-methoxythiophenol) as bidentate ligand, PPh_3 and $NaHCO_3$ in methanol.[2] The structure of (**2a**) and the expected mononuclear structure is presented in Scheme 6.4.

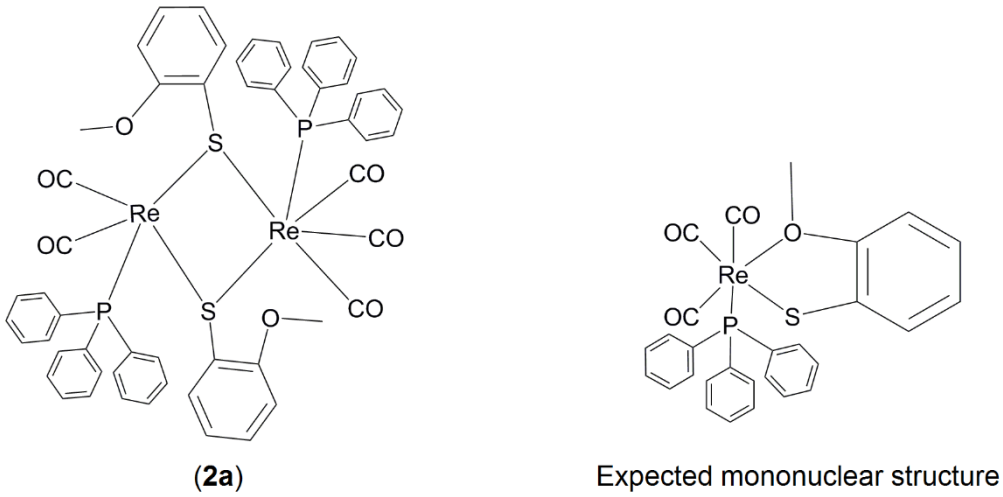

Scheme 6.4: Schematic presentation of (2a) and the expected mononuclear structure of *fac*-$[Re(CO)_3(BSOPhC)(PPh_3)]$.

As before, it was impossible to confirm the structure of (**2a**) with ^{1}H NMR. The NMR experiment was set up with one equivalent of (**2a**) and one equivalent of acetone as reference in deuterated DCM. The resulting integration and correlation between the hydrogen atoms of the ligands coordinated to the complex *versus* that of the acetone reference was in a 14:6 ratio as expected. The thirty aromatic hydrogen atoms for the two PPh_3 ligands were also confirmed (^{1}H NMR of (**2a**) - 7.76 - 6.70 (38H), 3.56 (6H)).

However, the crystal structure obtained from the recrystallization of (**2a**) in DCM and one equivalent of pyridine resulted in the formation of the dinuclear structure *fac*-$[Re_2(CO)_6(PPh_3)(BSOPhC)_2(Py)]$ (**2**), shown in Scheme 6.5. The ^{1}H NMR of (**2**) in

[2] Papagiannopoulou, D., Triantis, C., Vassileiadis, V., Raptopoulou, C.P., Psycharis, V., Terzis, A., Pirmettis, I., Papadopoulos, M.S. *Polyhedron* **68** (2014) 46-52.

deuterated DMSO confirmed that one PPh_3 ligand, one pyridine ligand and two BSOPhC ligands are in a 15:5:14 ratio (7.89 - 6.77 (28H), 3.83 (6H)). From this we assume that (**2a**) will also stay intact and are stable in solution.

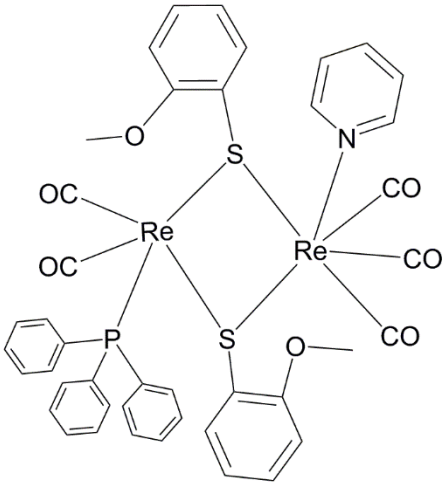

Scheme 6.5: Schematic representation of *fac*-[$Re_2(CO)_6(PPh_3)$(BSOPhC)(Py)] (2).

A literature search revealed five crystal structures similar to (**2**), with two sulphido bridges connecting the rhenium (I) tricarbonyl centres and with a non-sulphur ligand in the 6th position.[3,4,5] The five reported structures were all synthesized from dinuclear $Re_2(CO)_{10}$ as starting material, meaning that this is the first structure of this type that is synthesized from the *fac*-$[Re(CO)_3]^+$ synthon. By adding the bidentate ligand, triphenylphosphine and sodiumbicarbonate in methanol, the dinuclear structure is formed.

The bond distances and angles of the structure reported here (**2**) compare well with the similar structures in literature. ICP-OES and CHNS micro-analysis also confirmed the dinuclear nature of (**2a**). All the characterization data is presented in Chapter 4.

[3] Vanitha, A., Sathiya, P., Sangilipandi, S., Mobin, S.M., Manimaran, B. *J.Organomet.Chem.* **695** (2010) 1458-1463.

[4] Florke, U., Egold, H., Schwarze, D. *Acta Cryst.* **C56** (2000) 184-186.

[5] Eremenko, I.L., Pasynskii, A.A., Nefedov, S.E., Katugin, A.S., Kolobkov, B.I., Shaposhnikova, A.D., Stadnichenko, R.A., Yanovsky, A.I., Struchkov, Yu T. *Zh.Neorg.Khim.(Russ.)(Russ.J.Inorg.Chem.)* **37** (1992) 574-582.

6.4 *fac*-[NEt_4][$Re_2(CO)_6(BSOPhC)_3$] (3)

The Re (I) tricarbonyl complex (**3**) synthesized in Chapter 5 was prepared from *fac*-$[Re(CO)_3]^+$ and BSOPhCH (2-methoxythiophenol) as bidentate ligand. The expected structure is presented in Scheme 6.6.

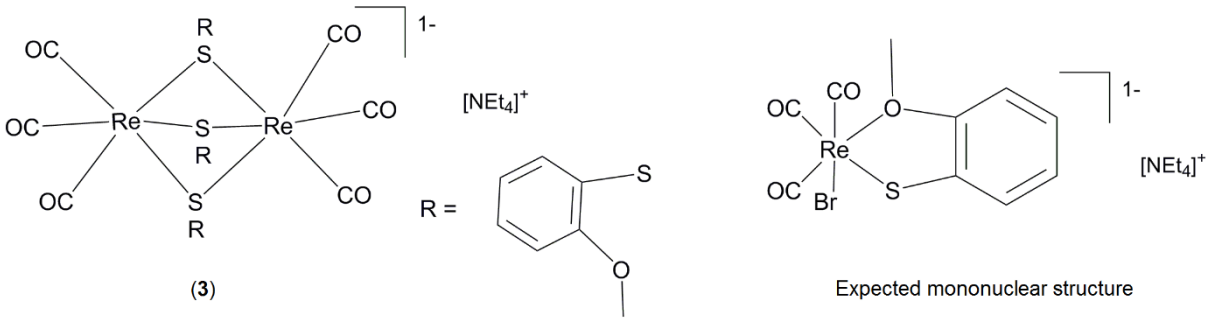

Scheme 6.6: Schematic representation of (3) and the expected structure of *fac*-[NEt_4][$Re(CO)_3$(BSOPhC)Br].

At first glance the IR data and the NMR data once again indicated the mononuclear complex. However, the crystals that formed from the slow evaporation of methanol as solvent yielded the dinuclear structure (**3**), presented in Scheme 6.6.

One equivalent of rhenium complex (**3**) and one equivalent of acetone was added to deuterated DCM. From the spectrum obtained it was confirmed that the complex synthesized was indeed the dinuclear structure, the same as the crystal structure. The resulting integration and correlation between the hydrogen atoms of (**3**) *versus* that of the acetone reference was in a 21:6 ratio as expected. The methyl hydrogen atoms of the ligand system are not equivalent and can be seen in a 6:3 ratio (7.42 (2H), 7.54 (2H), 7.20 (2H), 6.83 (6H), 3.94 (d, 9H), 2.93 (8H), 1.13(12H).

Only three other structures have been reported where three sulphido bridges connect the two rhenium (I) tricarbonyl centres.[6,7,8] The reported complexes are synthesized from $Re_2(CO)_{10}$ and $Re(CO)_5Br$ compared to the structure reported here where *fac*-$[Re(CO)_3]^+$ is used as starting material. The bond distances and angles, bite angles and non-bonding Re…Re distances of (**3**) and the three reported structures are in good agreement.

ICP-OES and CHNS micro-analysis also confirmed the dinuclear nature of (**3**). All the characterization data is presented in Chapter 4.

6.5 *fac*-[$Re_2(CO)_6$(μ-η^4-m-TolBSPh-S-S-m-TolBSPh)] (4)

The dinuclear compound (**4**) described in Chapter 5 was prepared with the aim of synthesizing the mononuclear complex presented in Scheme 6.7.

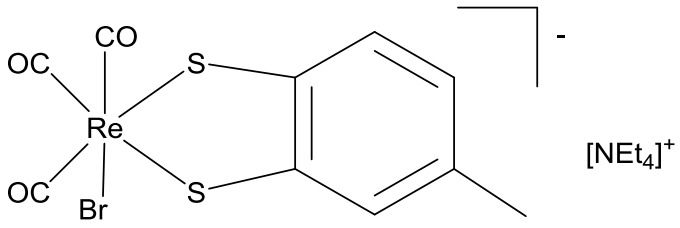

Scheme 6.7: Schematic presentation of the expected structure of *fac*-[NEt_4][$Re(CO)_3$(m-TolBSPh)Br].

However, the crystal structure obtained from the complex dissolved in acetone was the dinuclear complex *fac*-[$Re_2(CO)_6$(μ-η^4-m-TolBSPh-S-S-m-TolBSPh)] (**4**) shown in Scheme 6.8, with a disulphide bond between the two bidentate ligand backbones.

[6] Calhorda, M.J., de C.T.Carrondo, M.A.A.F., Dias, A.R., Felix, V., Galvao, A.M., Garcia, M.H., Matias, P.M., Villa de Brito, M.J. *J.Organomet.Chem.* **453** (1993) 231-240.

[7] Nefedov, S.E., Pasynskii, A.A., Eremenko, I.L., Papoyan, G.A., Rubinshtein, L.I., Yanovsky, A.I., Struchkov, Y.T. *Zh.Neorg.Khim.(Russ.)(Russ.J.Inorg.Chem.)* **38** (1993) 76.

[8] Mattes, R., Weber, H. *J.Organomet.Chem.* **178** (1979) 191-196.

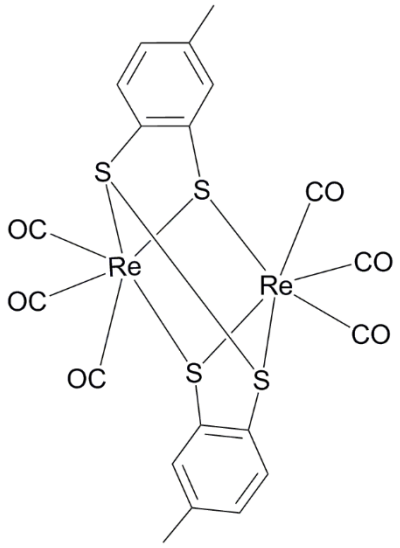

Scheme 6.8: Schematic representation of the structure of (4).

By considering the structures of the expected mononuclear (Scheme 6.7) and obtained dinuclear complex (Scheme 6.8), we expected one singulet for the methyl group on the ligand backbone. However, we observed two singulets. This does not provide conclusive evidence for the specific dinuclear structure presented in Scheme 6.8 as many other bonding modes are possible.

A ^{1}H NMR experiment was set up with one equivalent of rhenium complex (**4**) and one equivalent of DCM in deuterated DMF. The ^{1}H NMR revealed that the complex probably forms two isomers (1:5 ratio) in solution (Figure 6.1). This was confirmed in literature by Begum *et al*. The resulting integration and correlation between the hydrogen atoms of the complex *versus* that of the DCM reference was in a 12:2 ratio as expected and the dinuclear complex was confirmed (7.97 (2H), 7.46 (2H), 7.17 (2H), 2.41 (6H).

If the solid state structure of (**4**) corresponds to the major isomer, the minor isomer will have the structure shown in Scheme 6.9.

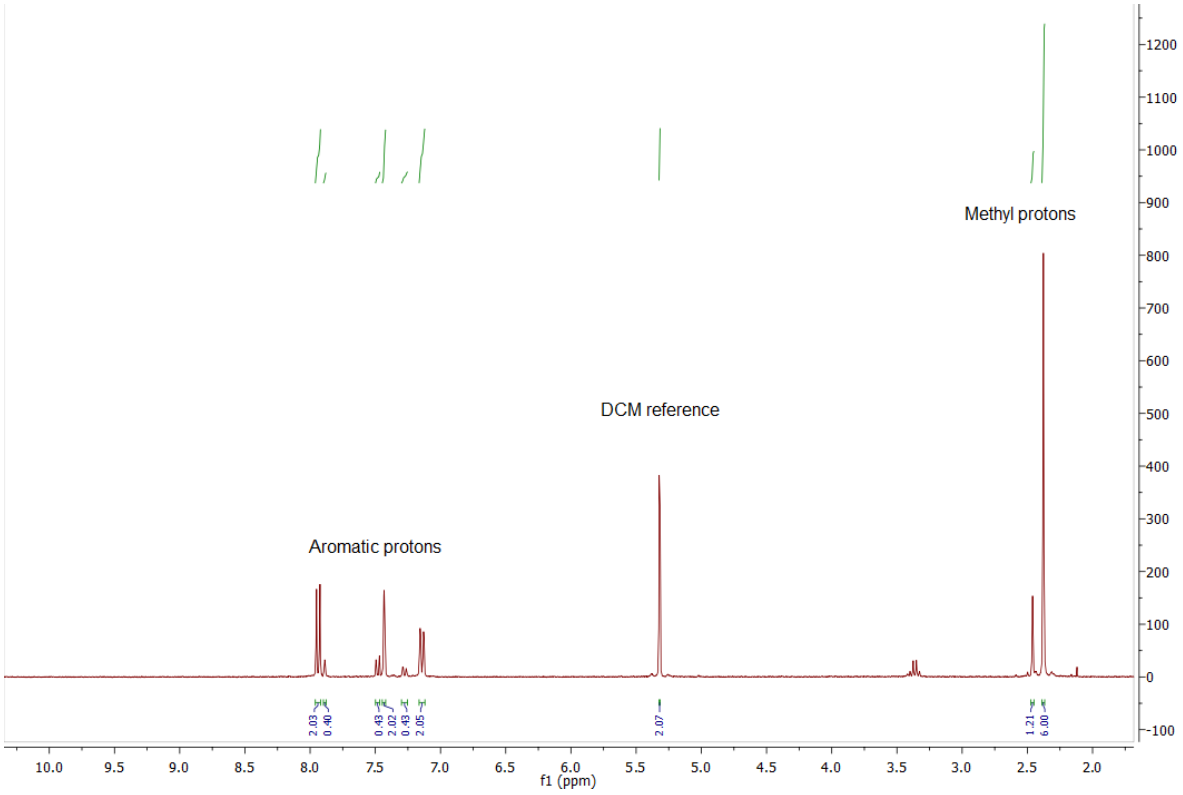

Figure 6.1: NMR spectrum of one equivalent of (4) and one equivalent of DCM. The 1:5 ratio of the two isomers is indicated.

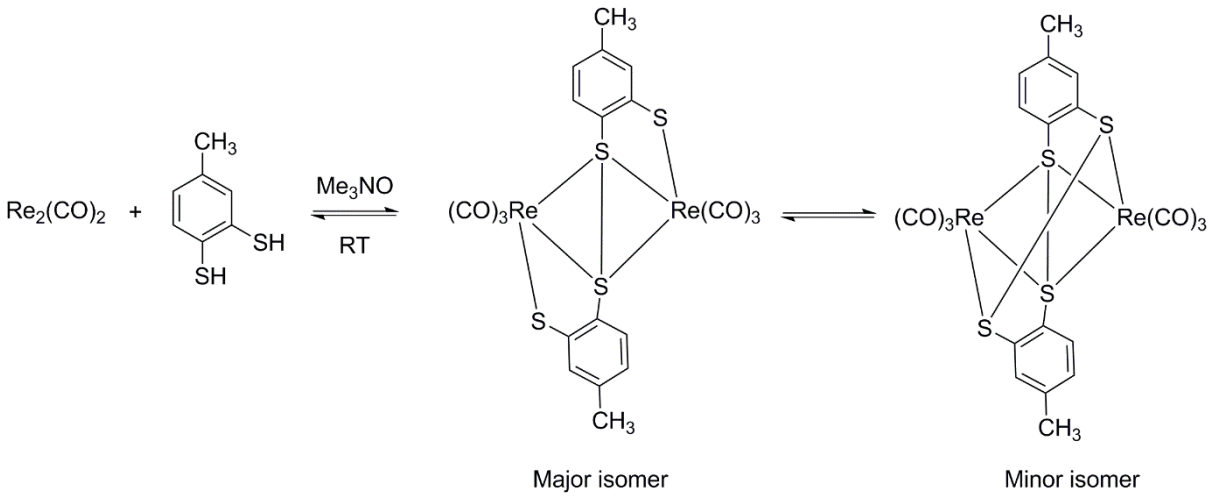

Scheme 6.9: Illustration of the synthetic procedure by Begum *et al*.

A literature search revealed that complexes with the disulphide bond, formed by interligand disulphide bond formation between the two ligand systems can be synthesized. Four similar structures are reported, three with Mn (I) and one with Re

(I).[9,10] Liaw *et al.*[9] synthesized *fac*-[(Mn(CO)$_3$)$_2$(μ-SC$_6$H$_4$-o-S-S-C$_6$H$_4$-o-μ-S-)] from [PPN][Mn(CO)$_5$] in a 5-step synthetic route. They found that a five-coordinate sixteen electron complex is chemically interconvertible with the bimetallic manganese (I)-bismercaptophenyl disulphide complex. The S-S bond is presumed to occur *via* the protonation of thiolate and the subsequent elimination of H_2. A more elaborate discussion is given in Chapter 2.

Begum *et al*.[10] found a direct method to synthesize disulphide complexes by adding $Re_2(CO)_{10}$, $Me_3NO.2H_2O$ and the S,S'-bidentate ligand to chloroform and by stirring it at room temperature (yields ranging from 18 % to 22 %) (Scheme 6.9). The structure reported by Begum *et al.* is the same as (**4**) reported here, the only difference being the synthetic procedure. Begum *et al*. used $Re_2(CO)_{10}$ as starting material in chloroform and then added $Me_3NO.2H_2O$ to the mixture with the ligand. The structure reported here is synthesized from *fac*-$[Re(CO)_3]^+$ and the ligand in methanol at room temperature. Both the structures contain the binucleating disulphide ligand that formed by interligand disulphide bond formation. Both the structures illustrate two isomers present in solution (as indicated in Chapter 2). The major isomer shows two doublets at 7.98 ppm and 7.17 ppm and a singlet at 7.46 ppm for the aromatic hydrogen atoms. The minor isomer exhibits two doublets at 7.51 ppm and 7.31 ppm and a singlet at 7.91 ppm. This same fingerprint is seen in the structure by Begum *et al*. In solid state, only the minor product is obtained with the disulphide bond found only between the sulphur atoms para to the methyl groups with a yield of 23 %, while Begum *et al.* reported an 18% yield of the crystals.

Because dithiols are known to condensate, a GC-MS analysis was performed to confirm that the bidentate ligand toluene-3,4-dithiol was still in the dithiol form and that no disulphide bridge has been formed. The results indicated a dithiol as expected.

[9] Liaw, W.-F., Hsieh, C.-K., Lin, G.-Y., Lee, G.-H. *Inorg. Chem*. **40** (2001) 3468-3475.

[10] Begum, N., Hyder, M.I., Kabir, S.E., Hossain, G.M.G., Nordlander, E., Rokhsana, D., Rosenberg, E. *Inorg. Chem*. **44** (2005) 9887-9894.

6.6 Conclusion

The ^{1}H NMR spectroscopic investigation contributed significantly to the available knowledge on the coordination of these S,O, S,S' and S,S',S'' ligands to the *fac*-$[Re(CO)_3]^+$ core. It was confirmed that the synthetic procedure of these complexes is complicated because the ligands are so versatile (many bonding modes). By considering the structure of (**2**) and (**3**) it is clear that a slight change in synthetic procedure has a big difference on the obtained structure. A lot more synthetic work is necessary in order to fully understand these systems. These ligands are very versatile and are able to form bridging complexes and in some cases (as in (**4**)) different isomers in solution. Our investigation shows that all of the dinuclear complexes probably retain their structure in solution. This is very important for the screening and cell studies of these complexes.

Some of the compounds synthesized as well as some of the ligands itself were tested for anti-mitochondrial activity, specifically anti-cancer activity. This will be discussed in Chapter 7.

7 SCREENING OF LIGANDS AND COMPOUNDS FOR ANTICANCER ACTIVITY

7.1 Introduction

Yeasts are eukaryotic single-celled organisms, widely used in various biotechnological processes, including for example beer brewing as well as commercial enzyme production. Of specific interest to this study, is the fact that yeasts are also used as model organisms to study for example ageing in humans. In this study, yeasts are used as indicator organisms to screen five ligand systems and four rhenium (I) tricarbonyl compounds for anticancer activity.

In 2009, a bio-assay was developed by Kock *et al*.[1], where changes in the colour of yeast sexual structures are used as biosensors to screen for anti-mitochondrial drugs (including anticancer compounds). This provides a cheaper, rapid, upstream screening method to determine if a compound should be considered for further testing using cancer cell lines.

In 2007, Kock and co-workers developed the Anti-mitochondrial Antifungal Hypothesis, which states that:[2]

- the asexual, vegetative reproductive phase of strictly aerobic yeasts are more sensitive to anti-mitochondrial drugs than are yeasts with an additional fermentative pathway,

[1] Kock, J.L.F., Swart, C.W., Ncango, D.M., Kock, J.L.F. (Jr), Munnik, I.A., Maartens, M.M.J., Pohl, C.H., Van Wyk, P.W.J. *Current Drug Discovery Technologies* **6** (2009) 186-191.

[2] Leeuw, N.J., Swart, C.W., Ncango, D.M., Pohl, C.H., Sebolai, O.M., Strauss, C.J., Botes, P.J., Van Wyk, P.W.J., Nigam, S., Kock, J.L.F. *Antonie van Leeuwenhoek* **91** (2007) 393-405.

- the sexual reproductive phase of yeasts is more sensitive to anti-mitochondrial drugs than is the asexual vegetative growth phase,

- flocculation in fermentative yeasts is partially inhibited by anti-mitochondrial drugs,

- these phenomena are probably attributable to mitochondrial inhibition by anti-mitochondrial compounds, which in turn may be linked to the inhibition of products such as 3-hydroxy (OH) oxylipins – not necessarily indicating oxylipin function and

- mitochondrial respiration and beta-oxidation are more pronounced during the sexual phase of yeasts than in the asexual vegetative phase.

This hypothesis was developed into a practical, visual bio-assay that can be used to screen compounds for antifungal, anticancer and anti-malarial activity.[1,3] In this bio-assay colour changes of yeast sexual stages (biosensors) of indicator yeasts are used to screen for compounds with the mentioned activities. Compounds such as some non-steroidal anti-inflammatory (NSAID's) drugs, anti-malarial, antifungal and anticancer drugs inhibit sexual spore formation by cutting off the power supply (mitochondria) of the cell and can therefore be regarded as anti-mitochondrial. A positive hit using the bio-assay will cause a colour change in the indicator organism. Compounds with anti-mitochondrial properties have the ability to selectively treat diseases such as cancer, fungal infections, malaria, etc. by targeting the power supplies of the causative agents. This bio-assay should however only be considered a first screen since other mechanisms of sexual reproduction may be involved (see detailed information at: http://vimeo.com/24167863).

As part of this study, the following ligand systems and rhenium (I) compounds were screened for anticancer activity using *Eremothecium ashbyii* and *Nadsonia fulvescens* as indicator organisms in the bio-assay:

- *fac*-[$Re_2(CO)_6(\mu\text{-}\eta^4$-m-TolBSPh-S-S-m-TolBSPh)] (**4**) – P1

[3] Kock, J.L.F., Swart, C.W., Pohl, C.H. *Expert Opinion on Drug Discovery* **6(6**) (2011) 671-681.

- reaction of fac-$[Re(CO)_3]^+$ with BSOC – P2
- reaction of *fac*-$[Re(CO)_3]^+$ with BSC – P3
- reaction of *fac*-$[Re(CO)_3]^+$ with BSOH – P4
- methyl benzo[b]thiophene-2-carboxylate – P11
- 2,2`-thiodiethanethiol – P12
- 2,2′-bithiophene-5-carboxylic acid – P13
- 5-bromo-2,2`-bithiophene – P14
- 2-mercaptoethanol – P15

7.2 Materials and Methods

7.2.1 Cultivation and bio-assay preparation

Eremothecium ashbyii (UOFS-1122) and *Nadsonia fulvescens* var. *elongata* (UFS-0932) (obtained from the yeast culture collection kept at the University of the Free State, Department of Microbial, Biochemical and Food Biotechnology) were streaked out on yeast malt (YM) agar plates and incubated at 25ºC for 48h to obtain significant growth. These cultures were then scraped from the plates and suspended in 5mL sterile distilled water. From these suspensions, 100µl aliquots of either *Eremothecium ashbyii* or *Nadsonia fulvescens* were placed on YM agar plates and spread across the plate to form a homogenous lawn of growth. Each of the compounds tested (P1 – P5, P11 – P15) were then placed in the middle of a petri dish containing either *Eremothecium ashbyii* or *Nadsonia fulvescens* as indicator organism and incubated for 48h and 7 days, respectively at 25ºC. In accordance with the diffusion plate method, the compound should diffuse throughout the plate with a decrease in concentration towards the periphery of the plate. Controls contained no compounds, only yeast cells of either *Eremothecium ashbyii* or *Nadsonia fulvescens*.

7.2.2 Light Microscopy (LM)

Should a compound test positive for anti-mitochondrial activity, two distinct zones should be observed on the plates, a white zone where only asexual growth can be observed (mitochondrial inhibition caused inhibition of sexual structure formation,

which needs large amounts of energy for production of mature spores); and a yellow (*Eremothecium ashbyii*) or brown (*Nadsonia fulvescens*) zone near the periphery of the plate, where asexual and sexual growth occurred. In certain cases the compound tested can also cause and inhibition zone close to the compound (high concentration of the compound), where no growth occurs. Cells from the white and yellow/brown zones were viewed with LM (Axioplan, Zeiss, Germany) coupled to a Colourview Soft Digital Imaging System (Münster, Germany) to determine the effect of the tested compounds on sexual structure development in the cells.

7.3 Results and Discussion

7.3.1 Bio-assay and Light Microscopy (LM)

Should a compound test positive for anti-mitochondrial activity, two distinct zones should be observed on the plates, a white zone where only asexual growth can be observed (mitochondrial inhibition caused inhibition of sexual structure formation) and a yellow (*Eremothecium ashbyii*) or brown (*Nadsonia fulvescens*) zone near the periphery of the plate, where asexual and sexual growth occurred. Near the periphery of the plate the compound concentration is low and thus does not inhibit growth or sexual structure formation. In certain cases the compound tested can also cause and inhibition zone close to the compound (high concentration of the compound), where no growth occurs.

From the results obtained using *Eremothecium ashbyii* as indicator organism (Figure 7.1), five of the compounds (P1, P3, P11, P13 and P14) exhibited anticancer activity. P1 displayed a small inhibition zone, where no growth occurred, followed by a very small white zone, where no sexual structures were produced (Figure 7.1 – P1, white zone) and a yellow zone where normal growth and sexual reproduction occurred (Figure 7.1 – P1, yellow zone). P3 displayed similar results with an inhibition zone, a larger white zone than observed for P1 and a yellow zone (Figure 7.1 – P3). Light Microscopy results indicate no sexual structure formation in the white zone (Figure 7.1 – P3, white zone) as compared to a large number of sickle-shaped ascospores produced in the yellow zone (Figure 7.1 – P3, yellow zone). P11 caused a large

inhibition zone, followed by a white zone (Figure 7.1 – P11). Here, no yellow zone was produced, indicating that the concentration of the compound, even at the periphery of the plate, inhibits mitochondrial function. Light Microscopy results indicated underdeveloped, empty asci in the white zone (Figure 7.1 – P11, white zone). Similar results were obtained for compound P13, with an inhibition zone, white zone and yellow zone observed (Figure 7.1 – P13). In the white zone no sexual structures can be observed (Figure 7.1 – P13, white zone), which is in sharp contrast to the yellow zone where mature ascospores can be observed inside asci (Figure 7.1 – P13, yellow zone). P14 did not cause an inhibition zone, however a very large white zone was observed, indicating that this compound does not inhibit growth as such, but does inhibit mitochondrial activity, even at low concentrations (Figure 7.1 – P14). Light Microscopy results indicate cells with no sexual structures (Figure 7.1 – P14, white zone). All the other compounds (P2, P4, P5, P12 and P15) tested were not effective and did not display inhibition or white zones (Figure 7.1). These compounds are not likely to have anticancer activity, however it should be kept in mind that this bio-assay is only an upstream screening method, since other mechanisms of sexual reproduction may be involved. In cases where there are no LM results in Figure 7.1, similar results as for the yellow zones of the other compounds were observed.

	Eremothecium	White Zone	Yellow Zone
P1			
P2			
P3	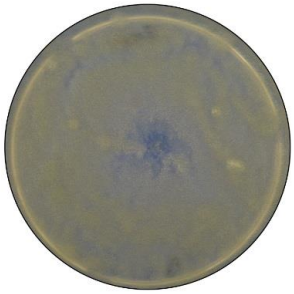	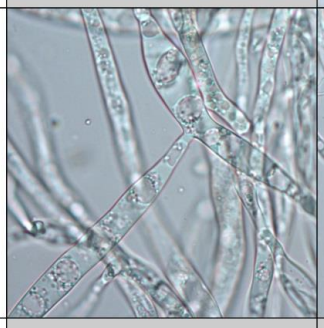	
P4			
P5			

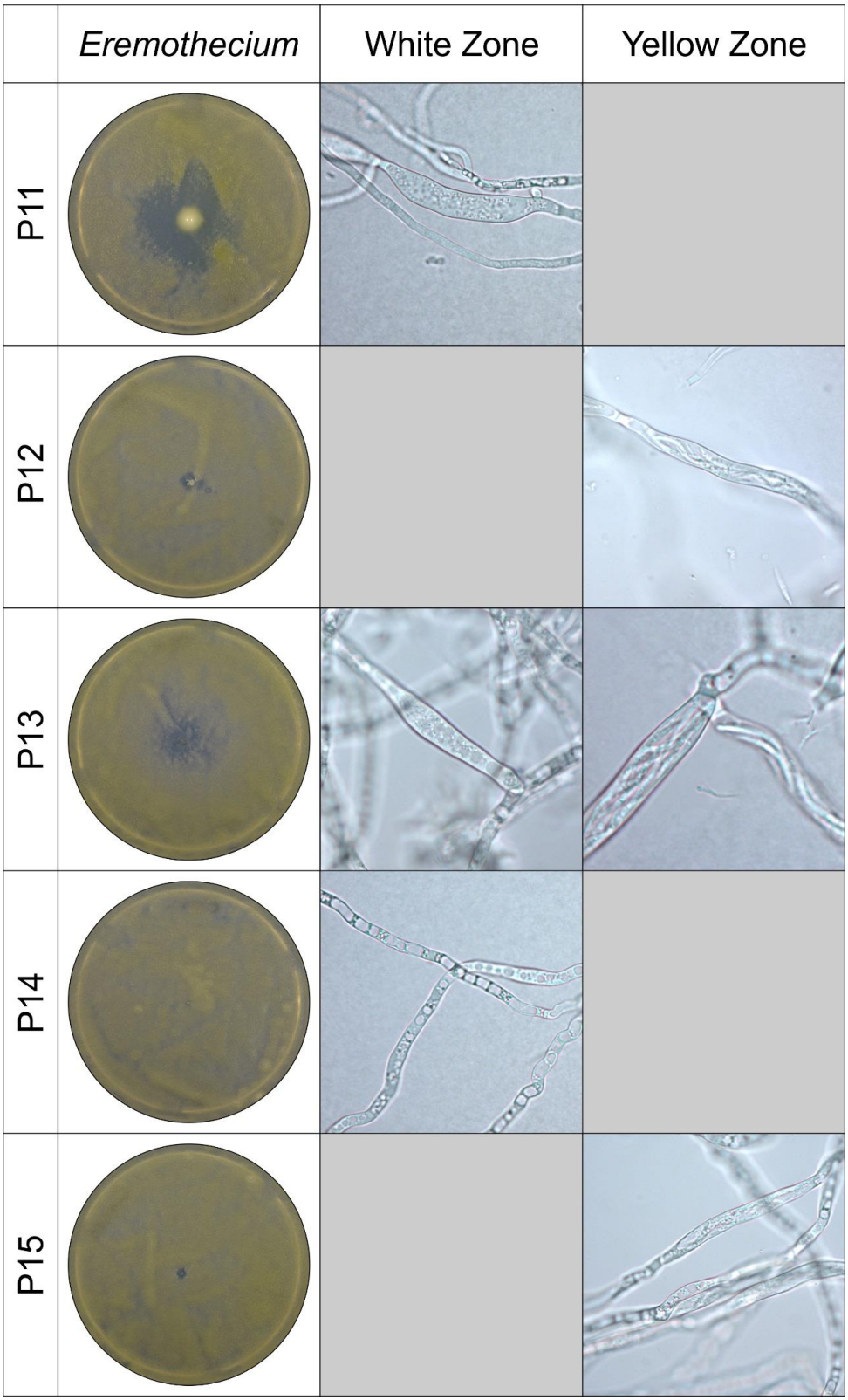

Figure 7.1: Column one indicates the bio-assay plate results for each compound tested when *Eremothecium ashbyii* was used as indicator organism. Column two indicates Light Microscopy (LM) results for compounds that exhibited white zones (no sexual structures can be observed here) and the third column indicates LM results for the yellow zones (mature ascospores inside asci can be observed).

When *Nadsonia fulvescens* was used as indicator organism (Figure 7.2), only two compounds tested positive for anticancer activity (P11 and P13). P11 and P13 caused an inhibition zone (larger zone caused by P11), a white and a brown zone (Figure 7.2 – P11, P13). From the LM results no mature sexual structures can be observed in the white zones of compounds P11 and P13 (Figure 7.2 – P11, white zone; P13, white zone). In the brown zone however, a large number of mature ascospores can be observed (Figure 7.2 – P11, brown zone; P13, brown zone). The other compounds tested were not effective using *Nadsonia fulvescens* as indicator organism (Figure 7.2). This could be due to the fact that *Eremothecium* ashbyii might be more sensitive towards the tested compounds as compared to *Nadsonia fulvescens*.

	Nadsonia	White Zone	Brown Zone
P1			
P2			
P3			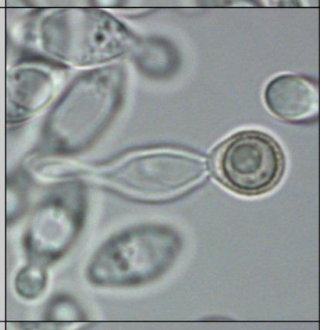
P4			
P5			

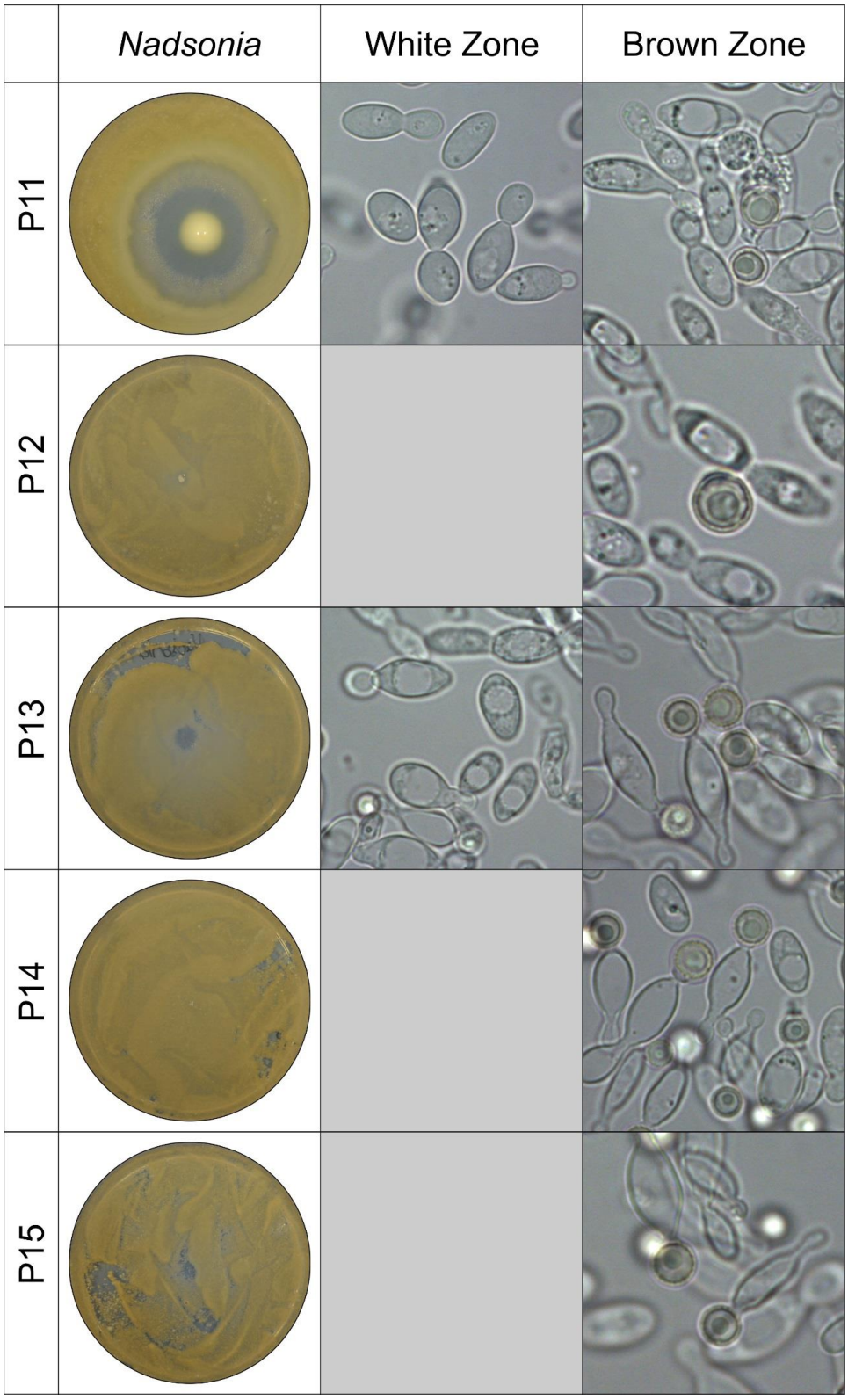

Figure 7.2: Column one indicates the bio-assay plate results for each compound tested when *Nadsonia fulvescens* was used as indicator organism. Column two indicates Light Microscopy (LM) results for compounds that exhibited white zones (no sexual structures can be observed here) and the third column indicates LM results for the brown zones (mature ascospores inside asci can be observed).

7.4 Conclusion

The bio-assay used in this study, should be regarded as a first screen to determine if a compound has probable anticancer activity. The method is however rapid and cheap and should therefore be considered as an upstream testing alternative instead of more expensive studies using cancer cell lines. Of the compounds tested, P1, P3, P11, P13 and P14 showed anti-mitochondrial activity when using *Eremothecium ashbyii* as indicator organism, while only P3 and P11 tested positive with *Nadsonia fulvescens* as indicator organism. This could be due to the fact that *Eremothecium* might be more sensitive towards the compounds tested than *Nadsonia*. The compounds that gave a positive hit should now be further tested using cancer cell lines to confirm activity.

8 EVALUTATION OF THE STUDY

8.1 Results obtained

The aim of the study was to investigate the ability of the chosen N,O; S,S'; S,O bidentate and S,S',S'' tridentate ligands to coordinate to the *fac*-$[Re(CO)_3]^+$ core. The results were compared to previous studies where N,O and O,O' bidentate ligand systems were used to see differences in the structures, reactivity and coordination behaviour.

Rhenium (I) tricarbonyl complexes were synthesized and characterized. Five complexes with N,O bidentate ligands were successfully synthesized and characterized. Unfortunately no suitable crystals were obtained. Two of the complexes with an S,O ligand, one of the complexes with a S,S' ligand and one complex with a S,S',S'' ligand were successfully synthesized and characterized by single crystal XRD.

- *fac*-$[Re_2(CO)_6(TS)(Py)]$ (**1**)
- *fac*-$[Re_2(CO)_6(PPh_3)(BSOPhC)_2(Py)]$ (**2**)
- *fac*-$[NEt_4][Re_2(CO)_6(BSOPhC)_3]$ (**3**)
- *fac*-$[Re_2(CO)_6(\mu\text{-}\eta^4\text{-m-TolBSPh-S-S-m-TolBSPh}]$ (**4**).

The rest if the complexes synthesized with S,O; S,S' and S,S',S'' ligands were characterized by means of IR, NMR, UV/Vis and elemental analysis, but no conclusive evidence could be found of the structures of the synthesized complexes. It was confirmed that single crystal XRD is imperative for these type of complexes since a wide variety of coordination modes is possible. This is seen in (**2**) and (**3**) where the same bidentate ligand is used with only a slight change in the synthetic procedure and two totally different complexes were found.

The treatment of ReAA with 2-methoxythiophenol (BSOPhC) in methanol at room temperature afforded the dinuclear complex (**3**). When triphenylphosphine is introduced during the same synthetic procedure, the dinuclear complex (**2**) is obtained. When triphenylphosphine was introduced, only two ligands and therefore two sulphur

bridges are formed between the two Re centres, and the 6th position is occupied by the triphenylphosphine ligand.

A good correlation is found in the bonding distances and angles of the four reported structures, also within each crystal structure between the two Re units. It was also in good agreement to similar dinuclear structures reported in literature. Although one cannot really compare the structures of (**1**) – (**4**) (dinuclear structures) to previously reported structures with N,O and O,O' bidentate ligands (mononuclear structures), the same trend was found for Re-O, Re-N, Re-S distances and N-Re-O, O-Re-O, S-Re-S bite angles: Re-O ≤ Re-N <Re-S and O,O' complexes < N,O complexes < S,O/S,S'/S,S',S'' complexes respectively. This can be explained by atomic radius of these atoms: O < N < S.

It is therefore imperative to investigate the synthetic process, bonding modes and coordination chemistry of these complexes in order to potentially obtain the mononuclear structures in future. Once mononuclear structures are obtained, it will be important to compare the reactivity of these complexes to the N,O and O,O' bidentate complexes to see the possible differences in stability, reactivity and mechanistic characteristics .

The anti-mitochondrial activity assay yielded excellent results. The next step will be to improve the water solubility of these complexes.

The results obtained contributed significantly to the little available knowledge of the S,O; S,S' and S,S',S'' ligand systems coordinated to the rhenium (I) tricarbonyl core. (**4**) is the first reported compound that is synthesized directly from the *fac*-$[Re(CO)_3]^+$ core and the dithiol in methanol that forms an internal disulphide linkage between the two ligand systems.

8.2 Future work

From the results obtained, various focus areas have been identified for future investigations. The available information and knowledge of the coordination of sulphur containing ligands on the rhenium (I) tricarbonyl core is limited.

Future research will therefore include:

- A crystallographic study of the coordination modes and manipulation of the coordination of these type of ligands to the Re (I) core.
- The investigation into the Re-S bond breaking and formation to determine if the formation of the mononuclear and dinuclear complexes are a reversible process or not.
- The synthesis of mononuclear complexes with S,O and possibly S,S' bidentate ligands and the kinetic investigation thereof including formation kinetics and substitution kinetics to evaluate the reactivity of the complexes.
- The synthesis of water soluble complexes and the testing of its biological activity.
- A computational study of the energy differences between the major and minor isomers of the structure of (**4**) and also other similar structures synthesized.

APPENDIX A

Table A.1: Atomic coordinates (x 10^4) and equivalent isotropic displacement parameters (Å^2 x 10^3) for *fac*-[$Re_2(CO)_6(TS)(Py)$] (1). U(eq) is defined as one third of the trace of the orthogonalized U^{ij} tensor.

	x	y	z	U(eq)
Re(2`)	8460(1)	8180(1)	3371(1)	30(1)
Re(2)	3612(1)	3280(1)	3241(1)	32(1)
Re(1)	4770(1)	1587(1)	1580(1)	34(1)
Re(1`)	9584(1)	6406(1)	1759(1)	34(1)
S(3)	4032(8)	3115(4)	1749(4)	35(1)
S(1)	3639(8)	1549(5)	2844(4)	36(1)
S(2')	5661(8)	7205(5)	2470(4)	36(1)
S(1')	8760(8)	6531(4)	3131(4)	34(1)
S(3')	8626(8)	7854(5)	1793(5)	38(1)
S(2)	820(8)	2435(5)	2248(5)	40(2)
C(18)	440(40)	1250(20)	2440(20)	52(8)
C(5)	3500(30)	4580(20)	3437(17)	41(7)
O(5)	3450(30)	5349(18)	3521(19)	65(7)
C(16)	2050(30)	2840(30)	942(19)	49(8)
C(18')	5550(30)	5898(17)	2037(19)	34(5)
C(11')	12570(40)	7340(20)	3600(20)	55(9)
C(16')	6580(30)	7370(20)	967(18)	43(7)
C(2')	10330(40)	5320(20)	1843(19)	49(8)
C(14)	9290(40)	3990(30)	3580(30)	66(10)
C(19)	1630(40)	710(20)	2300(20)	59(10)
N(1)	6940(30)	2551(18)	2801(16)	54(8)
O(3')	10960(40)	6530(30)	290(20)	81(9)
C(13')	14770(40)	8830(20)	4140(30)	63(11)
C(3)	5890(50)	1800(20)	780(20)	59(10)
O(6)	3080(30)	3469(17)	5052(14)	54(6)
O(4)	7040(30)	4300(19)	4612(16)	61(7)
N(1')	11810(40)	7524(19)	2840(18)	65(10)
O(6')	8230(30)	8595(17)	5292(15)	51(5)
C(11)	7510(40)	2220(20)	3490(20)	48(8)
C(6)	3260(30)	3360(20)	4379(16)	37(6)
C(17)	740(40)	2090(20)	1041(17)	41(6)
O(4')	11940(30)	9344(19)	4538(19)	70(8)
C(17')	5350(40)	7470(20)	1405(19)	42(7)
O(2')	10640(40)	4650(20)	1854(19)	79(9)
C(14')	13980(40)	9000(30)	3300(30)	67(12)
C(15)	7940(30)	3390(20)	2800(20)	44(7)
C(4')	10690(40)	8870(20)	4030(20)	46(7)
C(19')	6740(40)	5720(20)	2770(20)	50(8)
O(5')	7970(30)	10140(17)	3412(18)	61(7)

C(6')	8290(30)	8390(20)	4572(17)	34(4)
C(4)	5760(40)	3908(19)	4063(18)	38(6)
C(12')	14040(40)	8000(30)	4260(20)	57(10)
O(2)	5760(40)	-180(20)	1530(20)	92(11)
C(12)	8890(40)	2800(30)	4260(20)	64(10)
C(3')	10440(50)	6450(30)	800(20)	68(12)
O(3)	6520(30)	1940(20)	319(18)	65(7)
C(13)	9810(30)	3700(30)	4280(30)	59(10)
C(2)	5380(40)	480(20)	1550(19)	41(6)
C(15')	12570(50)	8310(20)	2680(30)	64(10)
C(1')	7760(30)	5430(20)	800(20)	51(8)
O(1')	6630(30)	4810(20)	209(18)	84(10)
O(1)	1830(30)	240(20)	-140(17)	77(9)
C(1)	3030(30)	720(20)	480(20)	47(7)
C(5')	8140(30)	9400(20)	3424(17)	34(4)

Table A.2: Bond distances (Å) and angles (°) for *fac*-[$Re_2(CO)_6$(TS)(Py)] (1).

Bond	Bond Distance	Bond Angle	Angle
Re(2')-C(5')	1.91(3)	C(5')-Re(2')-C(6')	87.6(11)
Re(2')-C(6')	1.93(3)	C(5')-Re(2')-C(4')	90.4(12)
Re(2')-C(4')	1.93(3)	C(6')-Re(2')-C(4')	87.1(12)
Re(2')-S(2')	2.465(6)	C(5')-Re(2')-S(2')	92.9(8)
Re(2')-S(1')	2.498(7)	C(6')-Re(2')-S(2')	95.0(7)
Re(2')-S(3')	2.512(7)	C(4')-Re(2')-S(2')	176.1(9)
Re(2)-C(4)	1.91(3)	C(5')-Re(2')-S(1')	174.3(8)
Re(2)-C(5)	1.92(4)	C(6')-Re(2')-S(1')	97.4(9)
Re(2)-C(6)	1.93(3)	C(4')-Re(2')-S(1')	92.4(9)
Re(2)-S(2)	2.459(7)	S(2')-Re(2')-S(1')	84.1(2)
Re(2)-S(3)	2.499(7)	C(5')-Re(2')-S(3')	93.6(8)
Re(2)-S(1)	2.513(7)	C(6')-Re(2')-S(3')	178.3(8)
Re(1)-C(2)	1.88(3)	C(4')-Re(2')-S(3')	94.1(10)
Re(1)-C(1)	1.90(3)	S(2')-Re(2')-S(3')	83.7(2)
Re(1)-C(3)	1.94(4)	S(1')-Re(2')-S(3')	81.3(2)
Re(1)-N(1)	2.22(2)	C(4)-Re(2)-C(5)	87.1(11)
Re(1)-S(3)	2.526(7)	C(4)-Re(2)-C(6)	83.5(11)
Re(1)-S(1)	2.562(7)	C(5)-Re(2)-C(6)	87.1(12)
Re(2)-C(1')	1.88(3)	C(4)-Re(2)-S(2)	176.8(8)
Re(2)-C(3')	1.94(3)	C(5)-Re(2)-S(2)	94.2(7)
Re(2)-C(2')	1.94(4)	C(6)-Re(2)-S(2)	93.7(7)
Re(2)-N(1')	2.22(2)	C(4)-Re(2)-S(3)	97.5(9)
Re(2)-S(1')	2.522(7)	C(5)-Re(2)-S(3)	94.7(8)
Re(2)-S(3')	2.546(8)	C(6)-Re(2)-S(3)	178.1(8)
S(3)-C(16)	1.83(3)	S(2)-Re(2)-S(3)	85.3(2)
S(1)-C(19)	1.81(3)	C(4)-Re(2)-S(1)	96.2(9)
S(2')-C(17')	1.81(3)	C(5)-Re(2)-S(1)	175.3(8)

S(2')-C(18')	1.86(3)	C(6)-Re(2)-S(1)	96.6(9)
S(1')-C(19')	1.83(3)	S(2)-Re(2)-S(1)	82.7(2)
S(3')-C(16')	1.84(3)	S(3)-Re(2)-S(1)	81.6(2)
S(2)-C(18)	1.84(3)	C(2)-Re(1)-C(1)	85.4(14)
S(2)-C(17)	1.85(3)	C(2)-Re(1)-C(3)	86.1(15)
C(18)-C(19)	1.58(6)	C(1)-Re(1)-C(3)	86.8(14)
C(5)-O(5)	1.15(4)	C(2)-Re(1)-N(1)	91.2(12)
C(16)-C(17)	1.53(4)	C(1)-Re(1)-N(1)	174.7(14)
C(18')-C(19')	1.52(4)	C(3)-Re(1)-N(1)	88.9(12)
C(11')-N(1')	1.36(4)	C(2)-Re(1)-S(3)	175.8(9)
C(11')-C(12')	1.40(4)	C(1)-Re(1)-S(3)	98.1(10)
C(16')-C(17')	1.54(5)	C(3)-Re(1)-S(3)	96.4(12)
C(2')-O(2')	1.12(4)	N(1)-Re(1)-S(3)	85.4(8)
C(14)-C(13)	1.32(6)	C(2)-Re(1)-S(1)	96.9(9)
C(14)-C(15)	1.39(5)	C(1)-Re(1)-S(1)	102.1(10)
N(1)-C(11)	1.35(4)	C(3)-Re(1)-S(1)	170.8(9)
N(1)-C(15)	1.38(3)	N(1)-Re(1)-S(1)	82.3(8)
O(3')-C(3')	1.09(4)	S(3)-Re(1)-S(1)	80.1(2)
C(13')-C(12')	1.36(6)	C(1')-Re(2)-C(3')	86.6(16)
C(13')-C(14')	1.45(6)	C(1')-Re(2)-C(2')	85.6(13)
C(3)-O(3)	1.10(4)	C(3')-Re(2)-C(2')	86.5(18)
O(6)-C(6)	1.12(3)	C(1')-Re(2)-N(1')	176.7(15)
O(4)-C(4)	1.17(4)	C(3')-Re(2)-N(1')	90.5(14)
N(1')-C(15')	1.35(4)	C(2')-Re(2)-N(1')	92.7(13)
O(6')-C(6')	1.14(3)	C(1')-Re(2)-S(1')	100.4(12)
C(11)-C(12)	1.40(4)	C(3')-Re(2)-S(1')	172.9(11)
O(4')-C(4')	1.14(4)	C(2')-Re(2)-S(1')	95.1(10)
C(14')-C(15')	1.36(5)	N(1')-Re(2)-S(1')	82.5(9)
O(5')-C(5')	1.16(4)	C(1')-Re(2)-S(3')	96.7(10)
O(2)-C(2)	1.13(4)	C(3')-Re(2)-S(3')	97.9(14)
C(12)-C(13)	1.40(5)	C(2')-Re(2)-S(3')	175.1(9)
C(1')-O(1')	1.18(3)	N(1')-Re(2)-S(3')	85.2(10)
O(1)-C(1)	1.17(3)	S(1')-Re(2)-S(3')	80.2(2)
		C(16)-S(3)-Re(2)	101.1(10)
		C(16)-S(3)-Re(1)	111.7(12)
		Re(2)-S(3)-Re(1)	98.1(2)
		C(19)-S(1)-Re(2)	108.1(13)
		C(19)-S(1)-Re(1)	108.5(13)
		Re(2)-S(1)-Re(1)	96.8(2)
		C(17')-S(2')-C(18')	99.9(13)
		C(17')-S(2')-Re(2')	101.6(10)
		C(18')-S(2')-Re(2')	105.8(8)
		C(19')-S(1')-Re(2')	101.9(11)
		C(19')-S(1')-Re(2)	111.2(11)
		Re(22)-S(1')-Re(2)	98.3(2)

		C(16')-S(3')-Re(2')	104.9(10)
		C(16')-S(3')-Re(2)	108.0(11)
		Re(22)-S(3')-Re(2)	97.3(2)
		C(18)-S(2)-C(17)	103.0(15)
		C(18)-S(2)-Re(2)	101.3(10)
		C(17)-S(2)-Re(2)	105.5(10)
		C(19)-C(18)-S(2)	115(2)
		O(5)-C(5)-Re(2)	177(3)
		C(17)-C(16)-S(3)	116(2)
		C(19')-C(18')-S(2')	109.4(18)
		N(1')-C(11')-C(12')	122(3)
		C(17')-C(16')-S(3')	115.5(18)
		O(2')-C(2')-Re(21)	175(3)
		C(13)-C(14)-C(15)	122(3)
		C(18)-C(19)-S(1)	112(2)
		C(11)-N(1)-C(15)	117(3)
		C(11)-N(1)-Re(1)	119.9(18)
		C(15)-N(1)-Re(1)	122.0(19)
		C(12')-C(13')-C(14')	117(3)
		O(3)-C(3)-Re(1)	178(4)
		C(15')-N(1')-C(11')	118(3)
		C(15')-N(1')-Re(21)	121(2)
		C(11')-N(1')-Re(21)	120(2)
		N(1)-C(11)-C(12)	121(3)
		O(6)-C(6)-Re(2)	176(3)
		C(16)-C(17)-S(2)	111.8(18)
		C(16')-C(17')-S(2')	115(2)
		C(15')-C(14')-C(13')	119(4)
		N(1)-C(15)-C(14)	121(3)
		O(4')-C(4')-Re(2')	169(3)
		C(18')-C(19')-S(1')	114.3(19)
		O(6')-C(6')-Re(2')	174(3)
		O(4)-C(4)-Re(2)	176(3)
		C(13')-C(12')-C(11')	121(4)
		C(13)-C(12)-C(11)	120(3)
		O(3')-C(3')-Re(2)	176(4)
		C(14)-C(13)-C(12)	118(3)
		O(2)-C(2)-Re(1)	179(3)
		N(1')-C(15')-C(14')	123(4)
		O(1')-C(1')-Re(2)	179(3)
		O(1)-C(1)-Re(1)	171(3)
		O(5')-C(5')-Re(2')	176(2)

Table A.3: Anisotropic displacement parameters ($Å^2$ x 10^3) for *fac*-[$Re_2(CO)_6$(TS)(Py)] (1). The anisotropic displacement factor exponent takes the form: $-2\pi^2[h2a^{*2}U^{11} + \ldots\ldots + 2hka^*b^*U^{12}]$.

	U_{11}	U_{22}	U_{33}	U_{23}	U_{13}	U_{12}
Re(2')	33(1)	19(1)	22(1)	2(1)	2(1)	-3(1)
Re(2)	34(1)	23(1)	23(1)	4(1)	2(1)	-3(1)
Re(1)	38(1)	22(1)	24(1)	3(1)	0(1)	-1(1)
Re(2)	33(1)	29(1)	22(1)	1(1)	-1(1)	2(1)
S(3)	41(3)	25(3)	27(3)	8(2)	7(2)	1(2)
S(1)	39(3)	26(3)	30(3)	9(2)	6(3)	-1(2)
S(2')	32(3)	31(3)	27(3)	3(2)	3(2)	-2(2)
S(1')	41(3)	20(2)	24(3)	4(2)	2(2)	-1(2)
S(3')	39(3)	35(3)	29(3)	12(3)	6(3)	5(3)
S(2)	32(3)	42(4)	29(3)	9(3)	2(2)	0(3)
C(18)	40(15)	48(17)	40(15)	21(13)	0(12)	-16(13)
C(5)	18(10)	65(19)	25(12)	-11(12)	12(9)	12(12)
O(5)	72(17)	38(12)	59(15)	5(11)	5(13)	11(12)
C(16)	38(14)	63(19)	26(13)	16(13)	5(11)	-9(13)
C(18')	26(11)	22(10)	40(13)	6(10)	-1(10)	7(9)
C(11')	60(20)	40(16)	32(14)	3(12)	-5(14)	-4(14)
C(16')	43(15)	56(17)	20(11)	16(11)	3(10)	9(13)
C(2')	59(19)	46(17)	25(13)	9(12)	2(12)	11(15)
C(14)	46(18)	48(19)	70(20)	3(17)	18(18)	-12(15)
C(19)	56(19)	33(14)	52(18)	14(13)	-1(15)	-18(14)
N(1)	63(16)	33(12)	24(11)	13(9)	-10(10)	-22(11)
O(3')	70(18)	130(30)	59(17)	29(18)	32(15)	47(19)
C(13')	45(17)	32(15)	70(20)	-28(15)	9(17)	5(13)
C(3)	70(20)	47(17)	24(13)	13(12)	-2(14)	-15(16)
O(6)	64(14)	54(13)	28(10)	12(9)	13(10)	1(11)
O(4)	35(11)	60(14)	43(12)	-13(10)	1(9)	-11(10)
N(1')	66(18)	37(13)	31(12)	3(10)	-14(12)	-36(13)
O(6')	64(14)	52(13)	34(11)	13(9)	19(10)	16(11)
C(11)	60(20)	33(13)	29(13)	9(11)	2(13)	5(13)
C(6)	31(12)	42(14)	18(11)	14(10)	-7(9)	-5(10)
C(17)	48(15)	38(14)	21(11)	-4(10)	12(11)	7(12)
O(4')	37(12)	54(14)	66(16)	-18(12)	2(11)	-12(11)
C(17')	51(16)	38(14)	27(12)	14(11)	2(11)	10(13)
O(2')	100(20)	60(16)	50(15)	5(12)	-4(15)	42(17)
C(14')	34(15)	49(19)	90(30)	-7(19)	34(19)	-4(14)
C(15)	36(14)	31(13)	58(18)	12(13)	21(13)	4(11)
C(4')	55(18)	23(12)	48(16)	-5(11)	21(15)	9(12)
C(19')	46(16)	29(13)	41(15)	11(11)	-4(13)	-14(12)
O(5')	76(17)	39(12)	63(15)	24(11)	15(13)	18(12)
C(6')	27(8)	41(10)	25(8)	8(7)	8(7)	4(7)
C(4)	54(16)	27(11)	28(12)	16(10)	8(12)	8(12)
C(12')	34(15)	70(20)	43(17)	-15(15)	14(13)	11(15)

O(2)	120(30)	59(17)	68(19)	7(14)	-3(18)	39(18)
C(12)	50(20)	60(20)	44(18)	11(15)	-18(15)	7(16)
C(3')	100(30)	70(20)	23(14)	5(14)	28(17)	0(20)
O(3)	60(15)	83(19)	51(14)	27(14)	16(12)	26(14)
C(13)	22(12)	49(18)	70(20)	-12(16)	-10(13)	11(12)
C(2)	52(16)	40(15)	32(13)	8(11)	21(12)	18(13)
C(15')	60(20)	29(14)	70(20)	8(15)	25(19)	-14(14)
C(1')	28(13)	48(17)	42(16)	-4(13)	-15(12)	12(12)
O(1')	54(15)	74(18)	48(15)	-32(13)	-16(12)	-4(13)
O(1)	65(16)	61(16)	40(13)	-12(11)	-16(12)	-12(13)
C(1)	31(13)	48(16)	36(14)	13(12)	-8(11)	-1(12)
C(5')	27(8)	41(10)	25(8)	8(7)	8(7)	4(7)

Table A.4: Hydrogen coordinates (x 10^4) and isotropic displacement parameters (Å^2 x 10^3) for *fac*-[$Re_2(CO)_6$(TS)(Py)] (1).

	x	y	z	U(eq)
H(18A)	460	1350	3057	63
H(18B)	-598	804	2001	63
H(16A)	1836	3445	1018	57
H(16B)	2010	2583	314	57
H(18C)	4509	5467	1920	40
H(18D)	5739	5766	1474	40
H(11')	12103	6776	3695	66
H(16C)	6499	7721	534	51
H(16D)	6314	6686	625	51
H(14)	9814	4615	3604	80
H(19A)	1384	408	1643	73
H(19B)	1520	199	2568	73
H(13')	15739	9277	4563	75
H(11)	6981	1592	3451	57
H(17A)	834	1452	856	48
H(17B)	-254	2063	634	48
H(17C)	4339	7027	952	52
H(17D)	5349	8137	1531	52
H(14')	14426	9553	3180	79
H(15)	7712	3573	2283	52
H(19C)	6685	5040	2518	59
H(19D)	6465	5785	3309	59
H(12')	14510	7862	4777	67
H(12)	9192	2600	4758	75

H(13)	10770	4070	4760	71
H(15')	12121	8400	2125	74

Table A.5: Hydrogen bond distances (Å) and angles (º) for *fac*-[$Re_2(CO)_6$(TS)(Py)] (1).

D-H…A	d (D-H)	d (H…A)	d (D…A)	D-H…A angle
C13-H13...O6[a]	0.93	2.54	3.14(5)	122
C19'-H19D…O6[b]	0.96	2.44	3.33(4)	154
C17'-H17D...O2[c]	0.97	2.43	3.37(4)	163
C13-H13 ...O4[d]	0.93	2.51	3.29(5)	142'
C11-H11 …O5'[e]	0.93	2.56	3.22(4)	128
C18-H18A ...O6'[f]	0.97	2.55	3.42(4)	149

Symmetry code, transformations used to generate equivalent atoms: [e]x,-1+y,z; [a]1+x,y,z; [b,f]1-x,1-y,1-z; [d]2-x,1-y,1-z; [c]x,1+y,z

Table A.6: Torsion angles (º) for *fac*-[$Re_2(CO)_6$(TS)(Py)] (1).

Torsion Angles	Angle	Torsion Angles	Angle
S2-C18-C19-S1	44.585(36)	Re2-S2-C17-C16	-32.085(32)
C18-C19-S1-Re2	14.310(33)	Re2-S1-Re1-S3	-13.883(16)
C19-S1-Re2-S2	-11.644 (22)	S1-Re1-S3-Re2	14.003(16)
S1-Re2-S2-C18	30.045(12)	Re1-S3-Re2-S1	-14.223(17)
Re2-S2-C18-C19	-51.033(30)	S3-Re2-S1-Re1	13.975(16)
S2-C17-C16-S3	53.124(36)	N1-C11-C12-C13	-7.734(55)
C17-C16-S3-Re2	-43.838(32)	C11-C12-C13-C14	3.996(53)
C16-S3-Re2-S2	16.608(21)	C12-C13-C14-C15	-6.188(55)
S3-Re2-S2-C17	5.133(22)	C13-C14-C15-N1	12.099(57)
Re2-S2-C17-C16	-32.085(32)	C14-C15-N1-C11	-14.974(53)
Re2-S1-Re1-S3	-13.883(16)	C15-N1-C11-C12	12.879(53)

APPENDIX B

Table B.1: Atomic coordinates (x 10^4) and equivalent isotropic displacement parameters ($Å^2$ x 10^3) for *fac*-[$Re_2(CO)_6(PPh_3)(BSOPhC)_2(Py)$] (2). U(eq) is defined as one third of the trace of the orthogonalized U^{ij} tensor.

	x	y	z	U(eq)
Re(1)	3583(1)	822(1)	8240(1)	27(1)
Re(2)	909(1)	1276(1)	6554(1)	32(1)
S(2)	1750(1)	1523(1)	7924(1)	32(1)
S(1)	3065(1)	1039(1)	6835(1)	29(1)
P(1)	4649(1)	1963(1)	8618(1)	28(1)
C(16)	6371(4)	1308(2)	9819(3)	42(1)
C(64)	1400(5)	3607(3)	6660(4)	66(2)
C(6)	393(4)	354(3)	6709(3)	42(1)
C(1)	3698(4)	675(2)	9270(3)	42(1)
O(1)	3731(3)	579(2)	9874(2)	64(1)
O(46)	5329(3)	567(2)	6778(2)	46(1)
O(2)	2407(3)	-619(2)	7810(2)	58(1)
C(41)	3337(4)	284(2)	6346(2)	31(1)
C(3)	5058(4)	381(2)	8376(2)	33(1)
O(3)	5943(3)	118(2)	8469(2)	52(1)
C(63)	1944(6)	3759(3)	6149(5)	87(2)
C(51)	723(4)	1236(2)	8356(3)	38(1)
C(11)	6093(4)	1869(2)	9323(2)	33(1)
C(31)	3984(3)	2620(2)	9061(2)	27(1)
C(13)	7979(5)	2353(3)	9949(3)	58(2)
C(43)	2662(5)	-657(2)	5455(3)	51(1)
C(2)	2818(4)	-78(2)	7962(3)	37(1)
C(36)	4404(4)	2763(2)	9820(3)	40(1)
C(33)	2530(4)	3523(2)	8945(3)	49(1)
C(32)	3029(4)	3001(2)	8623(3)	40(1)
C(42)	2451(4)	-139(2)	5914(3)	42(1)
C(24)	5737(5)	3081(3)	6785(3)	67(2)
C(26)	5509(4)	2063(2)	7446(3)	44(1)
C(62)	2206(6)	3217(4)	5759(5)	95(3)
C(47)	6508(4)	400(3)	6838(4)	70(2)
N(6)	1416(3)	2381(2)	6401(2)	42(1)
C(12)	6910(4)	2397(2)	9398(3)	42(1)
C(45)	4659(4)	-364(2)	5863(3)	43(1)
C(23)	5229(6)	3472(3)	7201(4)	74(2)
C(46)	4468(4)	156(2)	6334(2)	34(1)
C(34)	2988(5)	3664(3)	9696(3)	51(1)
C(35)	3904(5)	3285(3)	10136(3)	50(1)
C(65)	1144(4)	2917(3)	6771(3)	49(1)
C(61)	1935(5)	2543(3)	5898(4)	71(2)

C(21)	5005(4)	2444(2)	7882(2)	33(1)
C(14)	8238(5)	1799(3)	10436(3)	67(2)
C(25)	5879(5)	2382(3)	6909(3)	60(2)
O(6)	12(3)	-178(2)	6794(2)	64(1)
O(5)	-1590(3)	1663(2)	6435(2)	62(1)
O(4)	181(4)	1013(2)	4867(2)	74(1)
C(5)	-645(4)	1548(2)	6478(3)	41(1)
C(4)	449(4)	1110(3)	5494(3)	45(1)
C(44)	3755(5)	-755(2)	5427(3)	53(1)
C(15)	7444(5)	1273(3)	10368(3)	56(1)
C(22)	4867(5)	3153(3)	7759(3)	57(2)
O(56)	-153(3)	2345(2)	8021(2)	65(1)
C(52)	762(5)	592(3)	8693(3)	51(1)
C(56)	-171(4)	1709(3)	8342(3)	52(1)
C(53)	-75(6)	394(3)	9006(3)	72(2)
C(55)	-1035(5)	1493(4)	8643(4)	77(2)
C(54)	-974(6)	838(4)	8970(4)	84(2)
C(57)	-946(6)	2881(4)	8079(5)	102(3)

Table B.2: Bond distances (Å) and angles (°) for *fac*-[$Re_2(CO)_6(PPh_3)(BSOPhC)_2(Py)$] (2).

Bond	Bond Distance	Bond Angle	Angle
Re(1)-C(3)	1.922(4)	C(3)-Re(1)-C(1)	92.23(19)
Re(1)-C(1)	1.923(5)	C(3)-Re(1)-C(2)	89.84(18)
Re(1)-C(2)	1.939(5)	C(1)-Re(1)-C(2)	90.96(19)
Re(1)-S(2)	2.5006(13)	C(3)-Re(1)-S(2)	171.01(13)
Re(1)-P(1)	2.5103(12)	C(1)-Re(1)-S(2)	95.06(14)
Re(1)-S(1)	2.5507(13)	C(2)-Re(1)-S(2)	95.29(13)
Re(2)-C(6)	1.918(5)	C(3)-Re(1)-P(1)	88.00(13)
Re(2)-C(4)	1.919(5)	C(1)-Re(1)-P(1)	88.60(14)
Re(2)-C(5)	1.920(5)	C(2)-Re(1)-P(1)	177.77(13)
Re(2)-N(6)	2.235(4)	S(2)-Re(1)-P(1)	86.93(4)
Re(2)-S(2)	2.4974(13)	C(3)-Re(1)-S(1)	96.83(13)
Re(2)-S(1)	2.5439(15)	C(1)-Re(1)-S(1)	170.34(15)
S(2)-C(51)	1.782(5)	C(2)-Re(1)-S(1)	85.72(14)
S(1)-C(41)	1.794(4)	S(2)-Re(1)-S(1)	76.26(3)
P(1)-C(21)	1.827(4)	P(1)-Re(1)-S(1)	95.06(4)
P(1)-C(31)	1.830(4)	C(6)-Re(2)-C(4)	90.4(2)
P(1)-C(11)	1.840(5)	C(6)-Re(2)-C(5)	84.02(19)
C(16)-C(15)	1.382(7)	C(4)-Re(2)-C(5)	90.9(2)
C(16)-C(11)	1.388(6)	C(6)-Re(2)-N(6)	176.16(16)
C(64)-C(63)	1.363(9)	C(4)-Re(2)-N(6)	91.19(19)
C(64)-C(65)	1.381(7)	C(5)-Re(2)-N(6)	92.47(17)
C(6)-O(6)	1.145(5)	C(6)-Re(2)-S(2)	93.42(15)
C(1)-O(1)	1.141(5)	C(4)-Re(2)-S(2)	172.97(14)
O(46)-C(46)	1.359(5)	C(5)-Re(2)-S(2)	95.33(15)

O(46)-C(47)	1.438(5)	N(6)-Re(2)-S(2)	85.33(11)
O(2)-C(2)	1.140(5)	C(6)-Re(2)-S(1)	99.88(14)
C(41)-C(42)	1.381(6)	C(4)-Re(2)-S(1)	97.12(14)
C(41)-C(46)	1.405(6)	C(5)-Re(2)-S(1)	171.01(15)
C(3)-O(3)	1.148(5)	N(6)-Re(2)-S(1)	83.37(10)
C(63)-C(62)	1.362(10)	S(2)-Re(2)-S(1)	76.44(4)
C(51)-C(52)	1.373(6)	C(51)-S(2)-Re(2)	107.48(16)
C(51)-C(56)	1.406(6)	C(51)-S(2)-Re(1)	115.48(16)
C(11)-C(12)	1.387(6)	Re(2)-S(2)-Re(1)	100.60(4)
C(31)-C(36)	1.382(6)	C(41)-S(1)-Re(2)	112.54(15)
C(31)-C(32)	1.394(6)	C(41)-S(1)-Re(1)	112.23(14)
C(13)-C(14)	1.365(8)	Re(2)-S(1)-Re(1)	98.01(3)
C(13)-C(12)	1.382(7)	C(21)-P(1)-C(31)	104.52(19)
C(43)-C(44)	1.361(7)	C(21)-P(1)-C(11)	101.1(2)
C(43)-C(42)	1.389(6)	C(31)-P(1)-C(11)	101.28(19)
C(36)-C(35)	1.394(6)	C(21)-P(1)-Re(1)	116.37(14)
C(33)-C(34)	1.370(7)	C(31)-P(1)-Re(1)	117.23(13)
C(33)-C(32)	1.399(6)	C(11)-P(1)-Re(1)	114.09(14)
C(24)-C(25)	1.351(8)	C(15)-C(16)-C(11)	120.6(5)
C(24)-C(23)	1.364(8)	C(63)-C(64)-C(65)	119.5(6)
C(26)-C(25)	1.376(6)	O(6)-C(6)-Re(2)	175.3(4)
C(26)-C(21)	1.379(6)	O(1)-C(1)-Re(1)	177.8(5)
C(62)-C(61)	1.370(8)	C(46)-O(46)-C(47)	118.2(4)
N(6)-C(61)	1.332(6)	C(42)-C(41)-C(46)	118.2(4)
N(6)-C(65)	1.337(6)	C(42)-C(41)-S(1)	122.1(3)
C(45)-C(44)	1.363(7)	C(46)-C(41)-S(1)	119.4(3)
C(45)-C(46)	1.396(6)	O(3)-C(3)-Re(1)	179.1(4)
C(23)-C(22)	1.401(7)	C(62)-C(63)-C(64)	118.1(6)
C(34)-C(35)	1.362(7)	C(52)-C(51)-C(56)	119.4(4)
C(21)-C(22)	1.371(6)	C(52)-C(51)-S(2)	124.1(4)
C(14)-C(15)	1.369(8)	C(56)-C(51)-S(2)	116.5(4)
O(5)-C(5)	1.147(5)	C(12)-C(11)-C(16)	118.5(4)
O(4)-C(4)	1.136(6)	C(12)-C(11)-P(1)	119.4(3)
O(56)-C(56)	1.357(6)	C(16)-C(11)-P(1)	122.0(3)
O(56)-C(57)	1.432(6)	C(36)-C(31)-C(32)	118.1(4)
C(52)-C(53)	1.383(7)	C(36)-C(31)-P(1)	122.4(3)
C(56)-C(55)	1.408(7)	C(32)-C(31)-P(1)	119.5(3)
C(53)-C(54)	1.367(8)	C(14)-C(13)-C(12)	120.7(5)
C(55)-C(54)	1.382(9)	C(44)-C(43)-C(42)	120.0(5)
		O(2)-C(2)-Re(1)	177.4(4)
		C(31)-C(36)-C(35)	121.0(4)
		C(34)-C(33)-C(32)	119.8(5)
		C(31)-C(32)-C(33)	120.5(5)
		C(41)-C(42)-C(43)	121.0(4)
		C(25)-C(24)-C(23)	119.6(5)

		C(25)-C(26)-C(21)	121.3(5)
		C(63)-C(62)-C(61)	119.6(6)
		C(61)-N(6)-C(65)	116.6(4)
		C(61)-N(6)-Re(2)	121.5(4)
		C(65)-N(6)-Re(2)	121.7(3)
		C(13)-C(12)-C(11)	120.2(5)
		C(44)-C(45)-C(46)	120.2(4)
		C(24)-C(23)-C(22)	120.3(5)
		O(46)-C(46)-C(45)	123.2(4)
		O(46)-C(46)-C(41)	117.0(4)
		C(45)-C(46)-C(41)	119.8(4)
		C(35)-C(34)-C(33)	120.5(5)
		C(34)-C(35)-C(36)	120.0(5)
		N(6)-C(65)-C(64)	122.7(5)
		N(6)-C(61)-C(62)	123.4(6)
		C(22)-C(21)-C(26)	118.1(4)
		C(22)-C(21)-P(1)	125.2(4)
		C(26)-C(21)-P(1)	116.6(3)
		C(13)-C(14)-C(15)	119.8(5)
		C(24)-C(25)-C(26)	120.5(5)
		O(5)-C(5)-Re(2)	175.3(4)
		O(4)-C(4)-Re(2)	179.7(5)
		C(43)-C(44)-C(45)	120.7(5)
		C(14)-C(15)-C(16)	120.2(5)
		C(21)-C(22)-C(23)	120.2(5)
		C(56)-O(56)-C(57)	119.6(5)
		C(51)-C(52)-C(53)	121.4(5)
		O(56)-C(56)-C(51)	117.2(4)
		O(56)-C(56)-C(55)	124.2(5)
		C(51)-C(56)-C(55)	118.6(5)
		C(54)-C(53)-C(52)	119.8(6)
		C(54)-C(55)-C(56)	120.2(6)
		C(53)-C(54)-C(55)	120.5(5)

Table B.3: Anisotropic displacement parameters ($Å^2$ x 10^3) for *fac*-$[Re_2(CO)_6(PPh_3)(BSOPhC)_2(Py)]$ (2). The anisotropic displacement factor exponent takes the form: $-2\pi^2[h2a^{*2}U^{11} + ... + 2hka^*b^*U^{12}]$.

	U_{11}	U_{22}	U_{33}	U_{23}	U_{13}	U_{12}
Re(1)	28(1)	23(1)	29(1)	1(1)	10(1)	1(1)
Re(2)	26(1)	34(1)	36(1)	2(1)	9(1)	0(1)
S(2)	30(1)	30(1)	38(1)	0(1)	14(1)	2(1)
S(1)	27(1)	28(1)	31(1)	-1(1)	10(1)	0(1)
P(1)	29(1)	25(1)	28(1)	-1(1)	9(1)	0(1)
C(16)	36(3)	46(3)	36(3)	3(2)	0(2)	6(2)
C(64)	59(4)	42(3)	77(5)	9(3)	-6(3)	3(3)
C(6)	35(3)	45(3)	47(3)	-2(2)	14(2)	-1(2)
C(1)	47(3)	36(3)	46(3)	4(2)	19(2)	-1(2)
O(1)	79(3)	80(3)	35(2)	14(2)	23(2)	-6(2)
O(46)	32(2)	50(2)	58(2)	-14(2)	16(2)	-1(2)
O(2)	61(2)	30(2)	76(3)	-4(2)	13(2)	-13(2)
C(41)	37(2)	28(2)	31(2)	-1(2)	15(2)	-1(2)
C(3)	37(3)	24(2)	37(3)	0(2)	10(2)	-2(2)
O(3)	41(2)	49(2)	64(3)	2(2)	13(2)	18(2)
C(63)	68(5)	46(4)	140(8)	34(4)	22(5)	-10(3)
C(51)	35(3)	46(3)	35(3)	-8(2)	13(2)	-4(2)
C(11)	30(2)	34(2)	34(3)	-6(2)	9(2)	2(2)
C(31)	26(2)	25(2)	31(2)	-4(2)	9(2)	-2(2)
C(13)	42(3)	64(4)	60(4)	-17(3)	6(3)	-8(3)
C(43)	50(3)	40(3)	63(4)	-22(3)	16(3)	-9(2)
C(2)	36(3)	33(2)	42(3)	4(2)	15(2)	1(2)
C(36)	39(3)	48(3)	35(3)	-3(2)	16(2)	7(2)
C(33)	39(3)	34(3)	69(4)	-6(3)	11(3)	5(2)
C(32)	40(3)	34(2)	40(3)	-3(2)	4(2)	1(2)
C(42)	40(3)	36(3)	51(3)	-7(2)	17(2)	-1(2)
C(24)	85(5)	73(4)	52(4)	4(3)	34(3)	-32(4)
C(26)	54(3)	36(3)	45(3)	-4(2)	21(3)	-12(2)
C(62)	94(5)	65(4)	151(8)	50(5)	75(6)	12(4)
C(47)	40(3)	80(4)	94(5)	-23(4)	27(3)	-3(3)
N(6)	31(2)	39(2)	55(3)	12(2)	12(2)	5(2)
C(12)	34(3)	41(3)	47(3)	-8(2)	9(2)	-2(2)
C(45)	46(3)	40(3)	50(3)	-5(2)	24(3)	8(2)
C(23)	96(5)	45(3)	91(5)	22(3)	45(4)	-7(3)
C(46)	37(2)	33(2)	34(3)	2(2)	13(2)	0(2)
C(34)	49(3)	47(3)	66(4)	-18(3)	30(3)	-1(2)
C(35)	55(3)	65(3)	35(3)	-13(3)	22(3)	2(3)
C(65)	40(3)	39(3)	57(4)	7(3)	1(2)	-1(2)
C(61)	74(4)	55(4)	101(5)	24(3)	54(4)	13(3)
C(21)	39(3)	30(2)	28(2)	0(2)	10(2)	-9(2)
C(14)	41(3)	86(5)	57(4)	-17(3)	-8(3)	3(3)
C(25)	71(4)	63(4)	59(4)	-17(3)	38(3)	-32(3)

O(6)	59(2)	45(2)	87(3)	1(2)	22(2)	-19(2)
O(5)	29(2)	81(3)	79(3)	4(2)	22(2)	8(2)
O(4)	58(3)	117(3)	41(3)	-6(2)	7(2)	-8(2)
C(5)	39(3)	43(3)	42(3)	6(2)	13(2)	1(2)
C(4)	27(2)	59(3)	44(3)	1(3)	5(2)	-1(2)
C(44)	65(4)	37(3)	61(4)	-13(3)	27(3)	5(3)
C(15)	52(3)	62(4)	43(3)	7(3)	0(3)	10(3)
C(22)	75(4)	38(3)	68(4)	9(3)	39(3)	-2(3)
O(56)	55(2)	60(2)	85(3)	-1(2)	31(2)	24(2)
C(52)	51(3)	57(3)	52(3)	1(3)	27(3)	-4(3)
C(56)	45(3)	61(3)	58(4)	-15(3)	26(3)	7(3)
C(53)	84(5)	80(4)	72(4)	-4(3)	53(4)	-20(4)
C(55)	57(4)	106(5)	85(5)	-18(4)	45(4)	8(4)
C(54)	73(5)	105(5)	101(6)	-15(5)	67(5)	-25(4)
C(57)	77(5)	85(5)	152(8)	-14(5)	48(5)	40(4)

Table B.4: Hydrogen coordinates (x 10^4) and isotropic displacement parameters (Å^2 x 10^3) for *fac*-[$Re_2(CO)_6(PPh_3)(BSOPhC)_2(Py)$] (2).

	x	y	z	U(eq)
H(16)	5831	953	9783	50
H(64)	1204	3966	6932	79
H(63)	2131	4219	6069	105
H(13)	8527	2704	9989	69
H(43)	2055	-936	5166	62
H(36)	5029	2507	10124	48
H(33)	1890	3774	8651	59
H(32)	2720	2908	8113	48
H(42)	1702	-76	5931	50
H(24)	5983	3294	6419	80
H(26)	5602	1580	7518	52
H(62)	2566	3304	5401	114
H(47A)	7023	730	7168	105
H(47B)	6600	424	6352	105
H(47C)	6689	-66	7036	105
H(12)	6738	2781	9076	50
H(45)	5406	-444	5848	52
H(23)	5123	3952	7115	89
H(34)	2671	4020	9907	62
H(35)	4197	3375	10647	60
H(65)	767	2821	7118	58
H(61)	2122	2180	5627	85
H(14)	8953	1780	10813	80
H(25)	6229	2116	6628	72
H(44)	3887	-1092	5106	63
H(15)	7627	891	10692	67

H(22)	4531	3424	8045	68
H(52)	1363	284	8711	61
H(53)	-25	-40	9240	86
H(55)	-1649	1792	8623	92
H(54)	-1550	698	9166	101
H(57A)	-826	3297	7825	153
H(57B)	-817	2987	8598	153
H(57C)	-1729	2719	7854	153

Table B.5: Torsion angles (º) for *fac*-[$Re_2(CO)_6(PPh_3)(BSOPhC)_2(Py)$] (2).

Torsion Angles	Angle	Torsion Angles	Angle
S1-C41-C46-O16	8.24(35)	C64-C65-N6-C61	-1.358(40)
S2-C51-C56-O56-C57	-1.817(17)	C65-N6-C61-C62	0.994(40)
C41-C42-C43-C44	0.199(39)	C31-C32-C33-C34	0.398(39)
C42-C43-C44-C45	1.995(39)	C32-C33-C34-C35	-1.963(39)
C43-C44-C45-C46	-1.507(39)	C33-C34-C35-C36	1.766(39)
C44-C45-C46-C41	-1.142(39)	C34-C35-C36-C31	0.013(38)
C45-C46-C41-C42	3.221(38)	C35-C36-C31-C32	-1.568(38)
C46-C41-C42-C43	-2.770(38)	C36-C31-C32-C33	1.319(38)
C45-C46-O46-C47	-8.207(40)	C21- C22-C23C-24	-0.906(39)
C51-C52-C53-C54	1.262(39)	C22-C23-C24-C25	0.589(39)
C52-C53-C54-C55	-2.057(39)	C23-C24-C25-C26	0.421(39)
C53-C54-C55-C56	0.264(39)	C24-C25-C26-C21	-1.484(40)
C54-C55-C56-C51	2.287(38)	C25-C26-C21-C22	0.814(39)
C55-C56-C51-C52	-3.052(38)	C26-C21-C22-C23	0.199(38)
C56-C51-C52-C53	1.326(39)	C11-C12-C13-C14	-1.322(39)
C55-C56-O56-C57	9.665(40)	C12-C13-C14-C15	1.553(39)
N1-C61C62-C63	0.144(41)	C13-C14-C15-C16	-1.456(39)
C61-C62-C63-C64	-0.930(38)	C14-C15-C16-C11	1.139(39)
C62-C63-C64-C65	0.576(38)	C15-C16-C11-C12	-0.888(39)
C63-C64-C65-N6	0.601(40)	C16-C11-C12-C13	0.973(38)
Re1-S1-Re2-S2	21.961(11)	S2-Re1-S1-Re2	-21.949(11)

APPENDIX C

Table C.1: Atomic coordinates (x 10^4) and equivalent isotropic displacement parameters (Å^2 x 10^3) for *fac*-[NEt_4][$Re_2(CO)_3(BSOPhC)_3$] (3). U(eq) is defined as one third of the trace of the orthogonalized U^{ij} tensor.

	x	y	z	U(eq)
Re(01)	7999(1)	2165(1)	1667(1)	36(1)
Re(02)	7946(1)	3110(1)	3369(1)	35(1)
S(2)	9395(2)	2573(2)	2584(2)	34(1)
S(1)	7366(2)	3480(2)	2082(2)	39(1)
S(3)	7165(2)	1852(2)	2888(2)	36(1)
C(30)	7752(9)	1101(6)	3438(7)	34(3)
O(36)	6386(11)	1324(7)	4246(8)	87(4)
C(20)	10164(9)	3406(7)	2363(7)	37(3)
O(26)	11070(9)	3106(6)	3490(6)	66(3)
C(35)	7288(12)	912(8)	4102(8)	50(3)
O(5)	8982(11)	2459(8)	4772(6)	75(3)
C(10)	5991(10)	3576(7)	1880(8)	42(3)
O(1)	9147(13)	676(8)	1248(9)	97(5)
O(6)	8977(11)	4677(7)	3717(7)	78(4)
C(23)	11399(11)	4742(8)	2193(8)	53(3)
O(2)	8672(12)	2804(8)	182(7)	82(4)
C(6)	8594(13)	4093(9)	3579(8)	53(4)
C(32)	9102(11)	118(8)	3709(9)	54(4)
C(2)	8437(12)	2581(9)	740(8)	51(3)
C(13)	3906(12)	3840(9)	1486(11)	66(5)
C(11)	5236(11)	3535(10)	2390(9)	58(4)
C(34)	7716(13)	340(8)	4553(8)	53(4)
C(14)	4645(13)	3867(9)	954(10)	62(4)
C(22)	10623(11)	4545(8)	1666(8)	51(3)
C(31)	8666(10)	689(7)	3248(8)	44(3)
C(4)	6783(12)	3432(9)	3932(7)	51(3)
C(33)	8600(12)	-70(9)	4362(9)	54(4)
C(24)	11560(11)	4283(8)	2812(9)	52(3)
C(12)	4187(12)	3671(10)	2212(11)	61(4)
O(3)	5951(10)	1591(9)	919(7)	89(4)
O(16)	6483(9)	3780(8)	662(7)	73(3)
C(21)	10022(10)	3873(7)	1764(8)	45(3)
C(25)	10965(10)	3611(8)	2902(8)	44(3)
O(4)	6092(10)	3646(9)	4298(7)	90(4)
C(36)	5689(16)	1025(15)	4742(14)	108(8)
C(15)	5698(12)	3740(8)	1151(9)	54(4)
C(26)	11723(19)	3353(12)	4104(11)	88(7)
C(1)	8665(13)	1220(9)	1417(8)	55(4)
C(5)	8594(12)	2702(8)	4249(8)	47(3)

C(3)	6728(12)	1815(9)	1191(9)	55(4)
N(1)	2606(10)	1254(7)	1825(8)	55(3)
C(011)	3900(30)	1616(18)	2902(16)	141(13)
C(05)	3220(20)	587(16)	654(12)	116(10)
C(04)	3520(20)	1240(20)	1345(18)	56(8)
C(03)	1556(19)	1520(20)	1420(20)	60(9)
C(07)	1760(30)	1340(20)	2350(20)	74(7)
C(010)	2830(40)	1930(20)	2400(30)	89(9)
C(06)	2310(40)	560(20)	1240(20)	86(12)
C(09)	2410(30)	480(20)	2190(20)	74(7)
C(012)	3710(40)	1000(20)	2210(30)	89(9)
C(01)	2870(50)	2000(20)	1400(30)	110(20)
C(16)	6250(20)	3954(16)	-91(12)	116(9)
C(02)	1750(20)	2295(13)	972(14)	107(9)
C(8)	1566(19)	541(13)	2808(14)	94(7)

Table C.2: Bond distances [Å] and angles [°] for *fac*-[NEt_4][$Re_2(CO)_3(BSOPhC)_3$] (3).

Bond	Bond Distance	Bond Angle	Angle
Re(01)-C(1)	1.886(15)	C(1)-Re(01)-C(3)	90.1(7)
Re(01)-C(3)	1.909(15)	C(1)-Re(01)-C(2)	88.0(7)
Re(01)-C(2)	1.922(15)	C(3)-Re(01)-C(2)	88.9(6)
Re(01)-S(2)	2.501(3)	C(1)-Re(01)-S(2)	94.9(5)
Re(01)-S(1)	2.511(3)	C(3)-Re(01)-S(2)	165.2(5)
Re(01)-S(3)	2.536(3)	C(2)-Re(01)-S(2)	105.2(4)
Re(02)-C(4)	1.900(15)	C(1)-Re(01)-S(1)	171.7(5)
Re(02)-C(6)	1.906(15)	C(3)-Re(01)-S(1)	98.2(5)
Re(02)-C(5)	1.910(14)	C(2)-Re(01)-S(1)	91.9(5)
Re(02)-S(1)	2.511(3)	S(2)-Re(01)-S(1)	77.16(10)
Re(02)-S(3)	2.517(3)	C(1)-Re(01)-S(3)	103.3(5)
Re(02)-S(2)	2.531(3)	C(3)-Re(01)-S(3)	87.8(5)
S(2)-C(20)	1.780(12)	C(2)-Re(01)-S(3)	168.3(5)
S(1)-C(10)	1.785(13)	S(2)-Re(01)-S(3)	77.52(10)
S(3)-C(30)	1.779(12)	S(1)-Re(01)-S(3)	77.48(10)
C(30)-C(35)	1.393(18)	C(4)-Re(02)-C(6)	88.6(7)
C(30)-C(31)	1.409(17)	C(4)-Re(02)-C(5)	88.9(6)
O(36)-C(35)	1.376(18)	C(6)-Re(02)-C(5)	88.9(6)
O(36)-C(36)	1.38(2)	C(4)-Re(02)-S(1)	102.3(4)
C(20)-C(21)	1.356(18)	C(6)-Re(02)-S(1)	94.5(4)
C(20)-C(25)	1.437(17)	C(5)-Re(02)-S(1)	168.3(4)
O(26)-C(25)	1.377(17)	C(4)-Re(02)-S(3)	97.4(5)
O(26)-C(26)	1.436(19)	C(6)-Re(02)-S(3)	171.1(5)
C(35)-C(34)	1.38(2)	C(5)-Re(02)-S(3)	97.8(4)
O(5)-C(5)	1.136(16)	S(1)-Re(02)-S(3)	77.82(10)
C(10)-C(11)	1.35(2)	C(4)-Re(02)-S(2)	174.7(5)

C(10)-C(15)	1.394(19)	C(6)-Re(02)-S(2)	96.6(5)
O(1)-C(1)	1.159(19)	C(5)-Re(02)-S(2)	91.9(5)
O(6)-C(6)	1.138(18)	S(1)-Re(02)-S(2)	76.60(10)
C(23)-C(24)	1.38(2)	S(3)-Re(02)-S(2)	77.31(10)
C(23)-C(22)	1.40(2)	C(20)-S(2)-Re(01)	117.3(4)
O(2)-C(2)	1.130(18)	C(20)-S(2)-Re(02)	104.4(4)
C(32)-C(31)	1.391(19)	Re(01)-S(2)-Re(02)	87.77(10)
C(32)-C(33)	1.40(2)	C(10)-S(1)-Re(01)	109.9(4)
C(13)-C(14)	1.37(3)	C(10)-S(1)-Re(02)	118.4(5)
C(13)-C(12)	1.39(2)	Re(01)-S(1)-Re(02)	87.97(10)
C(11)-C(12)	1.38(2)	C(30)-S(3)-Re(02)	105.5(4)
C(34)-C(33)	1.38(2)	C(30)-S(3)-Re(01)	117.6(4)
C(14)-C(15)	1.39(2)	Re(02)-S(3)-Re(01)	87.28(9)
C(22)-C(21)	1.395(17)	C(35)-C(30)-C(31)	117.8(12)
C(4)-O(4)	1.173(18)	C(35)-C(30)-S(3)	118.1(10)
C(24)-C(25)	1.387(18)	C(31)-C(30)-S(3)	124.1(10)
O(3)-C(3)	1.157(17)	C(35)-O(36)-C(36)	119.1(14)
O(16)-C(15)	1.35(2)	C(21)-C(20)-C(25)	118.6(11)
O(16)-C(16)	1.42(2)	C(21)-C(20)-S(2)	126.1(9)
N(1)-C(07)	1.46(4)	C(25)-C(20)-S(2)	115.2(10)
N(1)-C(04)	1.47(3)	C(25)-O(26)-C(26)	117.3(12)
N(1)-C(09)	1.51(4)	O(36)-C(35)-C(34)	124.6(14)
N(1)-C(01)	1.53(4)	O(36)-C(35)-C(30)	114.8(13)
N(1)-C(010)	1.57(4)	C(34)-C(35)-C(30)	120.6(13)
N(1)-C(03)	1.57(3)	C(11)-C(10)-C(15)	118.9(13)
N(1)-C(012)	1.60(5)	C(11)-C(10)-S(1)	124.3(11)
N(1)-C(06)	1.63(5)	C(15)-C(10)-S(1)	116.7(11)
C(011)-C(012)	1.65(5)	C(24)-C(23)-C(22)	120.4(13)
C(011)-C(010)	1.70(6)	O(6)-C(6)-Re(02)	178.7(14)
C(05)-C(06)	1.59(5)	C(31)-C(32)-C(33)	119.2(14)
C(05)-C(04)	1.71(4)	O(2)-C(2)-Re(01)	177.4(13)
C(03)-C(02)	1.59(4)	C(14)-C(13)-C(12)	120.9(14)
C(03)-C(07)	1.73(5)	C(10)-C(11)-C(12)	121.9(16)
C(07)-C(8)	1.62(4)	C(33)-C(34)-C(35)	121.6(14)
C(07)-C(010)	1.70(6)	C(13)-C(14)-C(15)	119.2(16)
C(06)-C(09)	1.74(6)	C(21)-C(22)-C(23)	119.4(14)
C(09)-C(8)	1.58(4)	C(32)-C(31)-C(30)	121.5(13)
C(09)-C(012)	1.87(6)	O(4)-C(4)-Re(02)	177.3(14)
C(01)-C(02)	1.67(6)	C(34)-C(33)-C(32)	119.3(13)
		C(23)-C(24)-C(25)	119.7(13)
		C(11)-C(12)-C(13)	118.7(17)
		C(15)-O(16)-C(16)	120.1(14)
		C(20)-C(21)-C(22)	121.7(12)
		O(26)-C(25)-C(24)	124.6(12)

		O(26)-C(25)-C(20)	115.3(11)
		C(24)-C(25)-C(20)	120.1(13)
		O(16)-C(15)-C(14)	122.9(15)
		O(16)-C(15)-C(10)	116.7(12)
		C(14)-C(15)-C(10)	120.4(16)
		O(1)-C(1)-Re(01)	174.3(16)
		O(5)-C(5)-Re(02)	179.8(17)
		O(3)-C(3)-Re(01)	178.2(14)
		C(07)-N(1)-C(04)	174(2)
		C(09)-N(1)-C(01)	174(3)
		C(07)-N(1)-C(010)	68(2)
		C(04)-N(1)-C(010)	106(2)
		C(07)-N(1)-C(03)	69(2)
		C(04)-N(1)-C(03)	113.8(19)
		C(010)-N(1)-C(03)	104(2)
		C(09)-N(1)-C(012)	74(2)
		C(01)-N(1)-C(012)	104(3)
		C(09)-N(1)-C(06)	67(2)
		C(01)-N(1)-C(06)	109(3)
		C(012)-N(1)-C(06)	106(2)
		N(1)-C(04)-C(05)	106(2)
		N(1)-C(03)-C(02)	110(2)
		N(1)-C(03)-C(07)	52.3(16)
		C(02)-C(03)-C(07)	129(3)
		N(1)-C(07)-C(8)	112(2)
		N(1)-C(07)-C(010)	59(2)
		C(8)-C(07)-C(010)	128(3)
		N(1)-C(07)-C(03)	58.3(18)
		C(8)-C(07)-C(03)	129(3)
		C(010)-C(07)-C(03)	92(3)
		N(1)-C(010)-C(07)	53.0(19)
		N(1)-C(010)-C(011)	105(3)
		C(07)-C(010)-C(011)	118(3)
		C(05)-C(06)-N(1)	105(3)
		C(05)-C(06)-C(09)	129(3)
		N(1)-C(06)-C(09)	53.1(19)
		N(1)-C(09)-C(8)	112(2)
		N(1)-C(09)-C(06)	60(2)
		C(8)-C(09)-C(06)	132(3)
		N(1)-C(09)-C(012)	55.3(19)
		C(8)-C(09)-C(012)	125(3)
		C(06)-C(09)-C(012)	91(3)
		N(1)-C(012)-C(011)	106(3)
		N(1)-C(012)-C(09)	50.7(17)

		C(011)-C(012)-C(09)	115(3)
		N(1)-C(01)-C(02)	107(3)

Table C.3: Anisotropic displacement parameters ($Å^2$ x 10^3) for *fac*-[NEt_4][$Re_2(CO)_3(BSOPhC)_3$] (3).The anisotropic displacement factor exponent takes the form: $-2\pi^2[h2a^{*2}U^{11} + ... + 2hka^*b^*U^{12}]$.

	U_{11}	U_{22}	U_{33}	U_{23}	U_{13}	U_{12}
Re(01)	39(1)	34(1)	34(1)	-2(1)	-3(1)	-9(1)
Re(02)	39(1)	32(1)	33(1)	-1(1)	-3(1)	1(1)
S(2)	34(1)	31(1)	37(2)	-2(1)	-4(1)	-5(1)
S(1)	38(2)	36(2)	42(2)	4(1)	-7(1)	-2(1)
S(3)	35(1)	35(1)	38(2)	3(1)	-1(1)	-5(1)
C(30)	43(7)	26(5)	32(6)	-3(5)	-7(5)	-1(5)
O(36)	102(9)	69(8)	92(10)	23(7)	51(8)	27(7)
C(20)	32(6)	33(6)	46(7)	-4(5)	-1(5)	-6(5)
O(26)	69(7)	68(7)	60(7)	8(5)	-22(6)	-28(5)
C(35)	65(9)	42(7)	44(8)	-4(6)	13(7)	-4(6)
O(5)	96(9)	82(8)	48(7)	4(6)	-18(6)	23(7)
C(10)	41(6)	33(6)	53(8)	-5(5)	-8(6)	2(5)
O(1)	130(12)	64(8)	96(11)	-14(7)	20(10)	16(8)
O(6)	111(10)	43(6)	79(9)	-12(6)	-15(7)	-18(6)
C(23)	51(8)	51(8)	58(9)	-3(7)	5(7)	-19(6)
O(2)	99(10)	96(10)	49(7)	17(6)	7(7)	-42(8)
C(6)	70(9)	48(8)	41(8)	-3(6)	-10(7)	-1(7)
C(32)	41(7)	40(7)	80(11)	0(7)	-13(7)	-6(6)
C(2)	57(8)	51(8)	45(8)	-6(6)	-1(7)	-12(7)
C(13)	45(8)	52(9)	100(14)	-7(8)	-30(9)	15(7)
C(11)	44(8)	69(10)	61(10)	-11(8)	-15(7)	5(7)
C(34)	82(10)	46(8)	32(7)	-2(5)	1(7)	-13(7)
C(14)	64(10)	53(9)	67(11)	3(7)	-25(8)	17(7)
C(22)	50(7)	42(7)	60(9)	1(6)	7(7)	-12(6)
C(31)	43(7)	43(7)	44(7)	2(5)	-6(6)	-5(5)
C(4)	63(9)	59(9)	30(7)	-1(6)	-4(7)	7(7)
C(33)	63(9)	45(8)	54(9)	7(6)	-18(7)	-9(7)
C(24)	43(7)	45(7)	67(10)	-9(7)	-9(7)	-13(6)
C(12)	42(8)	60(9)	82(12)	-16(9)	1(8)	3(7)
O(3)	67(7)	133(12)	67(8)	-4(8)	-21(6)	-49(8)
O(16)	69(7)	99(9)	53(7)	28(6)	-12(6)	6(7)
C(21)	43(7)	39(7)	54(8)	-3(6)	-7(6)	-10(5)
C(25)	37(6)	46(7)	49(8)	-4(6)	-2(6)	-4(5)
O(4)	77(8)	132(12)	62(8)	-12(8)	15(6)	45(8)
C(36)	77(13)	116(19)	130(20)	21(16)	44(14)	17(12)
C(15)	58(8)	48(8)	56(9)	9(6)	-20(7)	5(6)
C(26)	125(17)	76(12)	60(11)	13(9)	-43(11)	-36(12)

C(1)	80(10)	51(8)	36(7)	-10(6)	6(7)	3(8)
C(5)	55(8)	50(8)	36(7)	-5(6)	-7(6)	7(6)
C(3)	52(8)	70(10)	44(8)	4(7)	-2(7)	-21(7)
N(1)	53(7)	50(7)	64(8)	7(6)	8(6)	3(5)
C(011)	190(30)	120(20)	100(20)	32(17)	-70(20)	-60(20)
C(05)	140(20)	150(20)	53(12)	8(13)	38(13)	68(18)
C(04)	42(14)	65(19)	60(20)	-1(15)	13(13)	18(14)
C(03)	23(12)	70(20)	80(20)	10(17)	3(13)	17(12)
C(07)	63(14)	63(15)	100(20)	14(14)	20(14)	4(11)
C(010)	100(20)	62(16)	100(20)	-4(15)	-11(18)	-17(15)
C(06)	100(30)	80(30)	80(30)	20(20)	-10(20)	0(20)
C(09)	63(14)	63(15)	100(20)	14(14)	20(14)	4(11)
C(012)	100(20)	62(16)	100(20)	-4(15)	-11(18)	-17(15)
C(01)	160(50)	60(20)	120(40)	20(20)	-60(40)	-40(30)
C(16)	116(18)	160(20)	71(14)	42(15)	-45(13)	-13(17)
C(02)	160(20)	72(14)	91(17)	17(12)	-3(16)	43(15)

Table C.4: Hydrogen coordinates (x 10^4) and isotropic displacement parameters (Å^2 x 10^3) for *fac*-[NEt_4][$Re_2(CO)_3(BSOPhC)_3$] (3).

	x	y	z	U(eq)
H(23)	11810	5185	2127	64
H(32)	9719	-136	3583	65
H(13)	3204	3936	1359	79
H(11)	5427	3411	2874	70
H(34)	7399	228	4998	64
H(14)	4449	3969	466	74
H(22)	10510	4859	1253	61
H(31)	8985	801	2805	52
H(33)	8861	-469	4664	65
H(24)	12065	4423	3168	62
H(12)	3680	3651	2572	74
H(21)	9510	3742	1410	54
H(36A)	5100	1372	4780	162
H(36B)	6034	972	5216	162
H(36C)	5447	522	4575	162
H(26A)	11732	2955	4476	132
H(26B)	11449	3829	4303	132
H(26C)	12427	3441	3941	132
H(16A)	6891	3963	-360	173
H(16B)	5915	4456	-127	173
H(16C)	5788	3562	-295	173

Table C.5: Torsion angles (°) for *fac*-[NEt_4][$Re_2(CO)_3(BSOPhC)_3$] (3).

Torsion Angle	Angle	Torsion Angle	Angle
Re(02)-S(3)-C(30)-C(35)	86.2(10)	C(01)-N(1)-C(07)-C(8)	-177(3)
Re(01)-S(3)-C(30)-C(35)	-178.7(9)	C(010)-N(1)-C(07)-C(8)	-122(3)
Re(02)-S(3)-C(30)-C(31)	-93.0(10)	C(03)-N(1)-C(07)-C(8)	123(3)
Re(01)-S(3)-C(30)-C(31)	2.1(12)	C(012)-N(1)-C(07)-C(8)	-58(3)
Re(01)-S(2)-C(20)-C(21)	4.5(14)	C(06)-N(1)-C(07)-C(8)	60(3)
Re(02)-S(2)-C(20)-C(21)	-90.5(12)	C(09)-N(1)-C(07)-C(010)	126(3)
Re(01)-S(2)-C(20)-C(25)	-179.2(8)	C(01)-N(1)-C(07)-C(010)	-56(3)
Re(02)-S(2)-C(20)-C(25)	85.8(10)	C(03)-N(1)-C(07)-C(010)	-115(3)
C(36)-O(36)-C(35)-C(34)	-20(3)	C(012)-N(1)-C(07)-C(010)	63(3)
C(36)-O(36)-C(35)-C(30)	159.0(19)	C(06)-N(1)-C(07)-C(010)	-179(3)
C(31)-C(30)-C(35)-O(36)	-178.7(12)	C(09)-N(1)-C(07)-C(03)	-119(3)
S(3)-C(30)-C(35)-O(36)	2.0(17)	C(01)-N(1)-C(07)-C(03)	60(3)
C(31)-C(30)-C(35)-C(34)	-0.1(19)	C(010)-N(1)-C(07)-C(03)	115(3)
S(3)-C(30)-C(35)-C(34)	-179.4(11)	C(012)-N(1)-C(07)-C(03)	179(2)
Re(01)-S(1)-C(10)-C(11)	105.3(12)	C(06)-N(1)-C(07)-C(03)	-63(2)
Re(02)-S(1)-C(10)-C(11)	6.5(14)	C(02)-C(03)-C(07)-N(1)	-85(3)
Re(01)-S(1)-C(10)-C(15)	-77.8(10)	N(1)-C(03)-C(07)-C(8)	-94(3)
Re(02)-S(1)-C(10)-C(15)	-176.6(9)	C(02)-C(03)-C(07)-C(8)	-180(3)
C(15)-C(10)-C(11)-C(12)	-2(2)	N(1)-C(03)-C(07)-C(010)	51(2)
S(1)-C(10)-C(11)-C(12)	175.1(12)	C(02)-C(03)-C(07)-C(010)	-35(4)
O(36)-C(35)-C(34)-C(33)	177.5(15)	C(04)-N(1)-C(010)-C(07)	-179(2)
C(30)-C(35)-C(34)-C(33)	-1(2)	C(09)-N(1)-C(010)-C(07)	-56(3)
C(12)-C(13)-C(14)-C(15)	-1(2)	C(01)-N(1)-C(010)-C(07)	128(3)
C(24)-C(23)-C(22)-C(21)	-1(2)	C(03)-N(1)-C(010)-C(07)	61(2)
C(33)-C(32)-C(31)-C(30)	2.3(19)	C(012)-N(1)-C(010)-C(07)	-122(3)
C(35)-C(30)-C(31)-C(32)	-0.6(18)	C(07)-N(1)-C(010)-C(011)	114(3)
S(3)-C(30)-C(31)-C(32)	178.6(10)	C(04)-N(1)-C(010)-C(011)	-65(3)
C(35)-C(34)-C(33)-C(32)	3(2)	C(09)-N(1)-C(010)-C(011)	58(3)
C(31)-C(32)-C(33)-C(34)	-3(2)	C(01)-N(1)-C(010)-C(011)	-118(4)
C(22)-C(23)-C(24)-C(25)	2(2)	C(03)-N(1)-C(010)-C(011)	174(3)
C(10)-C(11)-C(12)-C(13)	1(2)	C(012)-N(1)-C(010)-C(011)	-8(3)
C(14)-C(13)-C(12)-C(11)	0(2)	C(8)-C(07)-C(010)-N(1)	95(4)
C(25)-C(20)-C(21)-C(22)	-1(2)	C(03)-C(07)-C(010)-N(1)	-50.3(19)
S(2)-C(20)-C(21)-C(22)	175.5(11)	N(1)-C(07)-C(010)-C(011)	-88(4)
C(23)-C(22)-C(21)-C(20)	0(2)	C(8)-C(07)-C(010)-C(011)	7(6)
C(26)-O(26)-C(25)-C(24)	10(2)	C(03)-C(07)-C(010)-C(011)	-139(3)
C(26)-O(26)-C(25)-C(20)	-169.3(15)	C(012)-C(011)-C(010)-N(1)	8(3)
C(23)-C(24)-C(25)-O(26)	179.0(14)	C(012)-C(011)-C(010)-C(07)	64(4)
C(23)-C(24)-C(25)-C(20)	-2(2)	C(04)-C(05)-C(06)-N(1)	5(2)
C(21)-C(20)-C(25)-O(26)	-179.4(13)	C(04)-C(05)-C(06)-C(09)	-49(4)
S(2)-C(20)-C(25)-O(26)	4.0(16)	C(07)-N(1)-C(06)-C(05)	174(2)
C(21)-C(20)-C(25)-C(24)	1(2)	C(04)-N(1)-C(06)-C(05)	-6(2)

S(2)-C(20)-C(25)-C(24)	-175.3(11)	C(09)-N(1)-C(06)-C(05)	-128(3)
C(16)-O(16)-C(15)-C(14)	0(3)	C(01)-N(1)-C(06)-C(05)	48(4)
C(16)-O(16)-C(15)-C(10)	-179.2(17)	C(03)-N(1)-C(06)-C(05)	114(3)
C(13)-C(14)-C(15)-O(16)	-177.9(15)	C(012)-N(1)-C(06)-C(05)	-63(3)
C(13)-C(14)-C(15)-C(10)	1(2)	C(07)-N(1)-C(06)-C(09)	-58(2)
C(11)-C(10)-C(15)-O(16)	179.6(14)	C(04)-N(1)-C(06)-C(09)	122(2)
S(1)-C(10)-C(15)-O(16)	2.5(17)	C(01)-N(1)-C(06)-C(09)	176(3)
C(11)-C(10)-C(15)-C(14)	1(2)	C(03)-N(1)-C(06)-C(09)	-118(2)
S(1)-C(10)-C(15)-C(14)	-176.4(12)	C(012)-N(1)-C(06)-C(09)	64(3)
C(09)-N(1)-C(04)-C(05)	64(3)	C(07)-N(1)-C(09)-C(8)	-4(3)
C(01)-N(1)-C(04)-C(05)	-114(3)	C(04)-N(1)-C(09)-C(8)	170(2)
C(010)-N(1)-C(04)-C(05)	-173(2)	C(010)-N(1)-C(09)-C(8)	51(4)
C(03)-N(1)-C(04)-C(05)	-60(3)	C(03)-N(1)-C(09)-C(8)	-64(3)
C(012)-N(1)-C(04)-C(05)	121(3)	C(012)-N(1)-C(09)-C(8)	118(3)
C(06)-N(1)-C(04)-C(05)	6(2)	C(06)-N(1)-C(09)-C(8)	-126(3)
C(06)-C(05)-C(04)-N(1)	-6(2)	C(07)-N(1)-C(09)-C(06)	122(3)
C(07)-N(1)-C(03)-C(02)	125(3)	C(04)-N(1)-C(09)-C(06)	-64(3)
C(04)-N(1)-C(03)-C(02)	-49(3)	C(010)-N(1)-C(09)-C(06)	177(3)
C(09)-N(1)-C(03)-C(02)	-175(3)	C(03)-N(1)-C(09)-C(06)	63(2)
C(01)-N(1)-C(03)-C(02)	-1(3)	C(012)-N(1)-C(09)-C(06)	-116(3)
C(010)-N(1)-C(03)-C(02)	65(3)	C(07)-N(1)-C(09)-C(012)	-122(3)
C(06)-N(1)-C(03)-C(02)	-117(3)	C(04)-N(1)-C(09)-C(012)	52(2)
C(04)-N(1)-C(03)-C(07)	-174(3)	C(010)-N(1)-C(09)-C(012)	-67(3)
C(09)-N(1)-C(03)-C(07)	60(2)	C(03)-N(1)-C(09)-C(012)	178(3)
C(01)-N(1)-C(03)-C(07)	-125(3)	C(06)-N(1)-C(09)-C(012)	116(3)
C(010)-N(1)-C(03)-C(07)	-60(2)	C(05)-C(06)-C(09)-N(1)	79(4)
C(06)-N(1)-C(03)-C(07)	119(2)	C(05)-C(06)-C(09)-C(8)	172(3)
C(09)-N(1)-C(07)-C(8)	4(3)	N(1)-C(06)-C(09)-C(8)	93(4)
C(07)-N(1)-C(012)-C(011)	-50(3)	C(05)-C(06)-C(09)-C(012)	31(4)
C(04)-N(1)-C(012)-C(011)	124(3)	N(1)-C(06)-C(09)-C(012)	-47.9(19)
C(09)-N(1)-C(012)-C(011)	-110(3)	C(06)-C(09)-C(012)-C(011)	141(3)
C(01)-N(1)-C(012)-C(011)	75(4)	C(07)-N(1)-C(01)-C(02)	-57(4)
C(010)-N(1)-C(012)-C(011)	9(3)	C(04)-N(1)-C(01)-C(02)	130(4)
C(06)-N(1)-C(012)-C(011)	-170(3)	C(010)-N(1)-C(01)-C(02)	-110(4)
C(07)-N(1)-C(012)-C(09)	60(3)	C(03)-N(1)-C(01)-C(02)	1(3)
C(04)-N(1)-C(012)-C(09)	-126(3)	C(012)-N(1)-C(01)-C(02)	179(3)
C(01)-N(1)-C(012)-C(09)	-174(3)	C(06)-N(1)-C(01)-C(02)	67(4)
C(010)-N(1)-C(012)-C(09)	119(3)	N(1)-C(03)-C(02)-C(01)	1(3)
C(06)-N(1)-C(012)-C(09)	-60(2)	C(07)-C(03)-C(02)-C(01)	58(3)
C(010)-C(011)-C(012)-N(1)	-8(3)	N(1)-C(01)-C(02)-C(03)	-1(3)
C(010)-C(011)-C(012)-C(09)	-62(3)	N(1)-C(09)-C(8)-C(07)	4(3)
C(8)-C(09)-C(012)-N(1)	-94(3)	C(06)-C(09)-C(8)-C(07)	-65(4)
C(06)-C(09)-C(012)-N(1)	51(2)	C(012)-C(09)-C(8)-C(07)	66(3)
N(1)-C(09)-C(012)-C(011)	90(3)	N(1)-C(07)-C(8)-C(09)	-4(3)

C(8)-C(09)-C(012)-C(011)	-4(5)	C(010)-C(07)-C(8)-C(09)	-71(4)
		C(03)-C(07)-C(8)-C(09)	62(3)

Table C.6: Hydrogen bond distance (Å) and angles (º) for *fac*-[NEt_4][$Re_2(CO)_3(BSOPhC)_3$] (3).

D-H…A	d (D-H)	d (H…A)	d (D…A)	D-H…A angle
C36-H36A…O2[a]	0.96	2.42	3.37(3)	167

Symmetry code, transformations used to generate equivalent atoms:[a] -1/2+x, 1/2+y, 1/2+z

Table C.7: π-ring bond distances (Å) and angles (º) for *fac*-[NEt_4][$Re_2(CO)_3(BSOPhC)_3$] (3).

Y—X (I)	Res (I) Cg(J)	X..Cg	Y-X…Cg	Y..Cg
C5-O5	[1] → Cg6	3.806 (14)	82.4 (10)	3.826 (15)
C6-06	[1] → Cg5	3.666 (14)	82.6 (10)	3.695 (17)

Symmetry code, transformations used to generate equivalent atoms: x, y, z; Cg5 = centroid atoms of C20, C21, C22, C23, C24, C25; Cg6 = centroid atom of C30, C31, C32, C33, C34, C35.

APPENDIX D

Table D.1: Atomic coordinates (x 10^4) and equivalent isotropic displacement parameters (Å^2 x 10^3) for *fac*-[$Re_2(CO)_6$(μ-η^4-m-TolBSPh-S-S-m-TolBSPh)] (4). U(eq) is defined as one third of the trace of the orthogonalized U^{ij} tensor.

	x	y	z	U(eq)
Re(1)	5224(1)	3414(1)	2004(1)	20(1)
Re(2)	1810(1)	3023(1)	2748(1)	20(1)
S(1)	3023(2)	4266(2)	1703(2)	24(1)
S(3)	2085(2)	845(2)	1423(2)	25(1)
S(2)	3563(2)	1354(2)	413(2)	25(1)
S(4)	4368(2)	3221(2)	3789(2)	22(1)
O(5)	-1020(7)	2820(7)	947(6)	39(2)
O(2)	7279(8)	6169(7)	3716(6)	43(2)
O(1)	7582(7)	1955(7)	2507(6)	35(2)
O(6)	1625(7)	5673(7)	4747(6)	39(2)
C(13)	669(10)	1517(10)	-2430(9)	38(2)
C(11)	2360(9)	1918(9)	-475(8)	25(2)
O(4)	361(6)	1701(6)	4165(6)	31(1)
C(24)	4720(11)	-1082(10)	2813(10)	38(2)
C(25)	3555(11)	-843(9)	2082(9)	34(2)
C(16)	-487(13)	3297(12)	-2691(10)	53(3)
C(2)	6504(9)	5147(9)	3121(8)	27(2)
C(6)	1681(9)	4704(9)	3973(8)	27(2)
C(5)	-8(10)	2854(9)	1653(8)	27(2)
C(15)	1216(9)	3650(9)	-643(9)	30(2)
C(22)	5559(9)	1212(10)	4110(8)	30(2)
C(10)	2148(9)	3218(9)	78(8)	26(2)
C(12)	1616(10)	1076(10)	-1708(9)	35(2)
C(23)	5728(10)	-67(10)	3807(9)	34(2)
C(14)	483(10)	2809(10)	-1887(9)	35(2)
C(3)	5786(9)	3668(9)	660(8)	24(2)
O(3)	6145(8)	3859(7)	-109(6)	40(2)
C(1)	6737(9)	2513(9)	2308(8)	26(2)
C(21)	4446(10)	1526(9)	3432(8)	26(2)
C(20)	3428(9)	476(9)	2415(8)	27(2)
C(4)	914(9)	2163(8)	3627(8)	24(2)
C(26)	6977(12)	-367(13)	4485(11)	50(3)

Table D.2: Bond distances (Å) and angles (°) for *fac*-[$Re_2(CO)_6$(μ-η^4-m-TolBSPh-S-S-m-TolBSPh)] (4).

Bond	Bond Distance	Bond angle	Angle
Re(1)-C(3)	1.924(9)	C(3)-Re(1)-C(1)	93.6(4)
Re(1)-C(1)	1.939(9)	C(3)-Re(1)-C(2)	87.2(4)
Re(1)-C(2)	1.949(10)	C(1)-Re(1)-C(2)	91.0(4)

Re(1)-S(2)	2.442(2)	C(3)-Re(1)-S(2)	86.9(3)
Re(1)-S(1)	2.473(2)	C(1)-Re(1)-S(2)	93.2(3)
Re(1)-S(4)	2.543(2)	C(2)-Re(1)-S(2)	173.0(3)
Re(2)-C(5)	1.917(9)	C(3)-Re(1)-S(1)	94.8(2)
Re(2)-C(6)	1.935(9)	C(1)-Re(1)-S(1)	169.4(3)
Re(2)-C(4)	1.939(9)	C(2)-Re(1)-S(1)	95.8(2)
Re(2)-S(3)	2.432(2)	S(2)-Re(1)-S(1)	80.89(8)
Re(2)-S(4)	2.490(2)	C(3)-Re(1)-S(4)	175.4(2)
Re(2)-S(1)	2.541(2)	C(1)-Re(1)-S(4)	90.7(3)
S(1)-C(10)	1.799(9)	C(2)-Re(1)-S(4)	91.3(3)
S(3)-C(20)	1.781(9)	S(2)-Re(1)-S(4)	94.23(8)
S(3)-S(2)	2.228(3)	S(1)-Re(1)-S(4)	81.06(7)
S(2)-C(11)	1.759(8)	C(5)-Re(2)-C(6)	91.4(4)
S(4)-C(21)	1.785(9)	C(5)-Re(2)-C(4)	92.3(4)
O(5)-C(5)	1.147(10)	C(6)-Re(2)-C(4)	87.4(4)
O(2)-C(2)	1.146(11)	C(5)-Re(2)-S(3)	93.8(3)
O(1)-C(1)	1.134(10)	C(6)-Re(2)-S(3)	173.0(3)
O(6)-C(6)	1.146(11)	C(4)-Re(2)-S(3)	87.8(3)
C(13)-C(14)	1.390(14)	C(5)-Re(2)-S(4)	167.8(3)
C(13)-C(12)	1.399(12)	C(6)-Re(2)-S(4)	94.9(3)
C(11)-C(12)	1.389(12)	C(4)-Re(2)-S(4)	98.4(3)
C(11)-C(10)	1.409(12)	S(3)-Re(2)-S(4)	80.86(7)
O(4)-C(4)	1.145(10)	C(5)-Re(2)-S(1)	88.8(3)
C(24)-C(23)	1.369(14)	C(6)-Re(2)-S(1)	89.7(3)
C(24)-C(25)	1.405(13)	C(4)-Re(2)-S(1)	176.9(2)
C(25)-C(20)	1.398(12)	S(3)-Re(2)-S(1)	94.99(8)
C(16)-C(14)	1.510(12)	S(4)-Re(2)-S(1)	80.78(7)
C(15)-C(10)	1.383(11)	C(10)-S(1)-Re(1)	100.5(3)
C(15)-C(14)	1.397(13)	C(10)-S(1)-Re(2)	101.5(3)
C(22)-C(23)	1.370(13)	Re(1)-S(1)-Re(2)	93.55(8)
C(22)-C(21)	1.383(12)	C(20)-S(3)-S(2)	94.1(3)
C(23)-C(26)	1.470(14)	C(20)-S(3)-Re(2)	104.5(3)
C(3)-O(3)	1.140(10)	S(2)-S(3)-Re(2)	102.60(10)
C(21)-C(20)	1.400(12)	C(11)-S(2)-S(3)	97.0(3)
		C(11)-S(2)-Re(1)	103.4(3)
		S(3)-S(2)-Re(1)	103.20(10)
		C(21)-S(4)-Re(2)	102.7(3)
		C(21)-S(4)-Re(1)	97.7(3)
		Re(2)-S(4)-Re(1)	93.11(7)
		C(14)-C(13)-C(12)	118.7(9)
		C(12)-C(11)-C(10)	120.6(8)
		C(12)-C(11)-S(2)	119.9(7)
		C(10)-C(11)-S(2)	119.5(6)
		C(23)-C(24)-C(25)	122.0(9)
		C(20)-C(25)-C(24)	117.9(9)

		O(2)-C(2)-Re(1)	175.9(8)
		O(6)-C(6)-Re(2)	176.2(8)
		O(5)-C(5)-Re(2)	173.1(8)
		C(10)-C(15)-C(14)	120.7(9)
		C(23)-C(22)-C(21)	123.0(9)
		C(15)-C(10)-C(11)	118.6(9)
		C(15)-C(10)-S(1)	120.9(7)
		C(11)-C(10)-S(1)	120.5(6)
		C(11)-C(12)-C(13)	120.5(9)
		C(24)-C(23)-C(22)	118.3(8)
		C(24)-C(23)-C(26)	119.6(9)
		C(22)-C(23)-C(26)	122.1(10)
		C(13)-C(14)-C(15)	120.9(8)
		C(13)-C(14)-C(16)	118.2(9)
		C(15)-C(14)-C(16)	120.8(9)
		O(3)-C(3)-Re(1)	177.8(8)
		O(1)-C(1)-Re(1)	176.8(8)
		C(22)-C(21)-C(20)	117.9(8)
		C(22)-C(21)-S(4)	121.0(7)
		C(20)-C(21)-S(4)	121.0(7)
		C(25)-C(20)-C(21)	120.8(8)
		C(25)-C(20)-S(3)	119.4(7)
		C(21)-C(20)-S(3)	119.3(7)
		O(4)-C(4)-Re(2)	177.1(7)

Table D.3: Anisotropic displacement parameters ($Å^2$ x 10^3) for *fac*-[$Re_2(CO)_6$(μ-$η^4$-m-TolBSPh-S-S-m-TolBSPh)] (4). The anisotropic displacement factor exponent takes the form: $-2π^2[h^2a^{*2}U^{11} + ... + 2hka^*b^*U^{12}]$.

	U_{11}	U_{22}	U_{33}	U_{23}	U_{13}	U_{12}
Re(1)	16(1)	26(1)	20(1)	11(1)	4(1)	6(1)
Re(2)	16(1)	26(1)	20(1)	11(1)	4(1)	6(1)
S(1)	20(1)	28(1)	27(1)	15(1)	6(1)	9(1)
S(3)	24(1)	28(1)	24(1)	12(1)	5(1)	6(1)
S(2)	24(1)	30(1)	21(1)	12(1)	6(1)	9(1)
S(4)	20(1)	29(1)	20(1)	12(1)	3(1)	7(1)
O(5)	23(3)	63(5)	35(4)	27(4)	6(3)	11(3)
O(2)	51(4)	34(4)	30(4)	9(3)	4(3)	-4(4)
O(1)	25(3)	42(4)	46(4)	23(3)	12(3)	15(3)
O(6)	48(4)	35(4)	34(4)	12(3)	9(3)	17(3)
C(13)	31(5)	45(6)	26(5)	11(5)	-8(4)	1(5)
C(11)	19(4)	33(5)	22(4)	17(4)	0(3)	2(4)
O(4)	23(3)	37(4)	28(3)	15(3)	2(3)	-5(3)
C(24)	51(6)	36(5)	53(6)	35(5)	28(5)	25(5)
C(25)	43(6)	31(5)	29(5)	11(4)	13(4)	7(5)
C(16)	65(8)	63(8)	39(6)	26(6)	5(6)	40(7)
C(2)	24(4)	36(5)	28(5)	17(4)	10(4)	13(4)
C(15)	23(4)	38(5)	38(5)	22(4)	10(4)	13(4)
C(22)	23(4)	48(6)	30(5)	28(5)	4(4)	8(4)
C(10)	19(4)	39(5)	31(5)	25(4)	9(4)	7(4)
C(12)	38(5)	35(5)	29(5)	19(4)	-2(4)	4(4)
C(23)	35(5)	47(6)	34(5)	29(5)	13(4)	17(5)
C(14)	23(5)	50(6)	31(5)	22(5)	-1(4)	9(4)
C(3)	19(4)	26(4)	25(4)	11(4)	5(4)	5(4)
O(3)	55(5)	38(4)	33(4)	18(3)	19(3)	9(3)
C(1)	22(4)	30(5)	23(4)	12(4)	1(3)	5(4)
C(21)	30(5)	28(5)	30(5)	21(4)	14(4)	7(4)
C(20)	29(5)	27(5)	27(5)	13(4)	6(4)	5(4)
C(26)	46(6)	69(8)	53(7)	37(6)	19(6)	27(6)

Table D.4: Hydrogen coordinates (x 10^4) and isotropic displacement parameters ($Å^2$ x 10^3) for *fac*-[$Re_2(CO)_6$(μ-$η^4$-m-TolBSPh-S-S-m-TolBSPh)] (4).

	x	y	z	U(eq)
H(13)	173	957	-3257	46
H(24)	4808	-1956	2615	45
H(25)	2890	-1541	1398	41
H(16A)	-515	4199	-2202	80
H(16B)	-1440	2738	-3005	80
H(16C)	-124	3265	-3378	80
H(15)	1076	4510	-295	36
H(22)	6223	1900	4804	36
H(12)	1749	214	-2056	42

H(26A)	7581	445	5149	75
H(26B)	7511	-779	3922	75
H(26C)	6653	-964	4827	75

Table D.5: Torsion Angles (º) for *fac*-[$Re_2(CO)_6(\mu\text{-}\eta^4$-m-TolBSPh-S-S-m-TolBSPh)] (4).

Torsion Angle	Angle	Torsion Angle	Angle
S(3)-S(2)-C(11)-C(12)	-99.2(7)	C(21)-C(22)-C(23)-C(26)	175.5(9)
Re(1)-S(2)-C(11)-C(12)	155.4(7)	C(12)-C(13)-C(14)-C(15)	-0.6(15)
S(3)-S(2)-C(11)-C(10)	80.1(7)	C(12)-C(13)-C(14)-C(16)	177.2(10)
Re(1)-S(2)-C(11)-C(10)	-25.3(7)	C(10)-C(15)-C(14)-C(13)	0.2(14)
C(23)-C(24)-C(25)-C(20)	-1.4(14)	C(10)-C(15)-C(14)-C(16)	-177.4(9)
C(14)-C(15)-C(10)-C(11)	0.9(13)	C(23)-C(22)-C(21)-C(20)	2.0(13)
C(14)-C(15)-C(10)-S(1)	-176.7(7)	C(23)-C(22)-C(21)-S(4)	-174.4(7)
C(12)-C(11)-C(10)-C(15)	-1.8(13)	Re(2)-S(4)-C(21)-C(22)	-162.0(7)
S(2)-C(11)-C(10)-C(15)	178.9(6)	Re(1)-S(4)-C(21)-C(22)	103.1(7)
C(12)-C(11)-C(10)-S(1)	175.9(7)	Re(2)-S(4)-C(21)-C(20)	21.7(7)
S(2)-C(11)-C(10)-S(1)	-3.4(10)	Re(1)-S(4)-C(21)-C(20)	-73.3(7)
Re(1)-S(1)-C(10)-C(15)	-152.9(7)	C(24)-C(25)-C(20)-C(21)	1.1(13)
Re(2)-S(1)-C(10)-C(15)	111.3(7)	C(24)-C(25)-C(20)-S(3)	173.3(7)
Re(1)-S(1)-C(10)-C(11)	29.5(7)	C(22)-C(21)-C(20)-C(25)	-1.3(13)
Re(2)-S(1)-C(10)-C(11)	-66.4(7)	S(4)-C(21)-C(20)-C(25)	175.1(7)
C(10)-C(11)-C(12)-C(13)	1.5(14)	C(22)-C(21)-C(20)-S(3)	-173.6(6)
S(2)-C(11)-C(12)-C(13)	-179.2(8)	S(4)-C(21)-C(20)-S(3)	2.8(10)
C(14)-C(13)-C(12)-C(11)	-0.3(15)	S(2)-S(3)-C(20)-C(25)	-94.8(7)
C(25)-C(24)-C(23)-C(22)	2.0(14)	Re(2)-S(3)-C(20)-C(25)	161.1(7)
C(25)-C(24)-C(23)-C(26)	-175.9(9)	S(2)-S(3)-C(20)-C(21)	77.6(7)
C(21)-C(22)-C(23)-C(24)	-2.4(14)	Re(2)-S(3)-C(20)-C(21)	-26.5(8)

APPENDIX E

Preliminary results of the synthesis of complexes containing S,O and S, S' bidentate ligands

The synthesis of the following compounds were performed and the preliminary results are reported here, but it is not yet clear what the exact structure of these compounds is. The results of the elemental analysis was not yet available at the time of this dissertation and no suitable crystals for single crystal XRD were obtained. Therefore no conclusive evidence was found of the exact structure of these complexes. It is however expected that these compounds are dinuclear in nature, but how the ligands coordinated to the rhenium centre(s) is not known. The investigation into these complexes will form part of the future work on this project and an in depth NMR study and growing suitable crystals for XRD will form part of the main objectives.

ReAA reacted with BSOH

ReAA (100 mg, 0.130 mmol) was dissolved in 10 ml methanol. BSOH (21.3 mg, 0.130 mmol) was added to the mixture as a solid and stirred at room temperature for 2 hours. The product was collected by vacuum. The product obtained from the evaporation of methanol as solvent was crystalline but the crystals was not suitable for XRD. Yield: 70 %.

IR (KBr, cm^{-1}): ν_{CO} = 2004, 1860.

UV/Vis: λ_{max} = 204 nm, ε = 3125 M^{-1} cm^{-1}.

^{1}H NMR (150 MHz, Acetonitrile-*d*$_3$): δ (ppm) = 7.81 (m, 1H), 7.72 (dd, *J* = 6.6, 2.2, 1H), 7.30 (m, 2H), 7.22 (s, 1H), 4.83 (d, *J* = 5.3, 2H). 3.30 (q, 8H (NEt_4)), 1.28 (tt, 12H (NEt_4)).

^{13}C NMR (150 MHz, Acetonitrile-*d*$_3$): δ (ppm) = 148.13, 140.75, 140.45, 124.86, 124.23, 124.12, 121.21, 60.14, 53.29 (NEt_4), 7.35, 7.17 (NEt_4).

ReAA reacted with BSOC

ReAA (100 mg, 0.130 mmol) was dissolved in 10 ml methanol. BSOC (24.98 mg, 0.130 mmol) was added to the mixture as a solid and stirred at room temperature for 2 hours. The product was collected by vacuum. Yield: 78%.

IR (KBr, cm^{-1}): ν_{CO} = 2005, 1867.

UV/Vis: λ_{max} = 211 nm, ε = 2981 M^{-1} cm^{-1}.

^{1}H NMR (300 MHz, Methanol-*d*$_4$): δ (ppm) = 8.09 (s, 1H), 7.94 (m, 2H), 7.45 (m, 2H), 3.94 (d, *J* = 3.12, 3H), 3.32 (q, 8H (NEt_4)), 1.31(tt, 12H (NEt_4)).

^{13}C NMR (150 MHz, Methanol-*d*$_4$): δ (ppm) = δ (ppm) = 143.42, 140.13, 138.00, 134.35, 131.80, 128.22, 126.74, 126.19, 123.74, 53.27 (NEt_4), 53.03, 7.66 (NEt_4).

ReAA reacted with $BSOPhH_2$

ReAA (100 mg, 0.130 mmol) was dissolved in 10 ml methanol. $BSOPhH_2$ (13.05 µL, 0.130 mmol) was added to the mixture as a liquid and stirred at room temperature for 2 hours. The product was collected by vacuum. Yield: 66 %.

IR (KBr, cm^{-1}): ν_{CO} =2003, 1868.

UV/Vis: λ_{max} = 225 nm, ε = 3451 M^{-1} cm^{-1}.

^{1}H NMR (300 MHz, Methanol-*d*$_4$): δ (ppm) = 7.83 (d, *J* = 11.01, 1H), 7.37(dd, *J* = 7.61, 1.9 Hz, 1H), 7.08(dd, *J* = 7.41, 2.30 Hz, 1H), 6.78 (d, *J* = 18.1 Hz, 1H), 3.24 (NEt_4), 1.23 (NEt_4).

^{13}C NMR (150 MHz, Methanol-*d*$_4$): δ (ppm) = 130.21, 128.01, 126.31, 122.12, 120.10, 119.18, 51.40 (NEt_4), 7.15 (NEt_4).

ReAA reacted with BSBr

ReAA (100 mg, 0.130 mmol) was dissolved in 10 ml methanol. BSBr (31.8 mg, 0.130 mmol) was added to the mixture as a solid and stirred at room temperature for 2 hours. The product was collected by vacuum. The product obtained from the evaporation of methanol as solvent was crystalline but the crystals was not suitable for XRD. Yield: 63 %.

IR (KBr, cm^{-1}): ν_{CO} = 2004, 1868.

UV/Vis: λ_{max} = 261 nm, ε = 3853 M^{-1} cm^{-1}.

^{1}H NMR (300 MHz, Methanol-*d*$_4$): δ (ppm) = 7.36 (dd, *J* = 5.1, 1.1 Hz, 1H), 7.18 (dd, *J* = 3.6, 1.1 Hz, 1H), 7.04 (m, 2H), 7.00 (t, *J* = 4.2 Hz, 1H), 3.29 (q, 8H (NEt_4)), 1.29 (tt, 12H (NEt_4)).

^{13}C NMR (150 MHz, Methanol-*d*$_4$): δ (ppm) = 138.96, 135.88, 130.77, 127.67, 124.81, 123.87, 123.68, 110.10, 51.89 (NEt_4), 6.29 (NEt_4).

ReAA reacted with BSCH

ReAA (100 mg, 0.130 mmol) was dissolved in 10 ml methanol. BSCH (27.3 mg, 0.130 mmol) was added to the mixture as a solid and stirred at room temperature for 2 hours. The product was collected by vacuum. The product obtained from the evaporation of methanol as solvent was crystalline but the crystals was not suitable for XRD. Yield: 81 %.

IR (KBr, cm^{-1}): ν_{CO} = 2005, 1867.

UV/Vis: λ_{max} = 254 nm, ε = 2458 M^{-1} cm^{-1}.

^{1}H NMR (300 MHz, Methanol-*d*$_4$): δ (ppm) = 7.67 (d, *J* = 3.9 Hz, 1H), 7.44 (dd, *J* = 5.1, 1.1 Hz, 1H) 7.36 (dd, *J* = 3.7, 1.2 Hz, 1H), 7.24 (d, *J* = 3.9 Hz, 1H), 7.08 (dd, *J* = 5.1, 3.7Hz, 1H), 3.28 (q, 8H (NEt_4), 1.28(tt, 12H (NEt_4)).

^{13}C NMR (150 MHz, Methanol-*d*$_4$): δ (ppm) = 164.96, 145.74, 137.23, 135.75, 133.25, 129.22, 129.37, 126.52, 125.14, 53.25 (NEt_4), 7.63 (NEt_4).

ReAA reacted with $BSPhH_2$

ReAA (100 mg, 0.130 mmol) was dissolved in 10 ml methanol. $BSPhH_2$ (18.46 mg, 0.130 mmol) was added to the mixture as a liquid and stirred at room temperature for 2 hours. The product was collected by vacuum. The product obtained from the evaporation of methanol as solvent was crystalline but the crystals was not suitable for XRD. Yield: 63 %.

IR (KBr, cm^{-1}): ν_{CO} = 2000, 1870.

UV/Vis: λ_{max} = 260 nm, ε = 3458 M^{-1} cm^{-1}.

^{1}H NMR (300 MHz, Methanol-*d*$_4$): δ (ppm) = 7.36 (dd, *J* = 7.2, 1.2 Hz, 1H), 7.20 (dd, *J* = 6.9, 1.2 Hz, 1H), 6.94 (m, 2H), 3.19 (q, 8H (NEt_4), 1.15(tt, 12H (NEt_4)).

^{13}C NMR (150MHz, Methanol-*d*$_4$): δ (ppm) = 141.10, 133.27, 132.19, 130.49, 126.78, 115.03, 53.25 (NEt_4), 7.63 (NEt_4).

fac-$[Re(CO)_3(H_2O)_3]^+$ reacted with BSOH

ReAA (100 mg, 0.130 mmol) was dissolved in 20 ml of water and the pH was adjusted to ~2.0 using nitric acid. $AgNO_3$ (66.2 mg, 0.387 mmol) was added to the solution and stirred for 24 hours at room temperature. The precipitate, AgBr, was filtered off. BSOH (21.3 mg, 0.130 mmol) was added to the filtrate as a solid and stirred for 4 hours at room temperature. The product was filtered off, dried and weighed. Yield: 74 %.

IR (KBr, cm^{-1}): ν_{CO} = 2088, 2015,1881.

UV/Vis: λ_{max} = 271 nm, ε = 2548 M^{-1} cm^{-1}.

^{1}H NMR (300 MHz, DMSO-*d*$_6$): δ (ppm) = 7.90 (m, 1H), 7.76 (dd, *J* = 6.6, 2.2, 1H), 7.32 (m, 2H), 7.26 (s, 1H), 4.75 (s, *J* = 6.3 Hz, 2H), 3.18 (q, 8H (NEt_4)), 1.15 (tt, 12H (NEt_4)).

^{13}C NMR (151 MHz, Methanol-*d*$_4$): δ (ppm) = 147.24, 141.15, 125.27, 125.14, 123.27, 122.02, 60.68, 53.31 (NEt_4), 7.69 (NEt_4).

fac-$[Re(CO)_3(H_2O)_3]^+$ reacted with BSOPhCH

ReAA (100 mg, 0.130 mmol) was dissolved in 20 ml of water and the pH was adjusted to ~2.0 using Nitric acid. $AgNO_3$ (66.2 mg, 0.387 mmol) was added to the solution and stirred for 24 hours at room temperature. The precipitate, AgBr, was filtered off. BSOPhCH (15.8 µL, 0.130 mmol) was added to the filtrate as a solid and stirred for 6 hours. The product was filtered off, dried and weighed. Yield: 80 %.

IR (KBr, cm^{-1}): ν_{CO} = 2092, 2010, 1880.

UV/Vis: λ_{max} = 275 nm, ε = 3102 M^{-1} cm^{-1}.

^{1}H NMR (300 MHz, *DMSO-d*$_6$): δ (ppm) = 7.78 (dd, *J* = 7.7, 1.6 Hz, 1H), 7.12 (d, *J* = 7.7, 1.6 Hz, 1H), 6.88 (dtd, *J* = 22.2, 7.8, 1.6 Hz, 2H), 3.83 (s, 3H), 3.17 (q, 8H (NEt_4)), 1.14 (tt, 12H (NEt_4)).

^{13}C NMR (151 MHz, *DMSO-d*$_6$): δ (ppm) = 139.65, 134.23, 127.15, 12.30, 110.82, 55.92, 51.80(NEt_4), 7.52 (NEt_4).

fac-$[Re(CO)_3(H_2O)_3]^+$ reacted with $BSOPhH_2$

ReAA (100 mg, 0.130 mmol) was dissolved in 20 ml of water and the pH was adjusted to ~2.0 using nitric acid. $AgNO_3$ (66.2 mg, 0.387 mmol) was added to the solution and stirred for 24 hours at room temperature. The precipitate, AgBr, was filtered off. $BSOPhH_2$ (4.5 µL, 0.130 mmol) was added to the filtrate as a solid and stirred for 15 hours. The green product was filtered off, dried and weighed. Yield: 83 %.

IR (KBr, cm^{-1}): ν_{CO} = 2090, 2011, 1870

UV/Vis: λ_{max} = 263 nm, ε = 3102 M^{-1} cm^{-1}.

^{1}H NMR (300 MHz, Methanol-*d*$_4$): δ (ppm) = 9.39 (s, 1H), 7.84 (dd, *J* = 7.8, 1.6 Hz), 6.93 (td, *J* = 7.6, 1.6 Hz), 6.75 (m, 2H), 3.19 (q, 8H (NEt_4)), 1.11 (tt, 12H (NEt_4)).

^{13}C NMR (151 MHz, Methanol-*d*$_4$): δ (ppm) = 157.61, 135.07, 127.03, 125.33, 119.04, 114.75, 51.82 (NEt_4), 7.52 (NEt_4)